UNIVERSITÀ DI PARMA

Università degli Studi di Parma

Ph.D. program in Biotechnology and Life Sciences

XXXI cycle

A novel scaffold for nanobody selection and expression suitable for diagnostic and therapeutic applications

Coordinator:
Prof. Simone Ottonello

Tutor:
Prof. Angelo Bolchi

Ph.D. student: Valentina Garrapa

2015/2018

To those who
love me despite
of everything

Index

Abstract

A novelty in antibody field has recently been introduced after the discovery of the presence of heavy chain immunoglobulins G, lacking light chains molecules, in camelids blood. The potentiality of the variable domain of these heavy chain antibodies (called VHH or nanobody) was immediately exploited. These variable domains, singularly expressed, maintain a target affinity comparable to an entire antibody, are very soluble because of the absence of exposed hydrophobic amino acid residues and they are very small (~15 kDa), if compared to conventional antibodies (~150 kDa). All these features, combined with their easy expression as recombinant proteins in bacteria, determined their enrollment as new biotechnologial tools.

During my Ph.D., I produced and validated a novel scaffold suitable for nanobody expression and selection: the scaffold consists of four framework regions (FRs, conserved in sequence) derived from the alignment of more than 750 llama nanobodies. Within this scaffold, complementary determining regions (CDRs) of natural VHH or artificial random sequences can be grafted. The scaffold leads to an improvement of solubility and stability of the nanobodies and is the potential basis for antibody libraries construction.

I exploited the consensus framework scaffold (CFW) in the development of a platform for new nanobodies selection and for their improvement in order to render them diagnostic and therapeutic tools. Two artificial nanobody libraries are the basis of the platform. One, composed by the CFW and bearing semi-random artificial CDRs, presents a complexity of 10^{12} different nanobody clones (comparable to the natural llama VHH repertoire) and is selectable through ribosome display technique. I validated this library by selecting new Maltose binding protein (MBP) binders.

The second library is a humanized version of the previous one in which I introduced 12 point mutations in order to render CFW scaffold identical to human IgG VH III FRs. I confirmed the solubilizing and stabilizing effects of the humanized CFW scaffold and the library is now ready to be clone in a novel phage vector that I created to speed up phage display selection. From this humanized library potential directly human applicable nanobodies will be selected, avoiding any post-selection humanization which usually can lead to antibody target affinity alteration.

Additionally, I developed methods to improve nanobodies for diagnostic applications. Since nanobodies are not detectable through secondary antibodies, I applied an *in vitro* peptide ligation system to conjugate them to immunoglobulins Fc regions. With this modular and stable conjugation approach, I demonstrated the possibility to combine any purified VHHs to any expressed Fc regions, obtaining antibodies that mimic monoclonal antibodies activity.

In collaboration with Preclincs company, I further exploited my scaffold for the production of new *in vivo* imaging probes. Fusing nanobodies to a luciferase, a probe working for GFP imaging in mice has been validated, while other probes remain to be tested.

Introduction

Introduction

Since the development of hybridoma technology in 1970s by Köhler and Milstein[1] the world of monoclonal antibodies (mAb) and derivatives is exponentially growing: the development of a quicker and cheaper way to produce monoclonal antibodies determined their irruption in biomedical applications. With a global sales revenue near $ 75 billion for therapeutic[2] and 7.5 billion for diagnostic applications[3] they are currently the biggest piece of the market and continuous increase in pharmaceutical investments is expected (**Figure 1**).

In 1985 the first monoclonal antibody anti-CD3 was approved by Food and Drug Administration (OKT3®) and now 74 antibody-based molecules are available on the market, of which Rituximab (used in cancer treatment) is the best example of a tremendous medical and commercial success, being the fourth best-selling innovative drug of any kind[4].

The reasons for the diffusion of mAbs can be easily understood by noting their applications and advantages: they are specific, have a high affinity for their targets, can recruit immune response and can be easily detected. All these features make mAb suitable for *in vivo* and *in vitro* unlimited applications[5].

Furthermore, with the progress of scientific research, today not only naked mouse / humane / chimeric / humanized antibodies are available, but also derivatives like bivalent antibodies, conjugation to cytotoxic compound or immunomodulators are present[6,7].

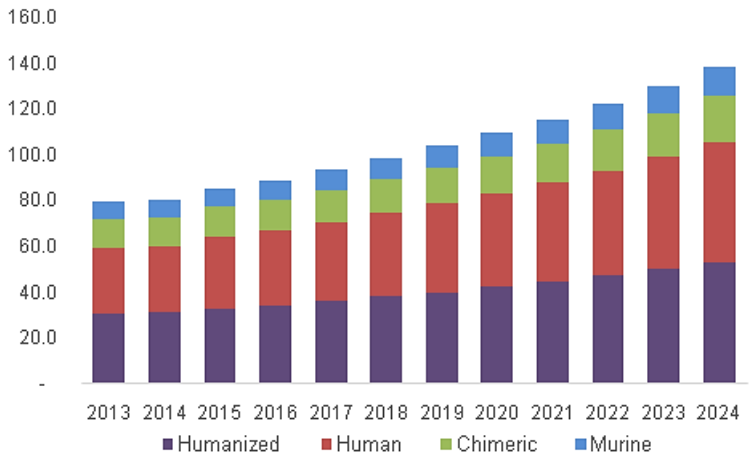

Figure 1 Monoclonal antibodies market by source type, 2013-2024 (USD Billion) (Monoclonal Antibodies Market Analysis, 2016. https://www.grandviewresearch.com/industry-analysis/monoclonal-antibodies-market)**.**

1. Heavy chain antibodies

In such a fast-moving field in 1993 a revolutionary and serendipitous discovery was made. During a lesson in which students did not want to analyse their own blood for HIV risk of infection and they did not want to kill a mouse, Hamers-Casterman and colleagues observed in the serum of camel (the only one ready-to-use present in the laboratory) the presence of naturally occurring antibodies devoid of light chains. In a short and concise article, they made a simple observation: two camel IgG subclasses did not show separation between heavy and light chains in presence of reducing agents (**Figure 2**).

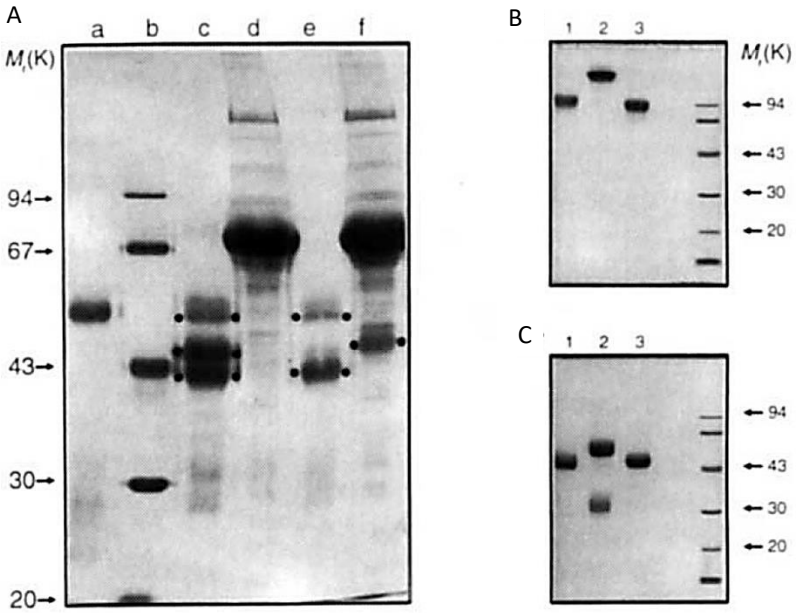

Figure 2 (modified by[8]) A) Adsorption of *C. dromedarius* serum on protein A (lane c) evidence the presence of three IgG subclasses (50, 46 and 43 kDa). B) The previous three subclasses are analysed separately on SDS-page. C) The same three subclasses are analysed on SDS-page after treatment with dithiothreitol.

They were also able to demonstrate that these peculiar subclasses of IgG generate an extensive repertoire of antibodies contributing to the immune response of the camel[8]. They called these antibodies heavy chain antibodies (hcAb) and they gave the starting point of a further proliferating pool of discoveries.

1.1. Generation of heavy chain antibodies in camelids

Today the generation, structure and features of hcAb are well known. Heavy chain antibodies can be found in the biological family of *Camelidae* that comprises camels (*Camelus dromedaries* and *Camelus bactrianus*), llama (*Lama glama* and *Lama guanicoe*)

and vicugna (*Vicugna vicugna* and *Vicugna pacos*). The percentage of hcAb if compared to the whole immunoglobulins repertoire in the serum of these animals is variable with the maximum ratio observed in camels (between 50-80%) and the minimum ratio observed in South American camelids (10-25%)[9].

They belong to the immunoglobulin γ antibody class (IgG) and in particular to IgG2 and IgG3 subclasses for their ability to bind protein A and protein G respectively[10]; in IgG2 subclass it is possible to identify with pH-controlled elution fractions of IgG2a and IgG2b[11].

The presence of heavy chain IgG subtype can be easily explained by their origin: a single-nucleotide G-to-A point mutation occurred in IGHG gene encoding IgGs heavy chains determining the loss of consensus splicing site (GT) at 5' end of the intron between the CH1–hinge exons; thus CH1 domain is eliminated during splicing[12]. This mutation explains contemporary the CH1 domains and light chains absence in mature hcAb: heavy and light chains of antibodies are expressed in endoplasmic reticulum (ER) and the heavy chains are retained in ER by the bind of BiP protein (heavy chain binding protein) to CH1 domain. BiP is the major ER protein involved in translocation, secretion, quality control and degradation of secreted proteins[13] and only when the light chains replace BiP in the binding to heavy chains, the mature Ab can be secreted. In absence of CH1 domain, hcAbs are not able to recruit BiP and they are secreted without light chains[14] (**Figure 3**).

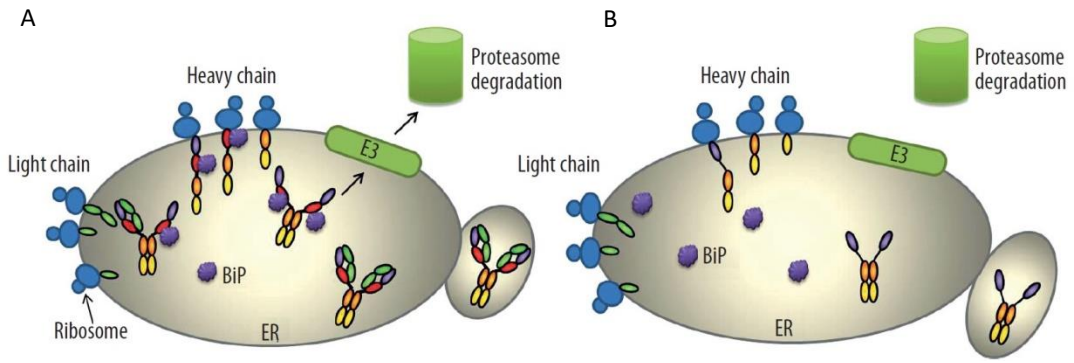

Figure 3[15] Schematic representation of antibody's expression in endoplasmic reticulum (ER). A) Physiological expression of antibodies in presence of CH1 domain. B) Expression of heavy chain antibodies in absence of CH1 domain.

Then it is possible to deduce that the elements that produce the heavy chain of hcAb are specific for them and present this typical point mutation even if they are located in the same locus of conventional antibodies in camelids genome.

Also, the variable domains of hcAb originate from dedicated germ line genes called IGHVH, probably derived from mutated IGHV genes (encoding for variable regions of

conventional Ab)[16]. The ratio of IGHVH comparing to IGHV genes varies between species ranging from 40% of IGHVH in dromedary to 20% in alpaca[17]. During B-cell lymphopoiesis both IGHVH and IGHV genes are involved in V-D-J recombination (i.e. the process during B-cell development in which one variable (V), one diversity (D) and one joining (J) segments are randomly rearranged from a gene cluster for the formation of the VH domain) and D and J gene pool are the same for both variable domains; then the principal differences between the variable domains of canonical IgGs and heavy chain IgGs reside in nucleotide sequence of V genes. The structure and sequence of the variable domain of hcAb will be discussed in depth in the next paragraph but it is interesting to note that the presence of peculiar sequences (i.e. palindromes) that are unstable, may lead to a faster gene evolution and consequently a faster expansion of IGHVH repertoire, promoting their maintenance during evolution[18].

1.2. Structure of heavy chain antibodies and their variable domains

The structure of IgGs is well known and highly conserved trough mammals: two identical heavy chains and two identical light chains join by hydrophobic interactions and disulphide bonds. After papain digestion, three fragments of IgG are obtained: two Fabs (antigen-binding fragments) and one Fc (fragment crystallizable)[19].

The structure of hcAb Fc region is the same of conventional IgG (**Figure 4**): every chain of the Fc is composed by two domain conserved in sequence and structure: constant heavy 3 and 2 domains (i.e. CH3 and CH2 respectively). Both domains fold in a constant structure of 3-strand/4-strand β sheet pinned together by an intrachain disulphide bond and are responsible for the effector function of the entire antibody[20].

HcAb lacks the CH1 domain so they are smaller than conventional IgG (~90 kDa compared to ~150 kDa) and the variable domain is directly connected to the constant domains through a hinge region. The hinge region of IgG2 fraction is longer than that of IgG3 subclass and contains Pro-Gln repeats which probably replace the CH1 domain[21].

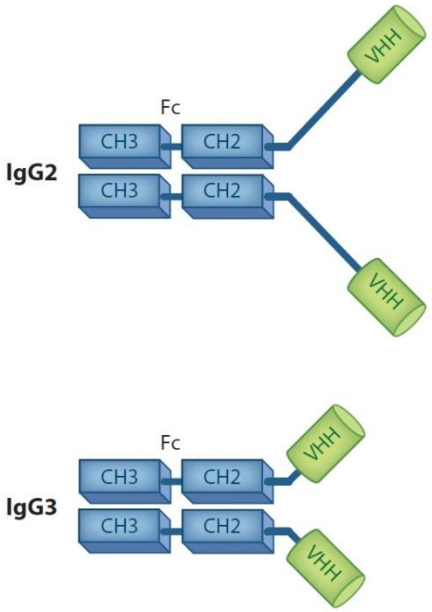

Figure 4 (modified by[21]) Schematic representation of IgG2 and IgG3 subclasses of hcAb.

HcAbs are also devoid of light chains thus their variable region consists of a single domain called VHH (variable heavy domain of heavy

chain antibody) or nanobody (Nb) that thanks to a set of characteristics renders the binding of hcAb to the antigen comparable to that of conventional antibodies (**Figure 5**)[22]. The folded variable domain comprises nine β strands (A-B-C-C'-C''-D-E-F-G) organized in a 4-strand/5-strand β sheet connected by loops and by a disulphide bond between Cys23 and Cys94. The sequence within β sheet is conserved and can be divided into 4 conserved and structural regions called framework (FR). FRs surround three hypervariable regions that represent loops and are called complementary determining regions (CDRs) primarily responsible for antigen binding[23].

What differs VHHs from canonical VH domains are notable differences mainly in FR2 (i.e. the second conserved region starting from the N-terminus) and in CDRs. A VH FR2 presents four conserved hydrophobic amino acids (Val47, Gly49, Leu50, Trp52) that interact with the VL (variable domain of the light chain) creating a hydrophobic core; in VHHs these four amino acids are replaced by hydrophilic or smaller ones (mostly Phe42, Glu49, Arg50, Gly52) probably for a more stable exposure to the solvent in absence of light chains[24].

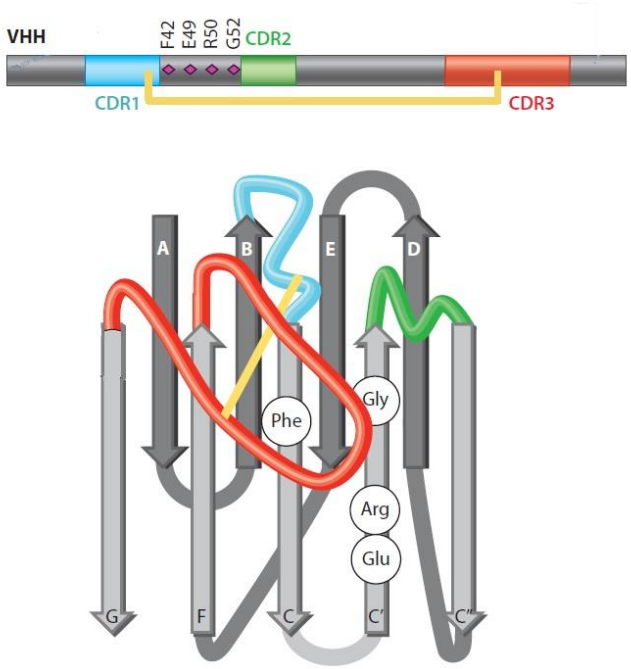

Figure 5 (modified by[21]) Schematic representation of a VHH with CDRs and FRs. FR are represented in grey and the disulphide bond in yellow. Peculiar amino acids of VHH are highlighted.

In order to contrast the lack of a VL domain and then of three CDRs that contact the antigen, VHHs have longer CDR1 and CDR3 that create an antigen-contacting surface of 600-800 Å^2 [25] comparable to classical VH-VL interacting surface (600-900 Å^2 [26]). While a longest CDR1 loop can be explained by the germline gene architecture, a longer CDR3, with an average length of 16 amino acids compared to 12 of a canonical CDR3, is probably selected during B cells maturation because contributes to a high affine and specific target binding[21].

Rather than sequence variability or length, for CDR1 and CDR2, high flexibility and structure variations are probably responsible for the high-affinity recruitment of the target[27,28].

An extended and flexible CDR3 loop (which position is probably determined by the first amino acid of FR4[29]) implies a counterproductive entropy; that is the reason why camel VHH often present an extra pair of cysteine that forms a disulphide bond in which CDR3 is involved[30]. The presence and the position of this extra S-S bridge vary between species: in llama, it is less frequent probably due to a shorter on average CDR3, in dromedary, it is frequently present between CDR1 and CDR3 and rarely between CDR3 and FR2[31]. In rare cases of short CDR3 the disulphide bridge is absent and the loop assumes a stretched twisted turn conformation similarly to VH domain to stabilize its structure[32].
VH domains of canonical immunoglobulins can be classified into three clans (I, II and III), which are defined as clusters containing an overall 80% DNA sequence identity[33]. Analysis of rearranged VHH clones classified them in clan III with a high identity with human IgG VH domain[24]. VHHs can also be classified in at least four subfamilies (1, 2, 3 and 4) based on five key residues (i.e. 4, 6, 7 and 10) and the additional disulphide bond position that characterise each subclass regardless of species origin[31].

1.3. Heavy chain antibodies in other species

Heavy chain antibodies are present in human and supposedly in other animals in case of aberrant conditions[34], but surprisingly the *Camelidae* family is not the only one that possesses heavy chain antibodies in its natural immune repertoire: in 1995 Greenberg and colleagues observed the presence of a new antigen receptor (NAR) in nurse shark (*Ginglymostoma cirratum*)[35]. Subsequent analysis revealed that NARs possess a structure similar to hcAb: they are composed by two covalently associated heavy chains that lack light chains and CH1 domains; the heavy chains are composed by six domains, of which five are constant and one variable[36]. Following studies demonstrated that after immunization an IgNAR response is elicited (i.e. they share some functional features with immunoglobulins) with a similar kinetic as IgM response[37], even if they probably originated from IgW subtype, a primordial immunoglobulin class presents in sharks[38].
Now the presence of IgNAR has been observed in many cartilaginous fishes (i.e. nurse sharks, wobbegong shark, spiny dogfish, banded houndshark, bamboo shark, rays and holocephalins)[39] and the presence of similar and peculiar antibodies in such diverse species arises a series of questions to which scientists are trying to answer.
Phylogenetic studies underline that heavy chain antibodies in camelids emerged and diverged from immunoglobulin-γ ~25 million years ago after *Tylopoda* split from other mammals and before the camel and llama speciation[40]. IgNAR is found in all elasmobranchs, thus emerged at least 220 million years ago, probably from IgW subtype even if it is impossible to exclude their classification as primordial immunoglobulins[41]. These data support a convergent evolution of heavy chain antibodies in different

species[18] that should involve different steps: the first constant domain (CH1) of the heavy chain should be absent or extensively modified, a repertoire of single V domain must be generated and the single V domain should be soluble. The concomitance of these events can be explained by a positive selective pressure that can be clarified by an advantage of the immune system to develop antibodies with a smaller antigen-binding site[42]. A minimal-size V domain has a smaller binding site on the antigen and provides access to cryptic and concave epitopes, like catalytic cleft of enzymes, that are inaccessible to classical antibodies[25].

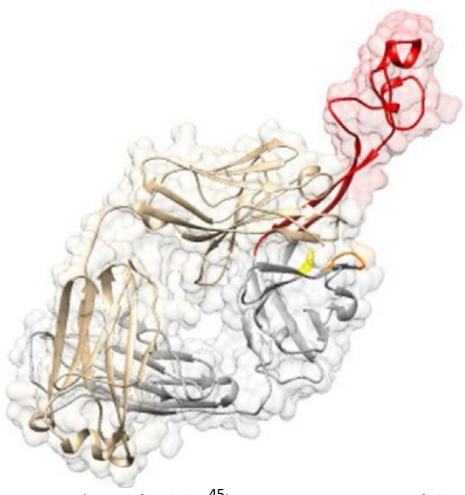

Figure 6 (modified by[45]) Representation of long CDR3 bovine antibodies, CDR3 is indicated in red and presents the "mushroom" shaped domain.

This functional explanation may be the reason why evolution promoted heavy chain antibody maintenance and this theory is supported by the fact that also other animals like cows and human produce immunoglobulins that compensate the flat antigen interaction of VH/VL paratope. In case of HIV type 1 infection in some humans, a broad and potent immune response occurs and recent studies identified the genes encoding for peculiar long CDR3 Abs as the responsibles[43,44]. In bovine unusual long CDR3 Abs naturally appeared: they can make up to 10-15% of the immune repertoire and their CDR3 can reach 60-70 amino acid length with a typical "mushroom" shaped domain (**Figure 6**)[45].

2. The debut of new immune-like biotechnological tools

The use of polyclonal and monoclonal antibodies in therapy and diagnosis is very spread and useful but it presents some limitations. It takes between six months and a year to develop ready-to-use antibodies and often the process involves animal vaccination. Their large size (~150 kDa) renders hard the penetration in small blood vessels like capillaries and they do not enter in cells where reducing intracellular environment, not appropriate for disulphide bonds formation, contributes to their lack of function[46]. Furthermore, in recent years a reproducibility crisis is the center of attention underlining that a lot of published antibodies present cross-reactivity, loss of structural integrity and batch-to-batch variances[47,48].

In order to overcome a part of these issues in the last decades a lot of antibodies derivatives have been developed: antibody Fab and $F(ab)_2$, which derive from IgGs proteolysis and lack of the Fc region, and single-chain Fvs, which consist only of interacting VH and VL domain connected by a flexible polypeptide linker[49] (**Figure 7**). These fragments conserve the VH-VL interface, thus maintain the target affinity of the entire antibody, but their reduced size permits better tissues penetration; nevertheless,

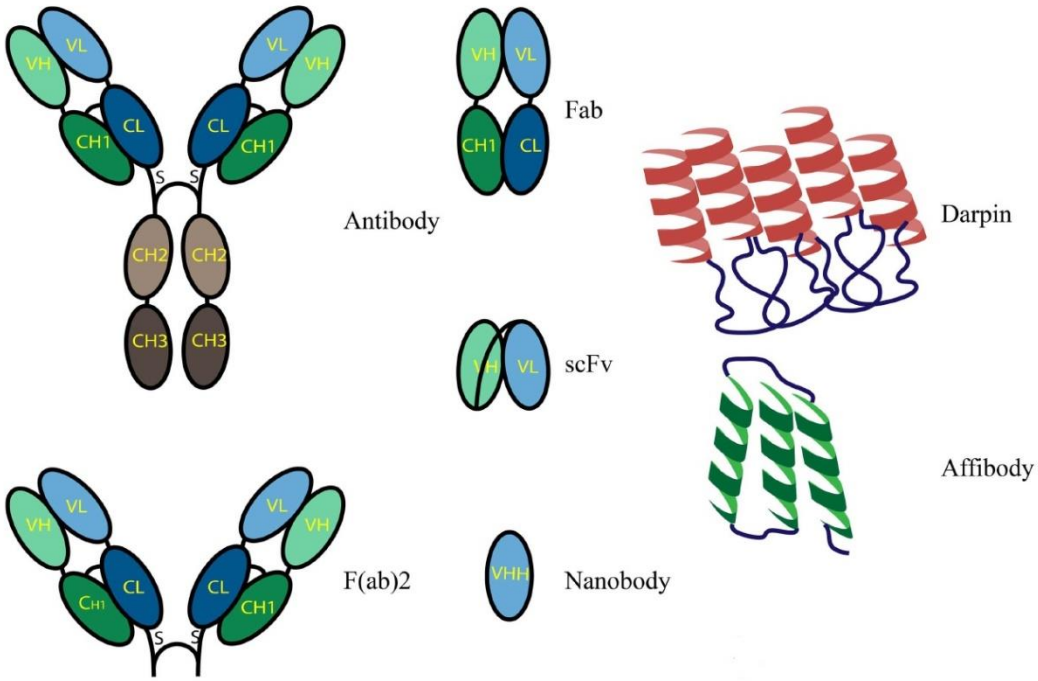

Figure 7 (modified by[49]) Schematic representation of IgG antibody, principal antibody fragments and antibody mimics.

shortcomings like a low level of expression, instability and a flat paratope still are present[50]. Trying to minimize the dimension of the binding domain, studies in which only the human VH domain is solubilized and modified are present, but without the respective VL domain the high risk of reducing target affinity is evident[51,52].
In parallel to antibody fragments, antibody mimics were developed: soluble scaffolds are exploited in order to introduce paratopes in loops mimicking variable domains of immunoglobulins. They can be usually produced in *Escherichia coli*, are cysteine-free, are immune-independent and offer more modularity and reproducibility compared to antibodies and antibody fragments[53].
Good illustrations of antibody-like molecules are Affibodies and Designed Ankyrin Repeat Proteins (DARPins), both currently studied for therapeutic and diagnostic applications (**Figure 7**). Affibody molecules are small (~7 kDa) and derived from alpha-helical Z-domain of Staphylococcal protein A; they are very soluble, stable and their loops can be engineered in order to simulate CDRs of antibodies[54]. Different Affibodies are now available, i.e. the Affibody that binds EGFR is an interesting example[55].
DARPins are synthetic binding proteins that present engineered loops in a stable scaffold composed of ankyrins alpha-helical structural motifs repeated in tandem[56]. They can reach picomolar affinity for their target and are very robust[57]; it is interesting to note that an anti-HER2 DARPin reached a similar sensibility to FDA-approved antibodies for the *in situ* identification of HER2 expression status in breast cancer tissue[58].

2.1. Nanobodies as a new biotechnological tool

During the research of smaller and smarter antibody-like molecules, the accidental discovery of heavy chain antibodies appeared like an interesting opportunity[59]. They bind the target with a single variable domain which if expressed alone is soluble and maintains the same binding affinity of the entire immunoglobulin[60]; it should not surprise that Muylerdmans and colleagues after their finding decided to open a university spin-off called Ablynx, specialized in the development and production of Nbs (name coined by them) as new immune biotechnological tolls[61]. Now the society has a turnover of € 55.5 million per year and has 8 product in clinical development[62].
What distinguishes Nbs from other antibody-like molecules is that they underwent selective pressure to be naturally soluble and they are subject to *in vivo* affinity maturation; thus despite the presence of only three CDRs their antigen specificity and affinity are of a good quality, routinely in a low nanomolar or picomolar equilibrium dissociation constant range. Their small size (~ 15 kDa) allows them to penetrate in the tissue where vascularisation is small or irregular (i.e. tumor tissues)[63] and to pass blood-brain barrier[64].

Nbs are encoded by only one small gene that can be easily manipulated and cloned in every expression vector of interest, furthermore *in vitro* affinity maturation (i.e. error-prone PCR, DNA shuffling) can be quickly performed[65]. For protein expression commonly a simple bacterial expression system is chosen (like *Escherichia coli*), in which a secretion signal exports the antibody fragment in periplasm where the oxidizing environment permits disulphide bonds proper fromation[66]. Usually, a single flask of bacterial culture allows obtaining several milligrams of protein. In addition, Nbs can be expressed in different microorganisms like yeast[67,68], mammalian cell lines[69], plants[70] or, if necessary, they can be easily recovered from inclusion bodies[71].

The VHH domain is very stable, can be conserved also high-concentrated and can be stored for a long time without losing its binding capacity. It resists under stringent conditions and thermal denaturation, showing in some cases the ability to renaturate: a VHH usually denatures in 2-3 M guanidinium solutions and at 60-80°C[72], though some VHHs can resist up to 90°C[73]. Different studies tried to explain the role of disulphide bonds in Nbs thermoresistance and refolding: disparate modifications were introduced (point mutation, disulphide bridge addiction) in order to enhance their intrinsic stability[74] but discordant results were obtained[75,76]; thus Nbs stability is probably a multifactorial phenomenon.

Nbs are low immunogenic due to their small size and rapid renal clearance from the blood[77], furthermore, they share a high sequence identity with human VH III family[78], indeed no immune response was observed when VHH where injected in mice or humans[79,80].

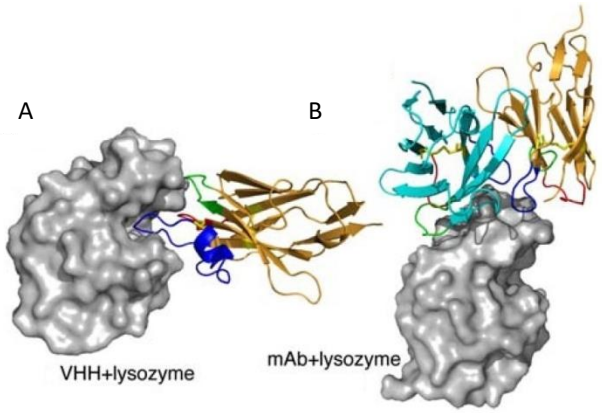

Figure 8 (modified by[84]) Pymol images: A) A VHH interacting with egg chicken lysozyme active site; B) A VH/VL fragment interacting with egg chicken lysozyme.

The unique convex paratope conformation of VHHs renders them particularly suitable to bind cryptic epitopes or to stabilize proteins in peculiar conformations[81,82] (**Figure 8**). For these reasons different Nbs were used during crystallisation experiments[83] or to inhibit/activate enzymatic activity[84,85].

Despite these undeniable advantages, Nbs have also shortcomings of which the mains are a complete lack of effector function (except for a possible steric encumbrance[86]) and a too quick clearance from the blood for therapeutic applications. Different solutions are reported in the literature to overcome these disadvantages: polyethylene glycol (PEG)-

ylation, coupling to abundant serum proteins, such albumin, for enhancing their retention in the body[87,88] or conjugation to Fc regions or enzymes to enhance their effector activity[89,90].

2.1.1. Production of nanobodies

The first and still most widespread way to obtain Nbs with a low nanomolar affinity against a target is to immunize a member of a *Camelidae* family with the antigen of interest, exploiting the natural immune response of the animal for *in vivo* affinity maturation. After 6-8 weeks immunization scheme with a purified protein or DNA[91,92] (i.e. when a purified antigen is difficult to obtain), 50 ml of anti-coagulated camelids blood are collected and mRNA is extracted. After reverse transcription, cDNA that codifies for Nbs can be cloned in any vector of interest and a size of 10^6 individual transformants for immune libraries is usually enough to obtain high-affinity binders[93]. Since llamas and camels are bulky and difficult to maintain, transgenic mice that express heavy-chain-only antibodies are available[94].

When antigens are pathogenic, toxic or in the case of small non-immunogenic molecules, immunization is not always feasible. In these cases, non-immune naïve libraries can be built using usually more than 1 liter of blood samples from different not immunized individuals[95]. A large size of the library is necessary (up to 10^9 different Nbs) in order to compensate the lack of antibodies somatic maturation and additional *in vitro* maturation techniques, such as DNA shuffling or error-prone PCR, are often requested[96–98].

In order to avoid animal care duties also *in vitro* production of antibodies, incubating peripheral blood mononuclear cells in presence of the antigen, were performed but often low affinity (μM) binders were obtained[99].

Also semisynthetic/synthetic libraries can be built bypassing the need of camelids blood; in these cases, a stable VHH (i.e. natural or synthetic) is chosen as a scaffold and its CDRs are randomized in order to mimic the *in vivo* diversification of natural Nbs. Thus semisynthetic/synthetic libraries have higher CDR3 diversity than the naturally occurring naïve VHH domains and are easily manipulable in their sequence, but also for these libraries a large diversity of different clones is needed to compensate the lack of antibodies somatic maturation[100,101].

The most interesting example of synthetic Nb library is the one described by Moutel and colleagues in 2016. Basing on a robust scaffold, they introduced synthetic diversity in CDRs controlling each position of CDR1 and CDR2 determined by statistical analysis of the diversity found in more than 200 natural VHHs; instead every position of CDR3, that could be of four variable lengths (9, 12, 15 and 18 amino acids), was randomized. A high-complexity library was obtained (10^9 different individual Nbs) and after phage display

analysis high-affinity binders (i.e. with dissociation constants from 10 nM to 50 pM) were found[102].

A plethora of techniques are available for the analysis of Nb libraries but the most robust and diffuse method is the phage display. First described in 1985[103], it exploits the fusion of peptides or proteins to coat proteins on phages surface. The library is cloned in a phagemid vector in frame with phage proteins (gIIIp or gVIIIp in case of the most common M13K07 phage) and transformed in appropriate *E. coli* strains. To generate phages that display Nbs on their surface, an infection with helper phage on *E. coli* is performed and displaying phages are used for biopanning. Usually the antigen of interest is adsorbed on microtiter plates wells and phages are added, only the ones that display binding Nbs on their surface will resist to successive washing step and will be recovered for analysis or further pannings (**Figure 9)**[15]; usually 2-3 rounds of panning are enough to obtain high-affinity binders for the most of biomedical applications. In the end single displaying phages (and then Nbs) are often analysed with an enzyme-linked immunosorbent assay (ELISA) and Nbs of interest subcloned in expression vectors for further analysis[104].

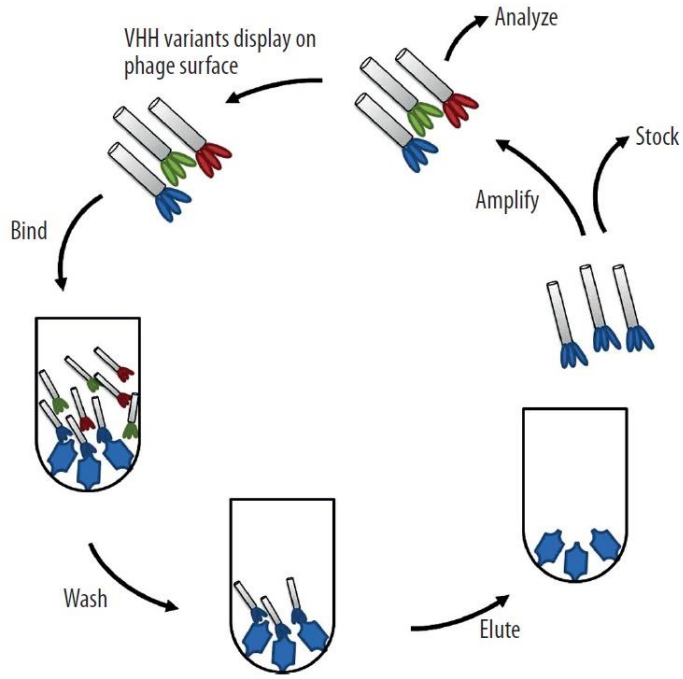

Figure 9[15] Schematic representation of biopanning with M13 phage.

The first Nb obtained by phage display was published by Arbabi Ghahroudi and colleagues in 1997[105] and since then myriads of new Nbs were identified with this technique[106,107].

Many alternatives to phage display method were developed in the last decades. Cell surface display permits the localisation of antibodies on the surface of yeast or bacteria, which are sufficiently large to be detected in flow cytometry. This approach enables fluorescence-based analysis (i.e. fluorescence-activated cell sorting (FACS)) and permits to directly quantify the target affinity of each displayed antibodies avoiding subcloning of the candidates. Furthermore, yeast has a secretory pathway similar to that of higher eukaryotes ensuring the secretion of only properly folded proteins[67,108–110].

The most interesting example of a Nb yeast display library is the one described by McMahon and colleagues. They produced a synthetic Nb scaffold based on a consensus sequence derived from the alignment of the VHHs present in Protein Data Bank and randomized four high variable position in CDR1 and CDR2 (in order to maintain a homogenous solubility and stability) and seven, eleven or fifteen positions in CDR3. The possible amino acids introduced in randomization were chosen analysing the frequency of each amino acid in every position of the previously mentioned alignment and they refined and speeded up the yeast display technique raising high-affinity binders against G protein-coupled β_2 adrenergic receptor[111,112].

Cloning a gene library in a vector of interest implicates the library complexity decrease due to molecular cloning and transformation procedures limitations. Thus different techniques to screen antibody libraries avoiding cloning procedures, like ribosome display (RD) and CIS display, were established.

In RD the coupling of genotype and phenotype (necessary in every screening procedure) is accomplished during *in vitro* translation by stabilizing the complex consisting of the ribosome, mRNA and the nascent Nb polypeptide. The DNA library is fused to a spacer sequence lacking the stop codon, which after *in vitro* translation occupies the ribosomal tunnel and thus allows the protein of interest to protrude out of the ribosome and fold. Indeed the ribosomal complexes that expose different Nbs are allowed to bind to the surface-immobilized target and to perform biopannings. In the end mRNAs of the complexes displaying a binding polypeptide can be recovered and sequences are available for further analysis[113].

CIS display (CD) exploits the ability of the DNA replication initiator protein RepA to bind exclusively to the template DNA from which it has been expressed. A peptide library can be fused to a DNA fragment that encodes RepA and after *in vitro* transcription and translation, a pool of protein–DNA complexes is formed where each protein is stably associated with the DNA that encodes for it. These complexes are able to be used for library screening[114]. Both techniques (RD and CD) were successfully used for Nb library screening providing new Nbs for biotechnological applications[115,116].

Ingenious methods can also be found in literature in order to speed up the final steps of a library screening: directly subcloning all the VHHs obtained from the third panning in a biotin acceptor peptide providing vector permits to obtain a pool of biotinylated Nbs suitable for flow cytometry and mass spectrometry final analysis. This technique is applicable to changeling and complex antigens located on whole cells, indeed antibodies against MHC II and mouse CD45 receptors were isolated[117].

One least to mention approach was developed in order to identify Nbs that work in reducing conditions (like intracellular environment) miming the yeast-two-hybrid system.

The antigen of interest is fused to the α-subunit of RNA polymerase and the VHH library is fused to λcI (that binds the phage λ operator). Both constructs are transformed in *E. coli* strains that present a reporter gene (i.e. aadA that confers streptomycin resistance) under the control of λ operator; thus clones, in which Nbs and antigen interact, can be easily identified because reporter gene transcription is permitted. This approach led to the isolation of VHH against HIV-1 integrase and GFP[118].

2.1.2. Applications of nanobodies

Despite some sharks VNAR tools were developed[39], the burst of Nbs application in the last years is much more appreciable, probably because of the much easier ways they can be obtained. Nbs are now commonly used in research, diagnosis and soon in therapy; here some examples will be reported.

2.1.2.1. *Nanobodies as research tools*

The first interesting to mention Nbs application is their tremendous and unexpected success as crystallisation chaperones[119]. Some hundreds crystal structure of Nbs are currently in Protein Data Bank and the majority of them are performed to solve the antigen structure[93,121–135]. Their success is probably due to their stability and their capacity to fix conformational variants of the target[135–138]. An example of crystallisation chaperones Nbs are the one against G-coupled receptors; since Rasmussen and colleagues identified the first VHH that fixed a receptor conformation, a lot of different crystal structure of β2 adrenergic and other G-coupled receptors (notably difficult to crystallise) are available[137,139–142].

Nbs can also be adsorbed on solid matrixes in order to extract their antigen from heterogeneous solutions or to analyse its post-transcriptional modification when VHHs can discriminate between their modified or not modified target[143–146]. The small size of Nbs permits a high-density coverage of the matrix and the absence of Fc region decreases unspecific binding on it; for these applications, a relative high dissociation constant for VHHs is requested in order to permit the antigen elution in mild conditions[147]. Also Nbs expressed in direct fusion with magnetic particles produced in *Magnetospirillum gryphiswaldense* are reported[148]; thanks to these features Nbs can be used for chromatin immune-precipitation[149].

Because of their stability in reducing environment Nbs can be used intracellularly as intrabodies[150,151]. They can interfere with the target activity or trace its movements in the cell; if conjugated to fluorescent proteins they are also known as chromobodies. Their capacity to trace the antigen was widely demonstrated conjugating different VHHs to the red fluorescent protein (RFP) and visualizing their antigen-coupled translocations by

confocal microscopy[152]. In order to reduce background signal a scaffold for the production of unstable VHHs is available, so the antibody is visible only if bound to its target, otherwise it is degraded by cell proteasome machinery[153].

Other nice and smart examples of the use of intrabodies are represented by the work of Bothma and colleagues and Tang and colleagues. Bothma and his team fused an anti-enhanced GFP (eGFP) Nb to transcription factors (TFs) involved in fruit fly development and induced constitutive expression of eGFP in the *Drosophila melanogaste*r embryo. When TFs are naturally expressed during maturation, the Nbs bind immediately eGFP enhancing its fluorescence and co-importing it in the nucleus; so following the fluorescence variation in single nuclei with confocal microscopy a real-time pattern of the TFs expression is visible[154].

Tang and colleagues exploited GFP endogenous expression for other purposes. Different constitutive GFP-expressing cell/mouse/zebrafish lines are commercially available and they demonstrated that GFP can be used as a scaffold suitable for gene manipulation. Different non-overlapping GFP Nb binders were selected and fused to DNA binding domain (DBD) or activation domain (AD) of various TFs and the correspondent expressing constructs were co-electroporated in GFP expressing cells (also in mouse retina or zebrafish embryo) with an additional vector bearing a reporter gene under the control of the selected TF. They demonstrated that the expression of the reporter gene was detected only in GFP expressing cell and in the case of effector reporter genes a GFP dependent effect was observed[155] (**Figure 10**).

Anti-GFP Nbs were used for a plethora of other creative applications like the degradation of endogenous proteins. The fusion of the Nb to the F-box of the ubiquitination machinery leads to GFP-tagged proteins enrolment in proteasomal degradation[156]. The system turned out to be functional *in vivo* in fruit flies, zebrafish, plants and human cell lines[157,158] and is applicable to other Nbs or degradation machinery domains[159,160].

It is also possible to use GFP binding VHHs to analyse protein-protein interactions (PPI). A versatile fluorescent-three-hybrid strategy was developed: fusing the Nb to a specific-located protein it is possible to observe the recruitment of GFP-tagged proteins at that level. Only if GFP-tagged protein of interest interacts with a second protein bound to RFP a co-localisation near the Nb can be observed[161]. To analyse PPI anti-GFP Nb can be also used as a delivery system for one element involved in the energy transfer in resonance energy transfer assays (i.e. Fluorescence Resonance Energy Transfer)[162].

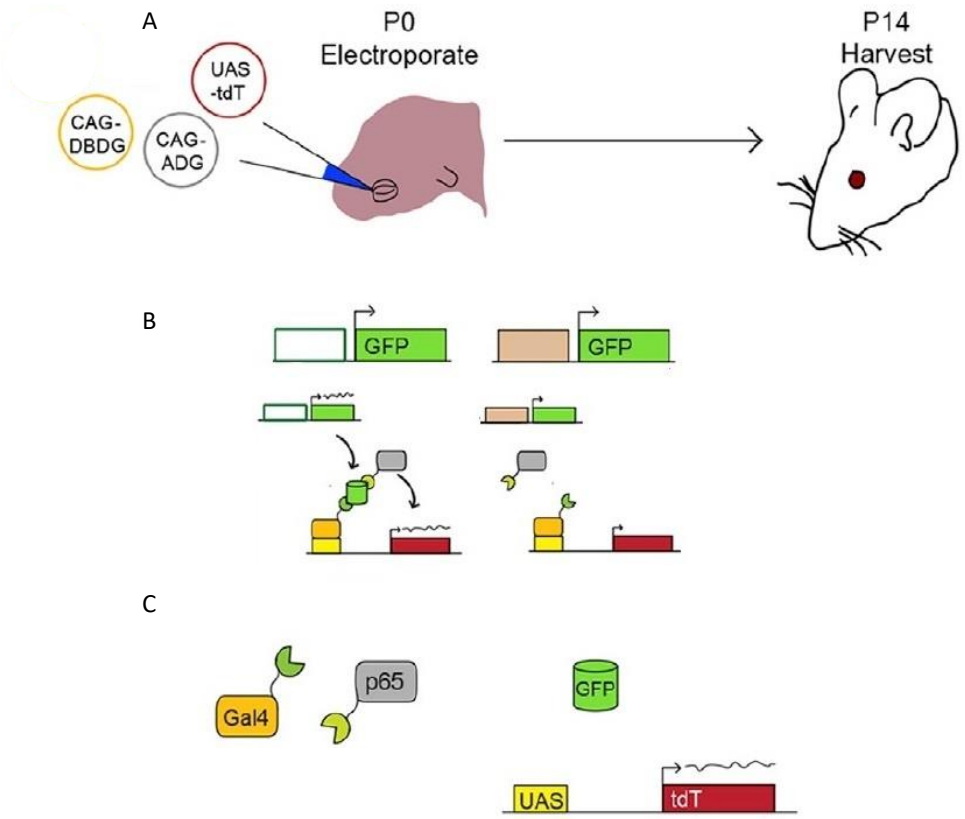

Figure 10 (modified by[155]) Schematic representation of the performed experiment: A) Three plasmids were electroporated in mouse retina, one bears the reporter gene, one the AD fused to an anti-GFP Nb and one the DBD fused to a second anti-GFP Nb; B) Only in presence of GFP the TF is complete and can activate the transcription of the reporter gene; C) Explanation of the single elements in the representation.

If attached to a transmembrane portion and exposed on the surface of the cell, anti-GFP VHH can trap secreted GFP-tagged proteins preventing their spreading into tissue in order to investigate the effect of secreted proteins[163]. Alternatively, GFP can be fused to synapsis membrane protein and the GFP binder can be loaded with quantum dots (a semiconductor material) in order to analyse cell communication[164].

Anti-GFP Nbs were further involved in optogenetic studies where the antibody was included in a light-activated reversible inhibition by the assembled trap (LARIAT). In presence of light, the complex assembles enclosing the GFP-tagged protein which is trapped and its function inhibited[165].

Nbs can be used to modify cellular localisation of the target protein: if fused to signal peptides they co-transport their target in the selected localisation[166], or if bound to

membrane and fuse to mCherry proteins retrograde transport to Golgi can be visualized[167].

When VHHs are exposed to the surface of the cell and their target is expressed on the surface of another cell, Nbs can also be used to induce cell-cell adhesion: Glass and colleagues demonstrated that a general and tunable cell-cell adhesion toolbox can be generated[168].

Taken together all these features strongly demonstrated the high stability and versatility of Nbs, which are going to be involved in more and more biotechnological applications.

2.1.2.2. *Nanobodies in diagnosis*

Nbs are perfect devices for diagnosis: they display high affinity and specificity like conventional antibodies but present lower unspecific binding and are easy to tailor[169].

Different Nb variants were developed for their use in diagnostic tests: if combined with different tags (i.e. c-myc tag, Fc region) or enzymes (i.e. horseradish peroxidase (HRP) or luciferase) they can be directly used for the their antigen detection in *in vitro* assays (i.e. ELISA, Western Blot or flow cytometry) or through microscopy[170–173]. More broadly applicable Nbs are the ones directed against tags suitable for immune-capturing or *in situ* detection of the antigen as primary or secondary antibodies[174,175].

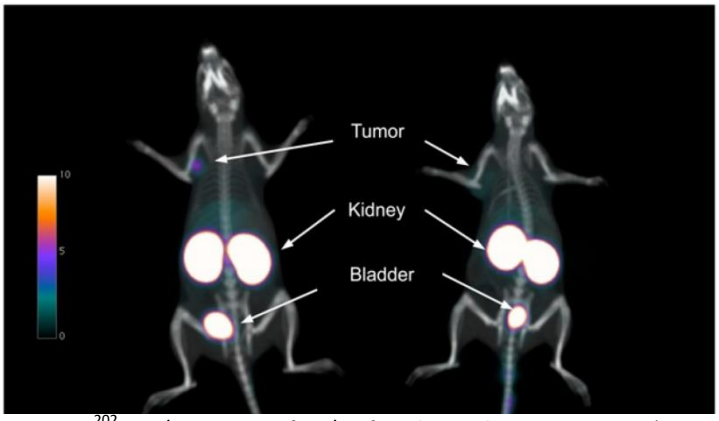

Figure 11[202] PET/CT images of nu/nu female rats bearing SK-OV-3 (HER2-positive) (left) or MDA-MB-435D (HER2-negative) (right) tumor xenografts at 1 h after injection of 68Ga-NOTA-2Rs15d.

Disparate biosensors with amperometric[178] or chemiluminescence[179] detection strategies that includes VHH have been produced[176,177]; one interesting example is the development of an electrochemiluminescent immunosensor with Nbs that bind human procalcitonin, a biomarker of sepsis[180,181]. Dipstick devices[182] and agglutination[183] tests with an immediate read-out for non-specialists in remote places are available.

Because of their small binding sites, VHHs are also able to bind small protein-like toxins and can be used for the detection of mycotoxin in food[184].

Nevertheless, the most surprising results for the application of Nbs in diagnostic were obtained for *in vivo* imaging. When injected intravenously the labelled Nbs extravasate

rapidly in tissues and localize specifically in the target tissue. Unspecific signal is visible in kidneys and bladder because the size of VHHs is below the renal cut-off, but at the same time, the rapid clearance of Nbs permits a perfect noise/signal ratio after short post-injection time compared to conventional antibodies. Furthermore, the short half-life *in vivo* reduces the side effects of labelled antibodies[185–190] and examples in which VHHs crossed blood-brain barrier (BBB) are reported, opening unexpected possibilities for brain imaging[191–193]. The most interesting field in which this application has been explored is the identification of cancer biomarkers (i.e. CEA, EGFR, HER2) for PET/SPECT imaging[194–198] or for image-guided surgey[199,200]. The most successful Nb probe is a VHH anti-HER2 conjugated to ^{68}Ga for PET imaging, which after preclinical experiments (**Figure 11**) in 2016 came to clinical phase I trial[201–203].

2.1.2.3. *Nanobodies as therapeutics*

Like immunoglobulins, Nbs have wide potentials for therapeutic applications. Despite their lack of effector function, they can be potent drugs, as demonstrated by the success that Caplacizumab (developed by Ablynx) had in the treatment of thrombotic thrombocytopenic purpura (TTP): the Nb completed Phase III studies and is expected to be launched on the market in 2018[80,204].

A shortcoming that inhibits the use of Nbs as therapeutics is a feature that renders them perfect diagnostic tools: their short half-life *in vivo*. A rapid renal clearance leads to a short permanence of the drug in the bloodstream and frequent administration steps are needed. Different strategies have been developed in order to enhance the permanence of Nbs in the blood: PEG-ylation inhibits renal clearance; conjugation to Fc domain of conventional antibodies or to nanoparticles increase the dimension of Nbs and enhance the interactions performed in the bloodstream; coupling the Nb to human abundant serum proteins (i.e. albumin) or to an another VHH that binds them, also boosts blood permanence increasing interactions with blood elements[205]. Namely, conjugation to an anti-albumin VHH leads to the accumulation of the complex in inflamed areas where albumin is abundant[206]. With these implementations, Nbs are currently studied as therapeutic molecules.

One of the branches in which antibody-based treatments are successful is cancer therapy, so also new Nb-based drugs are in active research[207,208]. Lacking of effector functions, Nbs can have a direct antagonist effect, suppressing for example signal transduction: their target should be preferentially extracellular, overexpressed in tumor cells (i.e. HER2, EGFR, HGF) and the Nb binding should interfere with receptor-ligand interaction. Different Nbs showed a successful inhibition of solid tumor growth *in vitro* and *in vivo*[209–212] and others show enhance anti-tumor activity when fused to cell-internalizing

peptides[213]. VHHs can also inhibit metastasis acting against cytoskeleton protiens[214] or proteins involved in angiogenesis[215–217].

Nbs can also act as agonist in cancer treatment as reported by Rozan and colleagues. In this case, a Nb against carcinoembryonic antigen (CEA) was fused to an anti-Fc-γ-RIIIa Nb. Fc-γ-RIIIa is a receptor exposed on natural killer cells (NK), mononuclear phagocytes and neutrophils and upon Nb binding to it, an agonistic reaction occurred boosting interferon-γ response[218,219].

To enhance effector activity of Nbs they can be conjugated to anti-tumor moieties like *Pseudomonas* exotoxin A[220,221], cytotoxic TRAIL protein[222], urase[223] or β-lactamase (which activates the cephalosporin nitrogen mustard prodrug[90]).

Nbs can also be used to engineer immune T cells with chimeric anti-tumor receptors: after patients administration, modified T cells accumulate on cancer cells. Furthermore, surface Nbs, linked to intracellular signal transduction domain through a hinge region, co-stimulate endodomains and immune response[224–226].

Likewise VHHs can be used to functionalize drug delivery systems in order to reduce the side effects of the drug and to enhance the circulating time of the antibody[227,228] (**Figure 12**). Examples of decorated liposomes are present in literature as well as cross-linked albumin nanoparticles[229] or PEG-liposomes. In the latter case, an interesting study demonstrated that loading a PEG-liposome with anti-EGFR Nbs and IGF-1R kinase inhibitor, induced accumulation of the nanoparticles on tumor cells and inhibited activities of both target receptors[230]. A new interesting class of carrier systems are polymerisomes, which are stabilized liposomes that can carry a large amount of drug[231,232]; also extracellular vesicles

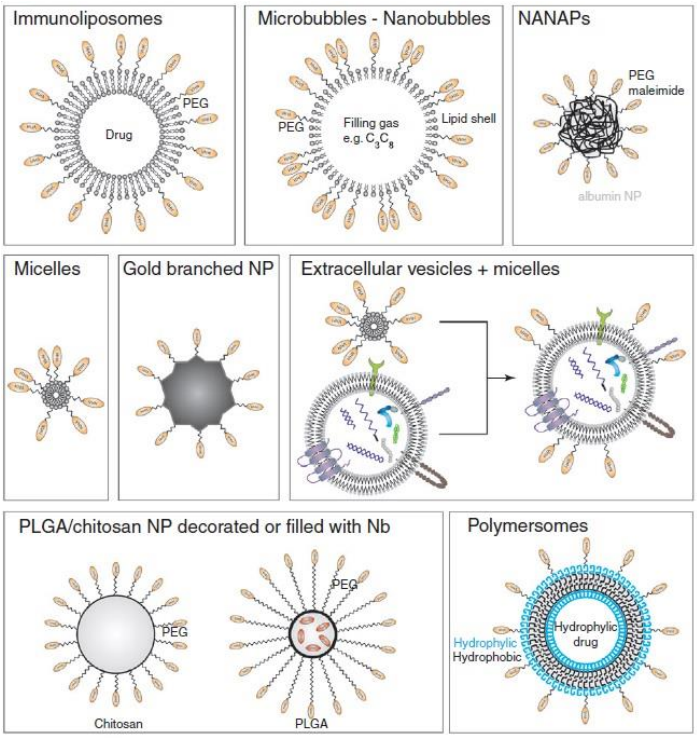

Figure 12 (modified by[205]) Schematic representation of nanoparticles that can be decorated with Nbs.

are rising as new drug delivery system because they are rapidly taken up by cells although with low specificity and they are rapidly cleared from bloodstream[233,234].

Linking radionuclides to Nbs can deliver a high dose of radiations directly to the tumor inducing cancer regression, indeed different radioisotopes were conjugated to VHHs[235–237]. However, the Nb high renal retention can lead to unwanted radiation damage, so D'Huyvetter and colleagues generated an anti-HER2 Nb linked to ^{177}Lu radionuclide and to overcome renal accumulation they co-infused the construct in mice with Gelofusin, a plasma expander. The research team demonstrated that Nbs could still reduce tumor growth and renal retention was significantly reduced[238].

An alternative to radionuclide treatment is photodynamic therapy (PDT) in which cell death is induced by activating a Nb-conjugated photosensitizer by light exposure[63,239,240] or photothermal gold nanoparticles after laser irradiation[241].

Cancer is strongly correlated with inflammation in which tumor necrosis factor (TNF) is the major key player, so it is not surprising that different VHHs against TNF have been developed[242–244]. A recent and interesting analysed construct is a trivalent biparatopic VHH linked to an anti-albumin Nb which competes with TNF on binding TNF receptor 1 (TNFR1); this complex is efficient *in vivo* and is a candidate for the treatment of autoimmune diseases that now are approached with anti-TNF blocker[245]. However, the most successful humanized, trivalent, bispecific Nb anti-TNF is ATN-103 or ozoralizumab developed by Ablynx which terminated with success the Phase IIa trial for the treatment of rheumatoid arthritis[246].

Nbs can also be used to interfere with T cells function: ADP-ribosyltransferase C2 (ARTC2.2) is an ectoenzyme expressed on the surface of T lymphocytes and, when activated by NAD^+ inflammation response, can lead to natural killer (NK) cell death. A VHH against ARTC2.2 restored NK cell population in diabetogenic mice, in which are naturally depleted, decreasing the development of type I diabetes mellitus[247].

Also interleukins (ILs) play an important role in immune response, indeed two anti-ILs Nbs, developed by Ablynx, are currently in clinical studies: ALX-0061 or vobarilizumab, that blocks IL-6 receptor, completed Phase II study for rheumatoid arthritis (RA) and systemic lupus erythematosus (SLE)[248,249] and ALX-0761 against IL-17A and IL-17F completed Phase Ib stage in patient with psoriasis[250].

Nbs can interfere at different levels with virus/bacterial infection, the simplest of which is to prevent pathogen attachment[251]. Intranasally administrated neutralising Nbs against influenza virus (i.e. H5N1 or H5N2) prevent viral attachment[252,253] and an anti-hepatitis C virus VHH inhibits virus cell entrance and virus transmission[254].

A Nb that can act intracellularly can interfere with further infection steps: different intracellularly expressed Nbs demonstrated their preventive activity[255–257] but

"tranbodies" that can penetrate in cells are more suitable for patient administration. The fusion of VHHs to cell-penetrating peptides or the use of penetrating positive scaffold[258,259] are exploited inducing Nbs anti-viral effects[260].

It is interesting to mention two peculiar approaches in the development of anti-viral Nbs: expression of Nbs against rotavirus (RV) on the surface of lactobacilli leads to lactobodies, which, when orally administrated, might be prophylactic against RV-induced diarrhea[261]. When the administration of live vaccines is contraindicated, exploiting a rice-based expression system for the expression of anti-RV VHHs may be useful[262]. In both cases, the high stability of Nbs permits their oral administration because they resist to proteolytical degradation in the upper gastrointestinal tract[263,264].

Also anti-viral Nbs reached clinical trials: an anti-RV Nb showed good results in Phase II/III for the treatment of diarrhea in India and further development are expected[265,266]. ALX-0171 Nb, when inhaled, block the uptake of respiratory syncytial virus (RSV) at the pulmonary level and is currently in Phase IIb trial[267,268].

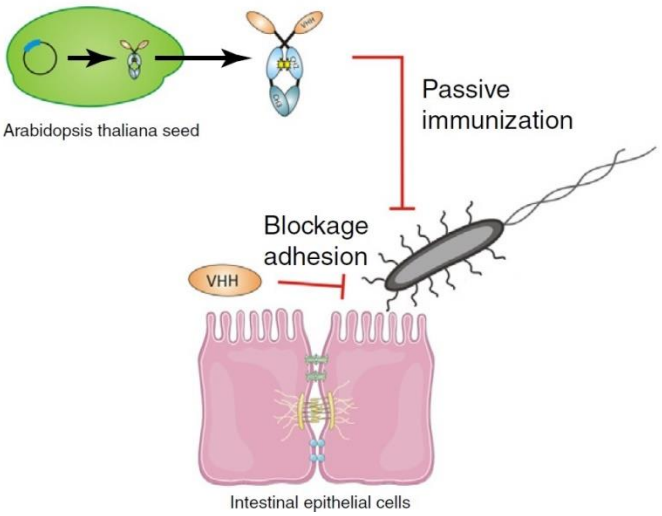

Figure 13 (modified by[205]) Schematic representation of the action of anti-ETEC Nb linked to IgA Fc region.

In order to enhance the prevention of enteric infections, Virdi and colleagues linked an anti-enterotoxigenic *Escherichia coli* (ETEC) Nb to a porcine IgA Fc region and expressed the fusion protein in *Arabidopsis thaliana* seeds. After administration of engineered seeds, the cumulative action of the antibody and of the mucosal immune response stimulated by the Fc region leads to the reduction of infection pressure in piglets[269] (**Figure 13**).

Furthermore, in order to overcome antibiotic resistance, Nbs against bacterial enzymes can be elicited: VHHs against β-lactamase (that confers antibiotic resistance) of *Bacillus cereus*[84] and UreC (a subunit of urease, fundamental for acidic resistance) of *Helicobacter pylori*[270] are reported.

Even if less described, Nbs can be generated also against parasite and fungi. The most interesting study is about the discovery of a potent VHH against Africa trypanosome parasite: the antibody is active *in vivo* and when bound to β-lactamase, which activates a

prodrug, leads to parasite kill[86,271]. Instead, when conjugated to truncated apolipoprotein L-I, that lysis Africa trypanosomes, or exposed on PEG-ylated polylactic-co-glycolic acid nanoparticles the Nb presents full curative activity in mice[79,272].
Highlighting their versatility, Nbs can also be found in medical shampoo. A Nb against a surface protein of *Malassezia furfur* fungi, implicated in the formation of dandruff, inhibits its epidermal adhesion[273].
Last but not least as conventional antibodies, Nbs can be used as detoxifying agents with a good tissue penetration potential; successful antidote were created against scorpions[274,275] and cobra[276] venoms. Also, VHHs against LPS of *Neisseria meningitidis*[277], cholera toxin[278], toxin of *Bacillus anthracis*[279] and botulinum neurotoxins[68,280] have been reported, even if it is not yet clear if they can be used in humans.

In conclusion, Nbs represent a new potent and promising tool that brought a breath of fresh air in research, diagnosis and therapy. Now remains to be seen how camelids will inspire new researches in the future.

3. Bibliography

1. Köhler G. Milstein C. Pillars Article : Continuous cultures of fused cells secreting antibody of predefined specificity. *Nature*. 1975;256(2453-2455).
2. Ecker DM, Jones SD, Levine HL. The therapeutic monoclonal antibody market. *MAbs*. 2015;7(1):9-14. doi:10.4161/19420862.2015.989042.
3. Saleem M. Monoclonal antibodies in clinical diagnosis: A brief review application. *African J Biotechnol*. 2008;7(8):923-925.
4. Strohl WR. Current progress in innovative engineered antibodies. *Protein Cell*. 2018;9(1):86-120. doi:10.1007/s13238-017-0457-8.
5. Waldmann TA. Monoclonal antibodies in diagnosis and therapy. *Sci* . 1991. doi:10.1126/science.2047874.
6. Almagro JC, Daniels-Wells TR, Perez-Tapia SM, Penichet ML. Progress and challenges in the design and clinical development of antibodies for cancer therapy. *Front Immunol*. 2018;8(JAN). doi:10.3389/fimmu.2017.01751.
7. Kremer L, Garcia-Sanz JA. Editorial: Is the recent burst of therapeutic anti-tumor antibodies the tip of an iceberg? *Front Immunol*. 2018;9(MAR):1-3. doi:10.3389/fimmu.2018.00442.
8. Hamers-Casterman C, Atarhouch T, Muyldermans S, et al. Naturally occurring antibodies devoid of light chains. *Nature*. 1993;363(6428):446-448. doi:10.1038/363446a0.
9. Blanc MR, Anouassi A, Abed MA, et al. A one-step exclusion-binding procedure for the purification of functional heavy-chain and mammalian-type γ-globulins from camelid sera. *Biotechnol Appl Biochem*. 2009;54(4):207-212. doi:10.1042/BA20090208.
10. Daley LP, Gagliardo LF, Duffy MS, Smith MC, Appleton JA. Application of Monoclonal Antibodies in Functional and Comparative Investigations of Heavy-Chain Immunoglobulins in New World Camelids. *Clin Vaccine Immunol*. 2005;12(3):380-386. doi:10.1128/CDLI.12.3.380.
11. Lauwereys M, Ghahroudi MA, Desmyter A, Genst E De, Wyns L, Muyldermans S. Potent enzyme inhibitors derived from dromedary heavy-chain antibodies. 1998;17(13):3512-3520.
12. Nguyen VK, Zou X, Lauwereys M, Brys L, Brüggemann M, Muyldermans S. Heavy-chain only antibodies derived from dromedary are secreted and displayed by mouse B cells. *Immunology*. 2003;109(1):93-101. doi:10.1046/j.1365-2567.2003.01633.x.
13. Dudek J, Benedix J, Cappel S, et al. Functions and pathologies of BiP and its interaction partners. *Cell Mol Life Sci*. 2009;66(9):1556-1569. doi:10.1007/s00018-009-8745-y.
14. Matheson LS, Osborn MJ, Smith JA, et al. Light chain-deficient mice produce novel multimeric heavy-chain-only IgA by faulty class switching. *Int Immunol*. 2009;21(8):957-966. doi:10.1093/intimm/dxp062.
15. Smolarek D, Bertrand O, Czerwinski M. Variable fragments of heavy chain antibodies (VHHs): A new magic bullet molecule of medicine? *Postepy Hig Med Dosw*. 2012;66:348-358. doi:10.5604/17322693.1000334.
16. Achour I, Cavelier P, Tichit M, Bouchier C, Lafaye P, Rougeon F. Tetrameric and Homodimeric Camelid IgGs Originate from the Same IgH Locus. *J Immunol*. 2008;181(3):2001-2009. doi:10.4049/jimmunol.181.3.2001.
17. Nguyen V, Hamers R, Wyns L, Muyldermans S. Camel heavy chain antibodies: diverse germline VHH and specific mechanisms enlarge the antigen binding repertoire. *EMBO J*. 2000;19(5):921-930. http://scholar.google.com/scholar?q=Camel heavy chain antibodies: diverse germline V H H and specific mechanisms enlarge the antigen binding repertoire&btnG=&hl=en&num=20&as_sdt=0%2C22.
18. Nguyen V, Su C, Muyldermans S, Van Der Loo W. Heavy-chain antibodies in Camelidae; a case of evolutionary innovation. *Immunogenetics*. 2002;54(1):39-47. doi:10.1007/s00251-002-0433-0.
19. Padlan EA. Anatomy of the antibody molecule. *Mol Immunol*. 1994. doi:10.1016/0161-5890(94)90001-9.
20. Schroeder HW, Cavacini L, Schroeder Jr. HW, Cavacini L, Schroeder HW, Cavacini L. Structure and function of immunoglobulins. *J Allergy Clin Immunol*. 2010;125(2 Suppl 2):S41-52.

doi:10.1016/j.jaci.2009.09.046.
21. Muyldermans S. Nanobodies : Natural Single-Domain Antibodies. 2013. doi:10.1146/annurev-biochem-063011-092449.
22. Mahesh N, Rohan N, Mangesh M. Single Domain Antibodies : A New Approach in Therapeutics. :839-852.
23. Chothia C, Lesk AM, Gherardi E, et al. Structural repertoire of the human VH segments. *J Mol Biol*. 1992. doi:10.1016/0022-2836(92)90224-8.
24. Muyldermans S, Atarhouch T, Saldanha J, Barbosa JARG, Hamers R. Sequence and structure of V_H domain from naturally occurring camel heavy chain immunoglobulins lacking light chains. *"Protein Eng Des Sel*. 1994;7(9):1129-1135. doi:10.1093/protein/7.9.1129.
25. De Genst E, Silence K, Decanniere K, et al. Molecular basis for the preferential cleft recognition by dromedary heavy-chain antibodies. *Proc Natl Acad Sci*. 2006;103(12):4586-4591. doi:10.1073/pnas.0505379103.
26. Sundberg EJ, Mariuzza RA. Molecular recognition in antibody-antigen complexes. *Adv Protein Chem*. 2002. doi:10.1016/S0065-3233(02)61004-6.
27. Mitchell LS, Colwell LJ. Comparative analysis of nanobody sequence and structure data. *Proteins Struct Funct Bioinforma*. 2018;(February). doi:10.1002/prot.25497.
28. Mitchell LS, Colwell LJ. Analysis of nanobody paratopes reveals greater diversity than classical antibodies. *Protein Eng Des Sel*. 2018;(July):1-9. doi:10.1093/protein/gzy017.
29. Noël F, Malpertuy A, de Brevern AG. Global analysis of VHHs framework regions with a structural alphabet. *Biochimie*. 2016;131:11-19. doi:10.1016/j.biochi.2016.09.005.
30. Govaert J, Pellis M, Deschacht N, et al. Dual beneficial effect of interloop disulfide bond for single domain antibody fragments. *J Biol Chem*. 2012;287(3):1970-1979. doi:10.1074/jbc.M111.242818.
31. Harmsen MM, Ruuls RC, Nijman IJ, Niewold TA, Frenken LGJ, De Geus B. Llama heavy-chain V regions consist of at least four distinct subfamilies revealing novel sequence features. *Mol Immunol*. 2000;37(10):579-590. doi:10.1016/S0161-5890(00)00081-X.
32. Sircar A, Sanni KA, Shi J, Gray JJ. Analysis and Modeling of the Variable Region of Camelid Single Domain Antibodies. *J Immunol*. 2011;186(11):6357-6367. doi:10.4049/jimmunol.1100116.Analysis.
33. Schroeder HW, Hillson JL, Perlmutter RM. Structure and evolution of mammalian VH families. *Int Immunol*. 1990;2(1):41-50. doi:10.1093/intimm/2.1.41.
34. Cogné M, Preud'homme JL, Guglielmi P. Immunoglobulin gene alterations in human heavy chain diseases. *Res Immunol*. 1989. doi:10.1016/0923-2494(89)90115-6.
35. Greenberg AS, Avila D, Hughes M, Hughes A, McKinney EC, Flajnik MF. A new antigen receptor gene family that undergoes rearrangement and extensive somatic diversification in sharks. *Nature*. 1995;374(6518):168-173. doi:10.1038/374168a0.
36. Roux KH, Greenberg a S, Greene L, et al. Structural analysis of the nurse shark (new) antigen receptor (NAR): molecular convergence of NAR and unusual mammalian immunoglobulins. *Proc Natl Acad Sci U S A*. 1998;95(20):11804-11809. doi:10.1073/pnas.95.20.11804.
37. Dooley H, Flajnik MF. Shark immunity bites back: Affinity maturation and memory response in the nurse shark, Ginglymostoma cirratum. *Eur J Immunol*. 2005;35(3):936-945. doi:10.1002/eji.200425760.
38. Berstein RM, Schluter SF, Shen S, Marchalonis JJ. A new high molecular weight immunoglobulin class from the carcharhine shark: implications for the properties of the primordial immunoglobulin. *Proc Natl Acad Sci U S A*. 1996;93(8):3289-3293. doi:10.1073/pnas.93.8.3289.
39. Zielonka S, Empting M, Grzeschik J, Könning D, Barelle CJ, Kolmar H. Structural insights and biomedical potential of IgNAR scaffolds from sharks. *MAbs*. 2015;7(1):15-25. doi:10.4161/19420862.2015.989032.
40. Conrath KE, Wernery U, Muyldermans S, Nguyen VK. Emergence and evolution of functional heavy-chain antibodies in Camelidae. *Dev Comp Immunol*. 2003;27(2):87-103. doi:10.1016/S0145-305X(02)00071-X.
41. Flajnik MF, Kasahara M. Origin and evolution of the adaptive immune system: Genetic events and selective pressures. *Nat Rev Genet*. 2010;11(1):47-59. doi:10.1038/nrg2703.

42. Flajnik MF, Deschacht N, Muyldermans S. A case of convergence: Why did a simple alternative to canonical antibodies arise in Sharks and Camels? *PLoS Biol*. 2011;9(8). doi:10.1371/journal.pbio.1001120.
43. Corti D, Lanzavecchia A. Broadly Neutralizing Antiviral Antibodies. *Annual Review of Immunology Vol 31*.; 2013. doi:10.1146/annurev-immunol-032712-095916.
44. Willis JR, Finn JA, Briney B, et al. Long antibody HCDR3s from HIV-naïve donors presented on a PG9 neutralizing antibody background mediate HIV neutralization. *Proc Natl Acad Sci U S A*. 2016;113(16):1518405113-. doi:10.1073/pnas.1518405113.
45. Muyldermans S, Smider V V. Distinct antibody species: Structural differences creating therapeutic opportunities. *Curr Opin Immunol*. 2016;40:7-13. doi:10.1016/j.coi.2016.02.003.
46. Bansal D. Using mimics to get around antibodies limitations. 2018:*The Scientist Magazine*.
47. Bradbury A, Plückthun A. Reproducibility: Standardize antibodies used in research. *Nature*. 2015;518(7537):27-29. doi:10.1038/518027a.
48. Baker M. Blame it on the antibodies. *Nature*. 2015;521(7552):274-276. doi:10.1038/521274a.
49. Gremel G, Grannas K, Sutton LA, Pontén F, Zieba A. In situ Protein Detection for Companion Diagnostics. *Front Oncol*. 2013;3(October):0-8. doi:10.3389/fonc.2013.00271.
50. Holliger P, Hudson PJ. Engineered antibody fragments and the rise of single domains. *Nat Biotechnol*. 2005;23(9):1126-1136. doi:10.1038/nbt1142.
51. Rouet R, Dudgeon K, Christie M, Langley D, Christ D. Fully human VH single domains that rival the stability and cleft recognition of camelid antibodies. *J Biol Chem*. 2015;290(19):11905-11917. doi:10.1074/jbc.M114.614842.
52. Drabek D, Janssens R, Boer E de, et al. Expression cloning and production of human heavy-chain-only antibodies from murine transgenic plasma cells. *Front Immunol*. 2016;7(DEC):3-12. doi:10.3389/fimmu.2016.00619.
53. Löfblom J, Frejd FY, Ståhl S. Non-immunoglobulin based protein scaffolds. *Curr Opin Biotechnol*. 2011;22(6):843-848. doi:10.1016/j.copbio.2011.06.002.
54. Löfblom J, Feldwisch J, Tolmachev V, Carlsson J, Ståhl S, Frejd FY. Affibody molecules: Engineered proteins for therapeutic, diagnostic and biotechnological applications. *FEBS Lett*. 2010;584(12):2670-2680. doi:10.1016/j.febslet.2010.04.014.
55. Friedman M, Nordberg E, Höidén-Guthenberg I, et al. Phage display selection of Affibody molecules with specific binding to the extracellular domain of the epidermal growth factor receptor. *Protein Eng Des Sel*. 2007;20(4):189-199. doi:10.1093/protein/gzm011.
56. Kohl A, Binz HK, Forrer P, Stumpp MT, Pluckthun A, Grutter MG. Designed to be stable: Crystal structure of a consensus ankyrin repeat protein. *Proc Natl Acad Sci*. 2003;100(4):1700-1705. doi:10.1073/pnas.0337680100.
57. Binz HK, Amstutz P, Kohl A, et al. High-affinity binders selected from designed ankyrin repeat protein libraries. *Nat Biotechnol*. 2004;22(5):575-582. doi:10.1038/nbt962.
58. Theurillat J-P, Dreier B, Nagy-Davidescu G, et al. Designed ankyrin repeat proteins: a novel tool for testing epidermal growth factor receptor 2 expression in breast cancer. *Mod Pathol*. 2010;23(9):1289-1297. doi:10.1038/modpathol.2010.103.
59. Smidt GL. Small but mighty. *J Orthop Sport Phys Ther*. 1992;15(6):1. http://www.ncbi.nlm.nih.gov/entrez/query.fcgi?cmd=Retrieve&db=PubMed&dopt=Citation&list_uids=18781006.
60. Nguyen VK, Desmyter A, Muyldermans S. Functional heavy-chain antibodies in Camelidae. *Adv Immunol*. 2001. doi:10.1016/S0065-2776(01)79006-2.
61. Wolfson W. Ablynx Makes Nanobodies from Llama Bodies. *Chem Biol*. 2006;13(12):1243-1244. doi:10.1016/j.chembiol.2006.12.003.
62. Woolworths Limited. 2017 Ablynx Annual Report. 2017:1-57. https://www.woolworthsgroup.com.au/icms_docs/188795_annual-report-2017.pdf.
63. van Lith SAM, van den Brand D, Wallbrecher R, et al. The effect of subcellular localization on the efficiency of EGFR-targeted VHH photosensitizer conjugates. *Eur J Pharm Biopharm*. 2018;124(September 2017):63-72. doi:10.1016/j.ejpb.2017.12.009.

64. Abulrob A, Sprong H, Van Bergen En Henegouwen P, Stanimirovic D. The blood-brain barrier transmigrating single domain antibody: Mechanisms of transport and antigenic epitopes in human brain endothelial cells. *J Neurochem*. 2005;95(4):1201-1214. doi:10.1111/j.1471-4159.2005.03463.x.
65. Yau KYF, Dubuc G, Li S, et al. Affinity maturation of a VHH by mutational hotspot randomization. *J Immunol Methods*. 2005;297(1-2):213-224. doi:10.1016/j.jim.2004.12.005.
66. Billen B, Vincke C, Hansen R, et al. Cytoplasmic versus periplasmic expression of site-specifically and bioorthogonally functionalized nanobodies using expressed protein ligation. *Protein Expr Purif*. 2017;133:25-34. doi:10.1016/j.pep.2017.02.009.
67. Frenken LGJ, Van Der Linden RHJ, Hermans PWJJ, et al. Isolation of antigen specific Llama V(HH) antibody fragments and their high level secretion by Saccharomyces cerevisiae. *J Biotechnol*. 2000;78(1):11-21. doi:10.1016/S0168-1656(99)00228-X.
68. Baghban R, Gargari SLM, Rajabibazl M, Nazarian S, Bakherad H. Camelid-derived heavy-chain nanobody against Clostridium botulinum neurotoxin E in Pichia pastoris. *Biotechnol Appl Biochem*. 2016;63(2):200-205. doi:10.1002/bab.1226.
69. Alirahimi E, Ashkiyan A, Kazemi-Lomedasht F, et al. Intrabody targeting vascular endothelial growth factor receptor-2 mediates downregulation of surface localization. *Cancer Gene Ther*. 2017;24(1):33-37. doi:10.1038/cgt.2016.76.
70. Ismaili A, Jalali-Javaran M, Rasaee MJ, Rahbarizadeh F, Forouzandeh-Moghadam M, Memari HR. Production and characterization of anti-(mucin MUC1) single-domain antibody in tobacco (Nicotiana tabacum cultivar Xanthi). *Biotechnol Appl Biochem*. 2007;47(Pt 1):11-19. doi:10.1042/BA20060071.
71. Maggi M, Scotti C. Enhanced expression and purification of camelid single domain VHH antibodies from classical inclusion bodies. *Protein Expr Purif*. 2017;136:39-44. doi:10.1016/j.pep.2017.02.007.
72. Dumoulin M, Conrath K, Van Meirhaeghe A, et al. Single-domain antibody fragments with high conformational stability. *Protein Sci*. 2009;11(3):500-515. doi:10.1110/ps.34602.
73. van Der Linden RH, Frenken LG, de Geus B, et al. Comparison of physical chemical properties of llama VHH antibody fragments and mouse monoclonal antibodies. *Biochim Biophys Acta*. 1999;1431(1):37-46. doi:10.1016/S0167-4838(99)00030-8.
74. Goldman ER, Liu JL, Zabetakis D, Anderson GP. Enhancing stability of camelid and shark single domain antibodies: An overview. *Front Immunol*. 2017;8(JUL):1-11. doi:10.3389/fimmu.2017.00865.
75. Akazawa-Ogawa Y, Uegaki K, Hagihara Y. The role of intra-domain disulfide bonds in heat-induced irreversible denaturation of camelid single domain VHH antibodies. *J Biochem*. 2016;159(1):111-121. doi:10.1093/jb/mvv082.
76. Kunz P, Zinner K, Mücke N, Bartoschik T, Muyldermans S, Hoheisel JD. The structural basis of nanobody unfolding reversibility and thermoresistance. *Sci Rep*. 2018;8(1):1-10. doi:10.1038/s41598-018-26338-z.
77. Vaneycken I, D'huyvetter M, Hernot S, et al. Immuno-imaging using nanobodies. *Curr Opin Biotechnol*. 2011;22(6):877-881. doi:10.1016/j.copbio.2011.06.009.
78. Vu KB, Ghahroudi MA, Wyns L, Muyldermans S. Comparison of llama V(H) sequences from conventional and heavy chain antibodies. *Mol Immunol*. 1997. doi:10.1016/S0161-5890(97)00146-6.
79. Baral TN, Magez S, Stijlemans B, et al. Experimental therapy of African trypanosomiasis with a nanobody-conjugated human trypanolytic factor. *Nat Med*. 2006;12(5):580-584. doi:10.1038/nm1395.
80. Peyvandi F, Scully M, Kremer Hovinga JA, et al. Caplacizumab for Acquired Thrombotic Thrombocytopenic Purpura. *N Engl J Med*. 2016;374(6):511-522. doi:10.1056/NEJMoa1505533.
81. Desmyter A, Transue TR, Ghahroudi MA, et al. Crystal structure of a camel single-domain V(H) antibody fragment in complex with lysozyme. *Nat Struct Biol*. 1996;3(9):803-811. doi:10.1038/nsb0996-803.
82. Wesolowski J, Alzogaray V, Reyelt J, et al. Single domain antibodies: Promising experimental and therapeutic tools in infection and immunity. *Med Microbiol Immunol*. 2009;198(3):157-174. doi:10.1007/s00430-009-0116-7.
83. Cromie K, Heeke G, Boutton C. Nanobodies and their Use in GPCR Drug Discovery. *Curr Top Med Chem*. 2015. doi:10.2174/1568026615666150701113549.

84. Conrath KE, Lauwereys M, Galleni M, et al. β-Lactamase inhibitors derived from single-domain antibody fragments elicited in the Camelidae. *Antimicrob Agents Chemother*. 2001;45(10):2807-2812. doi:10.1128/AAC.45.10.2807-2812.2001.
85. Saerens D, Kinne J, Bosmans E, Wernery U, Muyldermans S, Conrath K. Single domain antibodies derived from dromedary lymph node and peripheral blood lymphocytes sensing conformational variants of prostate-specific antigen. *J Biol Chem*. 2004;279(50):51965-51972. doi:10.1074/jbc.M409292200.
86. Stijlemans B, Caljon G, Natesan SKA, et al. High affinity nanobodies against the trypanosome brucei VSG are potent trypanolytic agents that block endocytosis. *PLoS Pathog*. 2011;7(6). doi:10.1371/journal.ppat.1002072.
87. Kontermann RE. Strategies for extended serum half-life of protein therapeutics. *Curr Opin Biotechnol*. 2011;22(6):868-876. doi:10.1016/j.copbio.2011.06.012.
88. Tijink BM, Laeremans T, Budde M, et al. Improved tumor targeting of anti-epidermal growth factor receptor Nanobodies through albumin binding: taking advantage of modular Nanobody technology. *Mol Cancer Ther*. 2008;7(8):2288-2297. doi:10.1158/1535-7163.MCT-07-2384.
89. Harmsen MM, Van Solt CB, Fijten HPD, Van Setten MC. Prolonged in vivo residence times of llama single-domain antibody fragments in pigs by binding to porcine immunoglobulins. *Vaccine*. 2005;23(41):4926-4934. doi:10.1016/j.vaccine.2005.05.017.
90. Cortez-Retamozo V, Backmann N, Senter PD, et al. Efficient Cancer Therapy with a Nanobody-Based Conjugate. *Cancer Res*. 2004;64(8):2853-2857. doi:10.1158/0008-5472.CAN-03-3935.
91. Peyrassol X, Laeremans T, Gouwy M, et al. Development by Genetic Immunization of Monovalent Antibodies (Nanobodies) Behaving as Antagonists of the Human ChemR23 Receptor. *J Immunol*. 2016;196(6):2893-2901. doi:10.4049/jimmunol.1500888.
92. Eden T, Menzel S, Wesolowski J, et al. A cDNA immunization strategy to generate nanobodies against membrane proteins in native conformation. *Front Immunol*. 2018;8(JAN):1-13. doi:10.3389/fimmu.2017.01989.
93. Romao E, Morales-Yanez F, Hu Y, et al. Identification of Useful Nanobodies by Phage Display of Immune Single Domain Libraries Derived from Camelid Heavy Chain Antibodies. *Curr Pharm Des*. 2017;22(43):6500-6518. doi:10.2174/1381612822666160923114417.
94. Janssens R, Dekker S, Hendriks RW, et al. Generation of heavy-chain-only antibodies in mice. *Proc Natl Acad Sci*. 2006;103(41):15130-15135. doi:10.1073/pnas.0601108103.
95. Liu W, Song H, Chen Q, et al. Recent advances in the selection and identification of antigen-specific nanobodies. *Mol Immunol*. 2018;96(February):37-47. doi:10.1016/j.molimm.2018.02.012.
96. Koide A, Tereshko V, Uysal S, Margalef K, Kossiakoff AA, Koide S. Exploring the Capacity of Minimalist Protein Interfaces: Interface Energetics and Affinity Maturation to Picomolar KD of a Single-domain Antibody with a Flat Paratope. *J Mol Biol*. 2007;373(4):941-953. doi:10.1016/j.jmb.2007.08.027.
97. Farasat A, Rahbarizadeh F, Hosseinzadeh G, Sajjadi S, Kamali M KA. Affinity enhancement of nanobody binding to EGFR: in silico site-directed mutagenesis and molecular dynamics simulation approaches. *J Biomol Struct Dyn*. 2017.
98. Hoseinpoor R, Mousavi Gargari SL, Rasooli I, Rajabibazl M, Shahi B. Functional mutations in and characterization of VHH against Helicobacter pylori urease. *Appl Biochem Biotechnol*. 2014;172(6):3079-3091. doi:10.1007/s12010-014-0750-4.
99. Comor L, Dolinska S, Bhide K, et al. Joining the in vitro immunization of alpaca lymphocytes and phage display: Rapid and cost effective pipeline for sdAb synthesis. *Microb Cell Fact*. 2017;16(1):1-13. doi:10.1186/s12934-017-0630-z.
100. Vincke C, Loris R, Saerens D, Martinez-Rodriguez S, Muyldermans S, Conrath K. General strategy to humanize a camelid single-domain antibody and identification of a universal humanized nanobody scaffold. *J Biol Chem*. 2009;284(5):3273-3284. doi:10.1074/jbc.M806889200.
101. Saerens D, Pellis M, Loris R, et al. Identification of a universal VHH framework to graft non-canonical antigen-binding loops of camel single-domain antibodies. *J Mol Biol*. 2005;352(3):597-607. doi:10.1016/j.jmb.2005.07.038.
102. Moutel S, Bery N, Bernard V, et al. NaLi-H1: A universal synthetic library of humanized nanobodies

providing highly functional antibodies and intrabodies. *Elife*. 2016;5(JULY):1-31. doi:10.7554/eLife.16228.
103. Smith GP. Filamentous fusion phage: Novel expression vectors that display cloned antigens on the virion surface. *Science (80-)*. 1985. doi:10.1126/science.4001944.
104. Lee CMY, Iorno N, Sierro F, Christ D. Selection of human antibody fragments by phage display. *Nat Protoc*. 2007;2(11):3001-3008. doi:10.1038/nprot.2007.448.
105. Arbabi Ghahroudi M, Desmyter A, Wyns L, Hamers R, Muyldermans S. Selection and identification of single domain antibody fragments from camel heavy-chain antibodies. *FEBS Lett*. 1997;414(3):521-526. doi:10.1016/S0014-5793(97)01062-4.
106. Xu C, Yang Y, Liu L, et al. Microcystin-LR nanobody screening from an alpaca phage display nanobody library and its expression and application. *Ecotoxicol Environ Saf*. 2018;151(December 2017):220-227. doi:10.1016/j.ecoenv.2018.01.003.
107. Monegal A, Ami D, Martinelli C, et al. Immunological applications of single-domain llama recombinant antibodies isolated from a naïve library. *Protein Eng Des Sel*. 2009;22(4):273-280. doi:10.1093/protein/gzp002.
108. Salema V, Fernández LÁ. Escherichia coli surface display for the selection of nanobodies. *Microb Biotechnol*. 2017;10(6):1468-1484. doi:10.1111/1751-7915.12819.
109. Fleetwood F, Devoogdt N, Pellis M, et al. Surface display of a single-domain antibody library on Gram-positive bacteria. *Cell Mol Life Sci*. 2013;70(6):1081-1093. doi:10.1007/s00018-012-1179-y.
110. Ryckaert S, Pardon E, Steyaert J, Callewaert N. Isolation of antigen-binding camelid heavy chain antibody fragments (nanobodies) from an immune library displayed on the surface of Pichia pastoris. *J Biotechnol*. 2010;145(2):93-98. doi:10.1016/j.jbiotec.2009.10.010.
111. McMahon C, Baier AS, Pascolutti R, et al. Yeast surface display platform for rapid discovery of conformationally selective nanobodies. *Nat Struct Mol Biol*. 2018;25(3):289-296. doi:10.1038/s41594-018-0028-6.
112. Rothbauer U. Speed up to find the right ones: Rapid discovery of functional nanobodies. *Nat Struct Mol Biol*. 2018;25(3):199-201. doi:10.1038/s41594-018-0038-4.
113. Zahnd C, Amstutz P, Plückthun A. Ribosome display: Selecting and evolving proteins in vitro that specifically bind to a target. *Nat Methods*. 2007;4(3):269-279. doi:10.1038/nmeth1003.
114. Odegrip R, Coomber D, Eldridge B, et al. CIS display: In vitro selection of peptides from libraries of protein-DNA complexes. *Proc Natl Acad Sci U S A*. 2004;101(9):2806-2810. doi:10.1073/pnas.0400219101.
115. Yau KYF, Groves MAT, Li S, et al. Selection of hapten-specific single-domain antibodies from a non-immunized llama ribosome display library. *J Immunol Methods*. 2003;281(1-2):161-175. doi:10.1016/j.jim.2003.07.011.
116. Patel S, Mathonet P, Jaulent AM, Ullman CG. Selection of a high-affinity WW domain against the extracellular region of VEGF receptor isoform-2 from a combinatorial library using CIS display. *Protein Eng Des Sel*. 2013;26(4):307-315. doi:10.1093/protein/gzt003.
117. Rossotti M, Tabares S, Alfaya L, Leizagoyen C, Moron G, González-Sapienza G. Streamlined method for parallel identification of single domain antibodies to membrane receptors on whole cells. *Biochim Biophys Acta - Gen Subj*. 2015;1850(7):1397-1404. doi:10.1016/j.bbagen.2015.03.009.
118. Pellis M, Pardon E, Zolghadr K, et al. A bacterial-two-hybrid selection system for one-step isolation of intracellularly functional Nanobodies. *Arch Biochem Biophys*. 2012;526(2):114-123. doi:10.1016/j.abb.2012.04.023.
119. Desmyter A, Spinelli S, Roussel A, Cambillau C. Camelid nanobodies: Killing two birds with one stone. *Curr Opin Struct Biol*. 2015;32:1-8. doi:10.1016/j.sbi.2015.01.001.
120. Lam AY, Pardon E, Korotkova K V., Hola WGJ, Steyaert J. Nanobody-aided structure determination of the EpsI:EpsJ pseudopilin heterodimer from Vibrio vulnificus. *J Struct Biol*. 2009;6(1):247-253. doi:10.1111/j.1743-6109.2008.01122.x.Endothelial.
121. Korotkov K V., Johnson TL, Jobling MG, et al. Structural and functional studies on the interaction of GspC and GspD in the type II secretion system. *PLoS Pathog*. 2011;7(9). doi:10.1371/journal.ppat.1002228.

122. Park YJ, Pardon E, Wu M, Steyaert J, Hol WGJ. Crystal structure of a heterodimer of editosome interaction proteins in complex with two copies of a cross-reacting nanobody. *Nucleic Acids Res*. 2012;40(4):1828-1840. doi:10.1093/nar/gkr867.
123. Baranova E, Fronzes R, Garcia-Pino A, et al. SbsB structure and lattice reconstruction unveil Ca2+ triggered S-layer assembly. *Nature*. 2012;487(7405):119-122. doi:10.1038/nature11155.
124. Khamrui S, Turley S, Pardon E, et al. The structure of the D3 domain of Plasmodium falciparum myosin tail interacting protein MTIP in complex with a nanobody. *Mol Biochem Parasitol*. 2013;190(2):87-91. doi:10.1016/j.molbiopara.2013.06.003.
125. Rivera-Calzada A, Fronzes R, Savva CG, et al. Structure of a bacterial type IV secretion core complex at subnanometre resolution. *EMBO J*. 2013;32(8):1195-1204. doi:10.1038/emboj.2013.58.
126. De Genst E, Chan PH, Pardon E, et al. A nanobody binding to non-amyloidogenic regions of the protein human lysozyme enhances partial unfolding but inhibits amyloid fibril formation. *J Phys Chem B*. 2013;117(42):13245-13258. doi:10.1021/jp403425z.
127. Kruse AC, Ring AM, Manglik A, et al. Activation and allosteric modulation of a muscarinic acetylcholine receptor. *Nature*. 2013;504(7478):101-106. doi:10.1038/nature12735.
128. Ward AB, Szewczyk P, Grimard V, et al. Structures of P-glycoprotein reveal its conformational flexibility and an epitope on the nucleotide-binding domain. *Proc Natl Acad Sci*. 2013;110(33):13386-13391. doi:10.1073/pnas.1309275110.
129. Löw C, Yau YH, Pardon E, et al. Nanobody Mediated Crystallization of an Archeal Mechanosensitive Channel. *PLoS One*. 2013;8(10):1-14. doi:10.1371/journal.pone.0077984.
130. Vuchelen A, Pardon E, Steyaert J, et al. Production, crystallization and X-ray diffraction analysis of two nanobodies against the Duffy binding-like (DBL) domain DBL6-FCR3 of the Plasmodium falciparum VAR2CSA protein. *Acta Crystallogr Sect F Struct Biol Cryst Commun*. 2013;69(3):270-274. doi:10.1107/S1744309113001917.
131. Abskharon RNN, Giachin G, Wohlkonig A, et al. Probing the N-terminal β-sheet conversion in the crystal structure of the human prion protein bound to a nanobody. *J Am Chem Soc*. 2014;136(3):937-944. doi:10.1021/ja407527p.
132. Wu M, Park YJ, Pardon E, et al. Structures of a key interaction protein from the Trypanosoma brucei editosome in complex with single domain antibodies. *J Struct Biol*. 2011;174(1):124-136. doi:10.1016/j.jsb.2010.10.007.
133. Guilliams T, El-Turk F, Buell AK, et al. Nanobodies raised against monomeric α-synuclein distinguish between fibrils at different maturation stages. *J Mol Biol*. 2013;425(14):2397-2411. doi:10.1016/j.jmb.2013.01.040.
134. De Genst EJ, Guilliams T, Wellens J, et al. Structure and properties of a complex of α-synuclein and a single-domain camelid antibody. *J Mol Biol*. 2010;402(2):326-343. doi:10.1016/j.jmb.2010.07.001.
135. Loris R, Marianovsky I, Lah J, et al. Crystal structure of the intrinsically flexible addiction antidote MazE. *J Biol Chem*. 2003;278(30):28252-28257. doi:10.1074/jbc.M302336200.
136. Moonens K, Gideonsson P, Subedi S, et al. Structural Insights into Polymorphic ABO Glycan Binding by Helicobacter pylori. *Cell Host Microbe*. 2016;19(1):55-66. doi:10.1016/j.chom.2015.12.004.
137. Steyaert J, Kobilka BK. Nanobody stabilization of G protein-coupled receptor conformational states. *Curr Opin Struct Biol*. 2011;21(4):567-572. doi:10.1016/j.sbi.2011.06.011.
138. Chaikuad A, Keates T, Vincke C, et al. Structure of cyclin G-associated kinase (GAK) trapped in different conformations using nanobodies. *Biochem J*. 2014;459(1):59-69. doi:10.1042/BJ20131399.
139. Westfield GH, Rasmussen SGF, Su M, et al. Structural flexibility of the Gαs α-helical domain in the β2 -adrenoceptor Gs complex. *Proc Natl Acad Sci U S A*. 2011;108(38):16086-16091. doi:10.1073/pnas.1113645108/-/DCSupplemental.www.pnas.org/cgi/doi/10.1073/pnas.1113645108.
140. Rasmussen SGF, Devree BT, Zou Y, et al. Crystal structure of the β 2 adrenergic receptor-Gs protein complex. *Nature*. 2011;477(7366):549-557. doi:10.1038/nature10361.
141. Rasmussen SGF, Choi HJ, Fung JJ, et al. Structure of a nanobody-stabilized active state of the β2adrenoceptor. *Nature*. 2011;469(7329):175-181. doi:10.1038/nature09648.
142. Ring AM, Manglik A, Kruse AC, et al. Adrenaline-activated structure of β 2-adrenoceptor stabilized by

an engineered nanobody. *Nature*. 2013;502(7472):575-579. doi:10.1038/nature12572.
143. Lewis W, Keshavarz-Moore E, Windust J, Bushell D, Parry N. Construction and Evaluation of Novel Fusion Proteins for Targeted Delivery of Micro Particles to Cellulose Surfaces. *WileyInterScience*. 2005. doi:10.1002/bit.
144. Hussack G, Luo Y, Veldhuis L, Hall JC, Tanha J, MacKenzie R. Multivalent anchoring and oriented display of single-domain antibodies on cellulose. *Sensors*. 2009;9(7):5351-5367. doi:10.3390/s90705351.
145. Tu Z, Xu Y, Fu J, et al. Preparation and characterization of novel IgG affinity resin coupling anti-Fc camelid single-domain antibodies. *J Chromatogr B Anal Technol Biomed Life Sci*. 2015;983-984:26-31. doi:10.1016/j.jchromb.2014.12.031.
146. Huang PJ, Tay LL, Tanha J, Ryan S, Chau LK. Single-domain antibody-conjugated nanoaggregate-embedded beads for targeted detection of pathogenic bacteria. *Chem - A Eur J*. 2009;15(37):9330-9334. doi:10.1002/chem.200901397.
147. Verheesen P, Ten Haaft MR, Lindner N, Verrips CT, De Haard JJW. Beneficial properties of single-domain antibody fragments for application in immunoaffinity purification and immuno-perfusion chromatography. *Biochim Biophys Acta - Gen Subj*. 2003;1624(1-3):21-28. doi:10.1016/j.bbagen.2003.09.006.
148. Pollithy A, Romer T, Lang C, et al. Magnetosome expression of functional camelid antibody fragments (nanobodies) in Magnetospirillum gryphiswaldense. *Appl Environ Microbiol*. 2011;77(17):6165-6171. doi:10.1128/AEM.05282-11.
149. Nguyen-Duc T, van Oeffelen L, Song N, et al. The genome-wide binding profile of the Sulfolobus solfataricus transcription factor Ss-LrpB shows binding events beyond direct transcription regulation. *BMC Genomics*. 2013;14(1):1-15. doi:10.1186/1471-2164-14-828.
150. Steels A, Bertier L, Gettemans J. Use, Applications and Mechanisms of Intracellular Actions of Camelid VHHs. *Web Sci*. 2013:29. doi:http://dx.doi.org/10.5772/46845.
151. Beghein E, Gettemans J. Nanobody technology: A versatile toolkit for microscopic imaging, protein-protein interaction analysis, and protein function exploration. *Front Immunol*. 2017;8(JUL):1-14. doi:10.3389/fimmu.2017.00771.
152. Rothbauer U, Zolghadr K, Tillib S, et al. Targeting and tracing antigens in live cells with fluorescent nanobodies. *Nat Methods*. 2006;3(11):887-889. doi:10.1038/nmeth953.
153. Tang JC, Drokhlyansky E, Etemad B, et al. Detection and manipulation of live antigen-expressing cells using conditionally stable nanobodies. *Elife*. 2016. doi:10.7554/eLife.15312.
154. Bothma JP, Norstad MR, Alamos S, Garcia HG. LlamaTags: A Versatile Tool to Image Transcription Factor Dynamics in Live Embryos. *Cell*. 2018;173(7):1810-1822.e16. doi:10.1016/j.cell.2018.03.069.
155. Tang JCY, Szikra T, Kozorovitskiy Y, et al. A nanobody-based system using fluorescent proteins as scaffolds for cell-specific gene manipulation. *Cell*. 2013;154(4):928-939. doi:10.1016/j.cell.2013.07.021.
156. Caussinus E, Kanca O, Affolter M. Fluorescent fusion protein knockout mediated by anti-GFP nanobody. *Nat Struct Mol Biol*. 2011;19(1):117-121. doi:10.1038/nsmb.2180.
157. Baudisch B, Pfort I, Sorge E, Conrad U. Nanobody-Directed Specific Degradation of Proteins by the 26S-Proteasome in Plants. *Front Plant Sci*. 2018;9(February):1-8. doi:10.3389/fpls.2018.00130.
158. Fulcher LJ, Macartney T, Bozatzi P, Hornberger A, Rojas-Fernandez A, Sapkota GP. An affinity-directed protein missile system for targeted proteolysis. *Open Biol*. 2016;6(10). doi:10.1098/rsob.160255.
159. Kuo CL, Oyler GA, Shoemaker CB. Accelerated neuronal cell recovery from botulinum neurotoxin intoxication by targeted ubiquitination. *PLoS One*. 2011;6(5). doi:10.1371/journal.pone.0020352.
160. Shin YJ, Park SK, Jung YJ, et al. Nanobody-targeted E3-ubiquitin ligase complex degrades nuclear proteins. *Sci Rep*. 2015;5:14269. doi:10.1038/srep14269.
161. Herce HD, Deng W, Helma J, Leonhardt H, Cardoso MC. Visualization and targeted disruption of protein interactions in living cells. *Nat Commun*. 2013;4(May):1-8. doi:10.1038/ncomms3660.
162. Drees C, Raj AN, Kurre R, Busch KB, Haase M, Piehler J. Engineered Upconversion Nanoparticles for Resolving Protein Interactions inside Living Cells. *Angew Chemie - Int Ed*. 2016;55(38):11668-11672. doi:10.1002/anie.201603028.

163. Harmansa S, Hamaratoglu F, Affolter M, Caussinus E. Dpp spreading is required for medial but not for lateral wing disc growth. *Nature*. 2015;527(7578):317-322. doi:10.1038/nature15712.
164. Modi S, Higgs N, Sheehan D, Griffin LD, Kittler J. Quantum Dot conjugated nanobodies for multiplex imaging of protein dynamics at synapses. *J Name*. 2016;8(00):1-660. doi:10.1039/x0xx00000x.
165. Lee S, Park H, Kyung T, et al. Reversible protein inactivation by optogenetic trapping in cells. *Nat Methods*. 2014;(May). doi:10.1007/978-1-4939-3512-3_25.
166. Beghein E, Van Audenhove I, Zwaenepoel O, Verhelle A, De Ganck A, Gettemans J. A new survivin tracer tracks, delocalizes and captures endogenous survivin at different subcellular locations and in distinct organelles. *Sci Rep*. 2016;6(April):11-15. doi:10.1038/srep31177.
167. Buser DP, Schleicher KD, Prescianotto-Baschong C, Spiess M. A versatile nanobody-based toolkit to analyze retrograde transport from the cell surface. *Proc Natl Acad Sci*. 2018:201801865. doi:10.1073/pnas.1801865115.
168. Glass DS, Riedel-Kruse IH. A Synthetic Bacterial Cell-Cell Adhesion Toolbox for Programming Multicellular Morphologies and Patterns. *Cell*. 2018:1-10. doi:10.1016/j.cell.2018.06.041.
169. Saerens D, Huang L, Bonroy K, Muyldermans S. Antibody fragments as probe in biosensor development. *Sensors*. 2008;8(8):4669-4686. doi:10.3390/s8084669.
170. de Beer MA, Kuipers J, van Bergen en Henegouwen PMP, Giepmans BNG. A small protein probe for correlated microscopy of endogenous proteins. *Histochem Cell Biol*. 2018;149(3):261-268. doi:10.1007/s00418-018-1632-6.
171. Yamagata M, Sanes JR. Reporter–nanobody fusions (RANbodies) as versatile, small, sensitive immunohistochemical reagents. *Proc Natl Acad Sci*. 2018;(18):201722491. doi:10.1073/pnas.1722491115.
172. Bruce VJ, McNaughton BR. Evaluation of Nanobody Conjugates and Protein Fusions as Bioanalytical Reagents. *Anal Chem*. 2017;89(7):3819-3823. doi:10.1021/acs.analchem.7b00470.
173. Djender S, Schneider A, Beugnet A, et al. Bacterial cytoplasm as an effective cell compartment for producing functional VHH-based affinity reagents and Camelidae IgG-like recombinant antibodies. *Microb Cell Fact*. 2014;13(1):1-10. doi:10.1186/s12934-014-0140-1.
174. Braun MB, Traenkle B, Koch PA, et al. Peptides in headlock - A novel high-affinity and versatile peptide-binding nanobody for proteomics and microscopy. *Sci Rep*. 2016;6(December 2015):1-10. doi:10.1038/srep19211.
175. Pleiner T, Bates M, Görlich D. A toolbox of anti – mouse and anti – rabbit IgG secondary nanobodies. *J Cell Biol*. 2018. doi:10.1083/jcb.201709115.
176. Anderson GP, Moore M, Charles PT, Goldman ER. Bead-based fluid array detection of pentaerythritol tetranitrate: Comparison of monoclonal vs. llama polyclonal antibodies. *Anal Lett*. 2010;43(18):2913-2922. doi:10.1080/00032711003763699.
177. Klein Á, Kovács M, Muskotál A, et al. Nanobody-Displaying Flagellar Nanotubes. *Sci Rep*. 2018;8(1):1-9. doi:10.1038/s41598-018-22085-3.
178. Campuzano S, Salema V, Moreno-Guzmán M, et al. Disposable amperometric magnetoimmunosensors using nanobodies as biorecognition element. Determination of fibrinogen in plasma. *Biosens Bioelectron*. 2014;52:255-260. doi:10.1016/j.bios.2013.08.055.
179. Dong JX, Li ZF, Lei HT, et al. Development of a single-chain variable fragment-alkaline phosphatase fusion protein and a sensitive direct competitive chemiluminescent enzyme immunoassay for detection of ractopamine in pork. *Anal Chim Acta*. 2012;736:85-91. doi:10.1016/j.aca.2012.05.033.
180. Yan J, Wang P, Zhu M, et al. Characterization and applications of Nanobodies against human procalcitonin selected from a novel naïve Nanobody phage display library. *J Nanobiotechnology*. 2015;13(1):1-11. doi:10.1186/s12951-015-0091-7.
181. Li H, Sun Y, Elseviers J, Muyldermans S, Liu S, Wan Y. A nanobody-based electrochemiluminescent immunosensor for sensitive detection of human procalcitonin. *Analyst*. 2014;139(15):3718-3721. doi:10.1039/c4an00626g.
182. Odongo S, Sterckx YGJ, Stijlemans B, et al. An Anti-proteome Nanobody Library Approach Yields a Specific Immunoassay for Trypanosoma congolense Diagnosis Targeting Glycosomal Aldolase. *PLoS Negl Trop Dis*. 2016;10(2):1-24. doi:10.1371/journal.pntd.0004420.

183. Habib I, Smolarek D, Hattab C, et al. VHH (nanobody) directed against human glycophorin A: A tool for autologous red cell agglutination assays. *Anal Biochem*. 2013;438(1):82-89. doi:10.1016/j.ab.2013.03.020.
184. Wang J, Mukhtar H, Ma L, Pang Q, Wang X. VHH antibodies: Reagents for mycotoxin detection in food products. *Sensors (Switzerland)*. 2018;18(2). doi:10.3390/s18020485.
185. De Vos J, Devoogdt N, Lahoutte T, Muyldermans S. Camelid single-domain antibody-fragment engineering for (pre)clinical *in vivo* molecular imaging applications: adjusting the bullet to its target. *Expert Opin Biol Ther*. 2013;13(8):1149-1160. doi:10.1517/14712598.2013.800478.
186. De Groeve K, Deschacht N, De Koninck C, et al. Nanobodies as Tools for In Vivo Imaging of Specific Immune Cell Types. *J Nucl Med*. 2010;51(5):782-789. doi:10.2967/jnumed.109.070078.
187. Movahedi K, Schoonooghe S, Laoui D, et al. Nanobody-based targeting of the macrophage mannose receptor for effective in vivo imaging of tumor-associated macrophages. *Cancer Res*. 2012;72(16):4165-4177. doi:10.1158/0008-5472.CAN-11-2994.
188. Zheng F, Put S, Bouwens L, et al. Molecular Imaging with Macrophage CRIg-Targeting Nanobodies for Early and Preclinical Diagnosis in a Mouse Model of Rheumatoid Arthritis. *J Nucl Med*. 2014;55(5):824-829. doi:10.2967/jnumed.113.130617.
189. Schoonooghe S, Laoui D, Van Ginderachter JA, et al. Novel applications of nanobodies for in vivo bio-imaging of inflamed tissues in inflammatory diseases and cancer. *Immunobiology*. 2012;217(12):1266-1272. doi:10.1016/j.imbio.2012.07.009.
190. Röder R, Helma J, Preiß T, Rädler JO, Leonhardt H, Wagner E. Intracellular Delivery of Nanobodies for Imaging of Target Proteins in Live Cells. *Pharm Res*. 2017;34(1):161-174. doi:10.1007/s11095-016-2052-8.
191. Li T, Vandesquille M, Koukouli F, et al. Camelid single-domain antibodies: A versatile tool for in vivo imaging of extracellular and intracellular brain targets. *J Control Release*. 2016;243:1-10. doi:10.1016/j.jconrel.2016.09.019.
192. Širochmanová I, Čomor Ľ, Káňová E, Jiménez-Munguía I, Tkáčová Z, Bhide M. Permeability of the Blood-Brain Barrier and Transport of Nanobodies Across the Blood-Brain Barrier. *Folia Vet*. 2018;62(1):59-66. doi:10.2478/fv-2018-0009.
193. Nabuurs RJA, Rutgers KS, Welling MM, et al. In vivo detection of amyloid-β deposits using heavy chain antibody fragments in a transgenic mouse model for alzheimer's disease. *PLoS One*. 2012;7(6):1-10. doi:10.1371/journal.pone.0038284.
194. Xavier C, Blykers A, Vaneycken I, et al. 18F-nanobody for PET imaging of HER2 overexpressing tumors. *Nucl Med Biol*. 2016;43(4):247-252. doi:10.1016/j.nucmedbio.2016.01.002.
195. Rashidian M, Wang L, Edens JG, et al. Enzyme-Mediated Modification of Single-Domain Antibodies for Imaging Modalities with Different Characteristics. *Angew Chemie - Int Ed*. 2016;55(2):528-533. doi:10.1002/anie.201507596.
196. Gainkam LOT, Huang L, Caveliers V, et al. Comparison of the Biodistribution and Tumor Targeting of Two 99mTc-Labeled Anti-EGFR Nanobodies in Mice, Using Pinhole SPECT/Micro-CT. *J Nucl Med*. 2008;49(5):788-795. doi:10.2967/jnumed.107.048538.
197. Rashidian M, Keliher EJ, Bilate AM, et al. Noninvasive imaging of immune responses. *Proc Natl Acad Sci U S A*. 2015;112(19):6146-6151. doi:10.1073/pnas.1502609112/-/DCSupplemental.www.pnas.org/cgi/doi/10.1073/pnas.1502609112.
198. Vaneycken I, Govaert J, Vincke C, et al. In Vitro Analysis and In Vivo Tumor Targeting of a Humanized, Grafted Nanobody in Mice Using Pinhole SPECT/Micro-CT. *J Nucl Med*. 2010;51(7):1099-1106. doi:10.2967/jnumed.109.069823.
199. Kijanka M, Warnders FJ, El Khattabi M, et al. Rapid optical imaging of human breast tumour xenografts using anti-HER2 VHHs site-directly conjugated to IRDye 800CW for image-guided surgery. *Eur J Nucl Med Mol Imaging*. 2013;40(11):1718-1729. doi:10.1007/s00259-013-2471-2.
200. Van Driel PBAA, Van Der Vorst JR, Verbeek FPR, et al. Intraoperative fluorescence delineation of head and neck cancer with a fluorescent Anti-epidermal growth factor receptor nanobody. *Int J Cancer*. 2014;134(11):2663-2673. doi:10.1002/ijc.28601.
201. Vaneycken I, Devoogdt N, Van Gassen N, et al. Preclinical screening of anti-HER2 nanobodies for

molecular imaging of breast cancer. *FASEB J*. 2011;25(7):2433-2446. doi:10.1096/fj.10-180331.
202. Xavier C, Vaneycken I, D'huyvetter M, et al. Synthesis, Preclinical Validation, Dosimetry, and Toxicity of 68Ga-NOTA-Anti-HER2 Nanobodies for iPET Imaging of HER2 Receptor Expression in Cancer. *J Nucl Med*. 2013;54(5):776-784. doi:10.2967/jnumed.112.111021.
203. Keyaerts M, Xavier C, Heemskerk J, et al. Phase I Study of 68Ga-HER2-Nanobody for PET/CT Assessment of HER2 Expression in Breast Carcinoma. *J Nucl Med*. 2016;57(1):27-33. doi:10.2967/jnumed.115.162024.
204. Scully M, Cataland S, Peyvandi F, et al. Results of the Randomized, Double-Blind, Placebo-Controlled, Phase 3 Hercules Study of Caplacizumab in Patients with Acquired Thrombotic Thrombocytopenic Purpura. *Ablynx*. 2017.
205. Steeland S, Vandenbroucke RE, Libert C. Nanobodies as therapeutics: Big opportunities for small antibodies. *Drug Discov Today*. 2016;21(7):1076-1113. doi:10.1016/j.drudis.2016.04.003.
206. Liu M, Huang Y, Hu L, et al. Selective delivery of interleukine-1 receptor antagonist to inflamed joint by albumin fusion. *BMC Biotechnol*. 2012;12:1-13. doi:10.1186/1472-6750-12-68.
207. Kijanka M, Dorresteijn B, Oliveira S, van Bergen en Henegouwen PMP. Nanobody-based cancer therapy of solid tumors. *Nanomedicine*. 2015;10(1):161-174. doi:10.2217/nnm.14.178.
208. Bannas P, Hambach J, Koch-Nolte F. Nanobodies and nanobody-based human heavy chain antibodies as antitumor therapeutics. *Front Immunol*. 2017;8(NOV):1-13. doi:10.3389/fimmu.2017.01603.
209. Vosjan MJWD, Vercammen J, Kolkman JA, Stigter-van Walsum M, Revets H, van Dongen GAMS. Nanobodies Targeting the Hepatocyte Growth Factor: Potential New Drugs for Molecular Cancer Therapy. *Mol Cancer Ther*. 2012;11(4):1017-1025. doi:10.1158/1535-7163.MCT-11-0891.
210. Roovers RC, Vosjan MJWD, Laeremans T, et al. A biparatopic anti-EGFR nanobody efficiently inhibits solid tumour growth. *Int J Cancer*. 2011;129(8):2013-2024. doi:10.1002/ijc.26145.
211. Schmidt Slørdahl T, Denayer T, Helen Moen S, et al. Anti-c-MET Nanobody® - A new potential drug in multiple myeloma treatment. *Eur J Haematol*. 2013;91(5):399-410. doi:10.1111/ejh.12185.
212. Omidfar K, Amjad Zanjani FS, Hagh AG, Azizi MD, Rasouli SJ, Kashanian S. Efficient growth inhibition of EGFR over-expressing tumor cells by an anti-EGFR nanobody. *Mol Biol Rep*. 2013;40(12):6737-6745. doi:10.1007/s11033-013-2790-1.
213. Sha H, Zou Z, Xin K, et al. Tumor-penetrating peptide fused EGFR single-domain antibody enhances cancer drug penetration into 3D multicellular spheroids and facilitates effective gastric cancer therapy. *J Control Release*. 2015;200:188-200. doi:10.1016/j.jconrel.2014.12.039.
214. Van Impe K, Bethuyne J, Cool S, et al. A nanobody targeting the F-actin capping protein CapG restrains breast cancer metastasis. *Breast Cancer Res*. 2013;15(6):1-15. doi:10.1186/bcr3585.
215. Maussang D, Mujić-Delić A, Descamps FJ, et al. Llama-derived single variable domains (nanobodies) directed against chemokine receptor CXCR7 reduce head and neck cancer cell growth in vivo. *J Biol Chem*. 2013;288(41):29562-29572. doi:10.1074/jbc.M113.498436.
216. Behdani M, Zeinali S, Karimipour M, et al. Expression, purification, and characterization of a diabody against the most important angiogenesis cell receptor: Vascular endothelial growth factor receptor 2. *Adv Biomed Res*. 2012;1(1):34. doi:10.4103/2277-9175.100126.
217. Ebrahimizadeh W, Mousavi Gargari SLM, Javidan Z, Rajabibazl M. Production of Novel VHH Nanobody Inhibiting Angiogenesis by Targeting Binding Site of VEGF. *Appl Biochem Biotechnol*. 2015;176(7):1985-1995. doi:10.1007/s12010-015-1695-y.
218. Behar G, Sibéril S, Groulet A, et al. Isolation and characterization of anti-FcγRIII (CD16) llama single-domain antibodies that activate natural killer cells. *Protein Eng Des Sel*. 2008;21(1):1-10. doi:10.1093/protein/gzm064.
219. Rozan C, Cornillon A, Petiard C, et al. Single-Domain Antibody-Based and Linker-Free Bispecific Antibodies Targeting FcγRIII Induce Potent Antitumor Activity without Recruiting Regulatory T Cells. *Mol Cancer Ther*. 2013;12(8):1481-1491. doi:10.1158/1535-7163.MCT-12-1012.
220. Bachran C, Schröder M, Conrad L, et al. The activity of myeloid cell-specific VHH immunotoxins is target-, epitope-, subset- and organ dependent. *Sci Rep*. 2017;7(1):2-11. doi:10.1038/s41598-017-17948-0.
221. Behdani M, Zeinali S, Karimipour M, et al. Development of VEGFR2-specific Nanobody Pseudomonas

exotoxin A conjugated to provide efficient inhibition of tumor cell growth. *N Biotechnol*. 2013;30(2):205-209. doi:10.1016/j.nbt.2012.09.002.

222. Water J a JM Van De, Bagci-onder T, Agarwal AS, Wakimoto H, Roovers RC. Therapeutic stem cells expressing variants of EGFR-specific nanobodies have antitumor effects. *Proc Natl Acad Sci U S A*. 2012:1-6. doi:10.1073/pnas.1202832109/-/DCSupplemental.www.pnas.org/cgi/doi/10.1073/pnas.1202832109.
223. Tian B, Wong WY, Hegmann E, Gaspar K, Kumar P, Chao H. Production and Characterization of a Camelid Single Domain Antibody-Urease Enzyme Conjugate for the Treatment of Cancer. *Bioconjug Chem*. 2015;26(6):1144-1155. doi:10.1021/acs.bioconjchem.5b00237.
224. Zhang G, Wang L, Cui H, et al. Anti-melanoma activity of T cells redirected with a TCR-like chimeric antigen receptor. *Sci Rep*. 2014;4(SREP03571):2-9. doi:10.1038/srep03571.
225. Jamnani FR, Rahbarizadeh F, Shokrgozar MA, et al. T cells expressing VHH-directed oligoclonal chimeric HER2 antigen receptors: Towards tumor-directed oligoclonal T cell therapy. *Biochim Biophys Acta - Gen Subj*. 2014;1840(1):378-386. doi:10.1016/j.bbagen.2013.09.029.
226. Sharifzadeh Z, Rahbarizadeh F, Shokrgozar MA, et al. Genetically engineered T cells bearing chimeric nanoconstructed receptors harboring TAG-72-specific camelid single domain antibodies as targeting agents. *Cancer Lett*. 2013;334(2):237-244. doi:10.1016/j.canlet.2012.08.010.
227. Hu Y, Liu C, Muyldermans S. Nanobody-based delivery systems for diagnosis and targeted tumor therapy. *Front Immunol*. 2017;8(NOV). doi:10.3389/fimmu.2017.01442.
228. Fan K, Jiang B, Guan Z, et al. Fenobody: A Ferritin-Displayed Nanobody with High Apparent Affinity and Half-Life Extension. *Anal Chem*. 2018;90(9):5671-5677. doi:10.1021/acs.analchem.7b05217.
229. Oliveira S, Heukers R, Sornkom J, Kok RJ, Van Bergen En Henegouwen PMP. Targeting tumors with nanobodies for cancer imaging and therapy. *J Control Release*. 2013;172(3):607-617. doi:10.1016/j.jconrel.2013.08.298.
230. Van Der Meel R, Oliveira S, Altintas I, et al. Tumor-targeted Nanobullets: Anti-EGFR nanobody-liposomes loaded with anti-IGF-1R kinase inhibitor for cancer treatment. *J Control Release*. 2012;159(2):281-289. doi:10.1016/j.jconrel.2011.12.027.
231. Debets MF, Leenders WPJ, Verrijp K, et al. Nanobody-Functionalized Polymersomes for Tumor-Vessel Targeting. *Macromol Biosci*. 2013;13(7):938-945. doi:10.1002/mabi.201300039.
232. Zou T, Dembele F, Beugnet A, et al. Nanobody-functionalized PEG-b-PCL polymersomes and their targeting study. *J Biotechnol*. 2015;214:147-155. doi:10.1016/j.jbiotec.2015.09.034.
233. El Andaloussi S, Mäger I, Breakefield XO, Wood MJA. Extracellular vesicles: Biology and emerging therapeutic opportunities. *Nat Rev Drug Discov*. 2013;12(5):347-357. doi:10.1038/nrd3978.
234. Kooijmans SAA, Fliervoet LAL, Van Der Meel R, et al. PEGylated and targeted extracellular vesicles display enhanced cell specificity and circulation time. *J Control Release*. 2016;224:77-85. doi:10.1016/j.jconrel.2016.01.009.
235. Lemaire M, D'Huyvetter M, Lahoutte T, et al. Imaging and radioimmunotherapy of multiple myeloma with anti-idiotypic Nanobodies. *Leukemia*. 2014;28(2):444-447. doi:10.1038/leu.2013.292.
236. Pruszynski M, Koumarianou E, Vaidyanathan G, et al. Improved Tumor Targeting of Anti-HER2 Nanobody Through N-Succinimidyl 4-Guanidinomethyl-3-Iodobenzoate Radiolabeling. *J Nucl Med*. 2014;55(4):650-656. doi:10.2967/jnumed.113.127100.
237. Krasniqi A, D'Huyvetter M, Xavier C, et al. Theranostic Radiolabeled Anti-CD20 sdAb for Targeted Radionuclide Therapy of Non-Hodgkin Lymphoma. *Mol Cancer Ther*. 2017;16(12):2828-2839. doi:10.1158/1535-7163.MCT-17-0554.
238. D'Huyvetter M, Vincke C, Xavier C, et al. Targeted Radionuclide Therapy with A 177Lu-labeled Anti-HER2 Nanobody. *Theranostics*. 2014;4(7):708-720. doi:10.7150/thno.8156.
239. Heukers R, van Bergen en Henegouwen PMP, Oliveira S. Nanobody-photosensitizer conjugates for targeted photodynamic therapy. *Nanomedicine Nanotechnology, Biol Med*. 2014;10(7):1441-1451. doi:10.1016/j.nano.2013.12.007.
240. Van Driel PBAA, Boonstra MC, Slooter MD, et al. EGFR targeted nanobody-photosensitizer conjugates for photodynamic therapy in a pre-clinical model of head and neck cancer. *J Control Release*. 2016;229:93-105. doi:10.1016/j.jconrel.2016.03.014.

241. Van De Broek B, Devoogdt N, Dhollander A, et al. Specific cell targeting with nanobody conjugated branched gold nanoparticles for photothermal therapy. *ACS Nano*. 2011;5(6):4319-4328. doi:10.1021/nn1023363.
242. Coppieters K, Dreier T, Silence K, et al. Formatted anti-tumor Necrosis Factor α VHH proteins derived from camelids show superior potency and targeting to inflamed joints in a murine model of collagen-induced arthritis. *Arthritis Rheum*. 2006;54(6):1856-1866. doi:10.1002/art.21827.
243. Van Hauwermeiren F, Vandenbroucke RE, Libert C. Treatment of TNF mediated diseases by selective inhibition of soluble TNF or TNFR1. *Cytokine Growth Factor Rev*. 2011;22(5-6):311-319. doi:10.1016/j.cytogfr.2011.09.004.
244. Abe M, Yuki Y, Kurokawa S, et al. A rice-based soluble form of a murine TNF-specific llama variable domain of heavy-chain antibody suppresses collagen-induced arthritis in mice. *J Biotechnol*. 2014;175(1):45-52. doi:10.1016/j.jbiotec.2014.02.005.
245. Steeland S, Puimege L, Vandenbroucke RE, et al. Generation and characterization of small single domain antibodies inhibiting human tumor Necrosis Factor receptor 1. *J Biol Chem*. 2015;290(7):4022-4037. doi:10.1074/jbc.M114.617787.
246. Fleischmann R, Nayiager S, Louw I, et al. A Multiple Ascending Dose/Proof of Concept study of ATN-103 (ozoralizumab) in Rheumatoid Arthritis Subjects on a background of Methotrexate. *Arthritis Rheum*. 2011.
247. Scheuplein F, Rissiek B, Driver JP, Chen YG, Koch-Nolte F, Serreze D V. A recombinant heavy chain antibody approach blocks ART2 mediated deletion of an iNKT cell population that upon activation inhibits autoimmune diabetes. *J Autoimmun*. 2010;34(2):145-154. doi:10.1016/j.jaut.2009.08.012.
248. Beneden K, Verschueren K, Willems W, et al. Impact of clinical remission on physical function in patients with rheumatoid arthritis treated with ALX-0061: Post-HOC analysis of phase I/II data. *Ann Rheum Dis*. 2014;73(1):9052. doi:10.1136/annrheumdis-2014-eular.2875.
249. Ablynx. ABLYNX INITIATES PHASE II SLE STUDY WITH ITS ANTI-IL-6R NANOBODY , PARTNERED WITH ABBVIE. *Ablynx*. 2015.
250. Svecova D, Krueger JG, Sverdlov O, et al. Safety and Efficacy of Multiple Ascending Doses of Subcutaneous M1095, an Anti-Interleukin-17A/F Bispecific Nanobody®, in Patients with Moderate-to- Severe Psoriasis. *Ablynx*. 2017.
251. Moonens K, De Kerpel M, Coddens A, et al. Nanobody mediated inhibition of attachment of F18 fimbriae expressing Escherichia coli. *PLoS One*. 2014;9(12):1-20. doi:10.1371/journal.pone.0114691.
252. Ibañez LI, De Filette M, Hultberg A, et al. Nanobodies with in vitro neutralizing activity protect mice against H5N1 influenza virus infection. *J Infect Dis*. 2011;203(8):1063-1072. doi:10.1093/infdis/jiq168.
253. Tillib S V., Ivanova TI, Vasilev LA, et al. Formatted single-domain antibodies can protect mice against infection with influenza virus (H5N2). *Antiviral Res*. 2013;97(3):245-254. doi:10.1016/j.antiviral.2012.12.014.
254. Tarr AW, Lafaye P, Meredith L, et al. An alpaca nanobody inhibits hepatitis C virus entry and cell-to-cell transmission. *Hepatology*. 2013;58(3):932-939. doi:10.1002/hep.26430.
255. Vercruysse T, Boons E, Venken T, et al. Mapping the Binding Interface between an HIV-1 Inhibiting Intrabody and the Viral Protein Rev. *PLoS One*. 2013;8(4). doi:10.1371/journal.pone.0060259.
256. Boons E, Li G, Vanstreels E, et al. A stably expressed llama single-domain intrabody targeting Rev displays broad-spectrum anti-HIV activity. *Antiviral Res*. 2014;112:91-102. doi:10.1016/j.antiviral.2014.10.007.
257. Liu H, Liang C, Duan H, et al. Intracellularly expressed nanobodies against non-structural protein 4 of porcine reproductive and respiratory syndrome virus inhibit virus replication. *Biotechnol Lett*. 2016;38(7):1081-1088. doi:10.1007/s10529-016-2086-3.
258. Löwik DWPM. Dodging Endosomes: Effective Cytosolic Antibody Delivery. *ChemBioChem*. 2017;18(22):2196-2198. doi:10.1002/cbic.201700510.
259. Bruce VJ, Lopez-Islas M, McNaughton BR. Resurfaced cell-penetrating nanobodies: A potentially general scaffold for intracellularly targeted protein discovery. *Protein Sci*. 2016;25(6):1129-1137. doi:10.1002/pro.2926.

260. Jittavisutthikul S, Thanongsaksrikul J, Thueng-In K, et al. Humanized-VHH transbodies that inhibit HCV protease and replication. *Viruses*. 2015;7(4):2030-2056. doi:10.3390/v7042030.
261. Pant N, Hultberg A, Zhao Y, et al. Lactobacilli Expressing Variable Domain of Llama Heavy-Chain Antibody Fragments (Lactobodies) Confer Protection against Rotavirus-Induced Diarrhea. *J Infect Dis*. 2006;194(11):1580-1588. doi:10.1086/508747.
262. Tokuhara D, Álvarez B, Mejima M, et al. Rice-based oral antibody fragment prophylaxis and therapy against rotavirus infection. *J Clin Invest*. 2013. doi:10.1172/JCI70266.
263. Moonens K, Van Den Broeck I, Okello E, et al. Structural insight in the inhibition of adherence of F4 fimbriae producing Enterotoxigenic Escherichia coli by llama single domain antibodies. *Vet Res*. 2015;46(1):1-7. doi:10.1186/s13567-015-0151-x.
264. Harmsen MM, Van Solt CB, Van Zijderveld-Van Bemmel AM, Niewold TA, Van Zijderveld FG. Selection and optimization of proteolytically stable llama single-domain antibody fragments for oral immunotherapy. *Appl Microbiol Biotechnol*. 2006;72(3):544-551. doi:10.1007/s00253-005-0300-7.
265. Sarker SA, Jäkel M, Sultana S, et al. Anti-rotavirus protein reduces stool output in infants with diarrhea: A randomized placebo-controlled trial. *Gastroenterology*. 2013;145(4):740-748.e8. doi:10.1053/j.gastro.2013.06.053.
266. Maffey L, Vega CG, Parreno V, Garaicoechea L. Controlling Rotavirus-associated diarrhea: Could single-domain antibody fragments make the difference? *Rev Argent Microbiol*. 2015;47(4):368-379. doi:10.1016/j.ram.2015.09.005.
267. Power UF, Stortelers C, Allosery K, Melero JA. Generation and Characterization of ALX-0171 , a Potent Novel Therapeutic Nanobody for the Treatment of Respiratory Syncytial Virus Infection. *Antimicrob Agents Chemother*. 2016;60(1):6-13. doi:10.1128/AAC.01802-15.Address.
268. Van Heeke G, Allosery K, De Brabandere V, De Smedt T, Detalle L, de Fougerolles A. Nanobodies® as inhaled biotherapeutics for lung diseases. *Pharmacol Ther*. 2017;169:47-56. doi:10.1016/j.pharmthera.2016.06.012.
269. Virdi V, Coddens A, De Buck S, et al. Orally fed seeds producing designer IgAs protect weaned piglets against enterotoxigenic Escherichia coli infection. *Proc Natl Acad Sci*. 2013;110(29):11809-11814. doi:10.1073/pnas.1301975110.
270. Ardekani LS, Gargari SLM, Rasooli I, et al. A novel nanobody against urease activity of Helicobacter pylori. *Int J Infect Dis*. 2013;17(9):e723-e728. doi:10.1016/j.ijid.2013.02.015.
271. Stijlemans B, Conrath K, Cortez-Retamozo V, et al. Efficient targeting of conserved cryptic epitopes of infectious agents by single domain antibodies: African trypanosomes as paradigm. *J Biol Chem*. 2004;279(2):1256-1261. doi:10.1074/jbc.M307341200.
272. Arias JL, Unciti-Broceta JD, Maceira J, et al. Nanobody conjugated PLGA nanoparticles for active targeting of African Trypanosomiasis. *J Control Release*. 2015;197:190-198. doi:10.1016/j.jconrel.2014.11.002.
273. Dolk E, Van Der Vaart M, Hulsik DL, et al. Isolation of llama antibody fragments for prevention of dandruff by phage display in shampoo. *Appl Environ Microbiol*. 2005;71(1):442-450. doi:10.1128/AEM.71.1.442-450.2005.
274. Hmila I, Cosyns B, Tounsi H, et al. Pre-clinical studies of toxin-specific Nanobodies: Evidence of in vivo efficacy to prevent fatal disturbances provoked by scorpion envenoming. *Toxicol Appl Pharmacol*. 2012;264(2):222-231. doi:10.1016/j.taap.2012.07.033.
275. Yardehnavi N, Behdani M, Bagheri KP, et al. A camelid antibody candidate for development of a therapeutic agent against Hemiscorpius lepturus envenomation. *FASEB J*. 2014;28(9):4004-4014. doi:10.1096/fj.13-247478.
276. Richard G, Meyers AJ, McLean MD, Arbabi-Ghahroudi M, MacKenzie R, Hall JC. In Vivo Neutralization of α-Cobratoxin with High-Affinity Llama Single-Domain Antibodies (VHHs) and a VHH-Fc Antibody. *PLoS One*. 2013;8(7):1-14. doi:10.1371/journal.pone.0069495.
277. El Khattabi M, Adams H, Heezius E, et al. Llama single-chain antibody that blocks lipopolysaccharide binding and signaling: Prospects for therapeutic applications. *Clin Vaccine Immunol*. 2006;13(10):1079-1086. doi:10.1128/CVI.00107-06.
278. Goldman ER, Andersen GP, Liu JL, et al. Facile generation of heat-stable antiviral and antitoxin single

domain antibodies from a semisynthetic llama library. *Anal Chem*. 2006;78(24):8245-8255. doi:10.1021/ac0610053.

279. Moayeri M, Leysath CE, Tremblay JM, et al. A heterodimer of a VHH (variable domains of camelid heavy chain-only) antibody that inhibits anthrax toxin cell binding linked to a VHH antibody that blocks oligomer formation is highly protective in an anthrax spore challenge model. *J Biol Chem*. 2015;290(10):6584-6595. doi:10.1074/jbc.M114.627943.

280. Swain MD, Anderson GP, Zabetakis D, et al. Llama-derived single-domain antibodies for the detection of botulinum A neurotoxin. *Anal Bioanal Chem*. 2010;398(1):339-348. doi:10.1007/s00216-010-3905-3.

Aim of the project

Aim of the project

Since nanobodies (Nb) are taking powerfully their place in biological and medical fields, the development of new technologies for their expression and discovery are growing exponentially[1].

In this evolving context, my Ph.D. project is located and has the aim of developing a novel platform for Nb expression, selection and improvement to render them appropriate for future applications. The platform is based on a scaffold used for Nb expression and selection. Among known camelid VHHs, 783 non-redundant llama sequences were selected from ABVDDB database (http://swift.cmbi.ru.nl/mcsis /systems/ABVDDB/) because were the most abundant and had the predominant presence of only one S-S bridge[2]. The alignment of the aforesaid sequences allowed me to obtain a consensus scaffold consisting of the conserved regions (framework regions, FRs) in which every position is occupied by the most represented amino acid in the alignment.

The use of this consensus framework scaffold (CFW) as universal acceptor of natural or artificial Nbs complementary determining regions (CDRs) is expected to permit bacterial expression of soluble and stable antibodies. Comparing to expression and selection of natural VHHs, these new Nbs with homogenous FRs should permit the standardization of their production and application protocols[3].

Starting from these assumptions, once established the possibility to obtain high-expressed, soluble and functional Nbs after CDRs grafting in the consensus scaffold, I set different goals to develop a functional platform for new Nbs selection and for their improvement for diagnostic and therapeutic applications:

1. By keeping the CFW as constant scaffold if artificial semi-random sequences, corresponding to the hypervariable CDRs, are grafted into it, a library of different artificial potential binders can be obtained. Thus I decided to build a semi-random artificial Nb library from which potential binders against any target of interest can be selected. I chose Ribosome Display as selection method because allows reaching a very high library complexity simulating the natural llama Nb repertoire so as to increase the possibility to select new binders[4] (Chapter 1).

2. To reduce the risk of immune rejection before their application on patients antibodies need to be humanized (i.e. render their sequence as similar as possible to human antibodies). For this reason, I decided to humanize the sequence of the CFW scaffold (hCFW) to render it suitable for human applications. Altering the sequence of functional antibodies can modify their solubility and activity[5]; thus after hCFW validation, I decided to build a humanized version of the semi-random

artificial Nb library to select already humanized new Nbs. I have chosen to use Phage Display as a selection method because is the easiest and most widespread technique and can be applied in almost every laboratory exploiting simple methodologies[6]. I also established to develop a new vector suitable for speeding up Phage Display selection (Chapter 2).

3. The low immunogenicity of Nbs can be an advantage in the therapeutic field but is a limitation for diagnostic applications because secondary antibodies against VHHs cannot be elicited[7]. In order to solve this problem, I decided to develop a quick and cheap method to conjugate Nbs to a part of immunoglobulin constant region (Fc region) for rendering them detectable through secondary antibodies. Since the direct fusion of Nbs to immunoglobulins Fc regions usually leads to difficult-to-express proteins[8], I introduced an *in vitro* protein ligation system (i.e. SpyTag - SpyCatcher[9]) for building conjugated VHH-Fc starting from already expressed modular peptides (Chapter 3).

4. In collaboration with the company Preclinics (Potsdam, Germany), I chose to develop a new method for the production of novel imaging probes suitable for preclinical studies. Fusing a CFW-derivative Nb to a small novel luciferase (NanoLuc)[10], a small antibody detectable through luminescence might be obtained. The novel probes are expected to be small, cheap, easily detectable and safe for the operator, unlike radionuclides labelled ones. Their potential commercialization will boost the nascent application of luciferases in preclinical *in vivo* imaging[11] (Chapter 4).

Therefore, exploiting CFW and hCFW scaffold features, selection of new Nbs for diagnostic or therapeutic purposes will be possible. All these goals taken together will provide my laboratory of complete novel platforms for the selection and the production of soluble and stable new Nbs.

Bibliography

1. Ingram JR, Schmidt FI, Ploegh HL. Exploiting Nanobodies' Singular Traits. *Annu Rev Immunol*. 2018;36(1):695-715. doi:10.1146/annurev-immunol-042617-053327.
2. Muyldermans S. Nanobodies : Natural Single-Domain Antibodies. 2013. doi:10.1146/annurev-biochem-063011-092449.
3. Saerens D, Pellis M, Loris R, et al. Identification of a universal VHH framework to graft non-canonical antigen-binding loops of camel single-domain antibodies. *J Mol Biol*. 2005;352(3):597-607. doi:10.1016/j.jmb.2005.07.038.
4. Zahnd C, Amstutz P, Plückthun A. Ribosome display: Selecting and evolving proteins in vitro that specifically bind to a target. *Nat Methods*. 2007. doi:10.1038/nmeth1003.
5. Vincke C, Loris R, Saerens D, Martinez-Rodriguez S, Muyldermans S, Conrath K. General strategy to humanize a camelid single-domain antibody and identification of a universal humanized nanobody scaffold. *J Biol Chem*. 2009;284(5):3273-3284. doi:10.1074/jbc.M806889200.
6. Lee CMY, Iorno N, Sierro F, Christ D. Selection of human antibody fragments by phage display. *Nat Protoc*. 2007;2(11):3001-3008. doi:10.1038/nprot.2007.448.
7. Bannas P, Hambach J, Koch-Nolte F. Nanobodies and nanobody-based human heavy chain antibodies as antitumor therapeutics. *Front Immunol*. 2017;8(NOV):1-13. doi:10.3389/fimmu.2017.01603.
8. Djender S, Schneider A, Beugnet A, et al. Bacterial cytoplasm as an effective cell compartment for producing functional VHH-based affinity reagents and Camelidae IgG-like recombinant antibodies. *Microb Cell Fact*. 2014:1-10. doi:10.1186/s12934-014-0140-1.
9. Zakeri B, Fierer JO, Celik E, et al. Peptide tag forming a rapid covalent bond to a protein, through engineering a bacterial adhesin. *Proc Natl Acad Sci U S A*. 2012;109(12):E690-7. doi:10.1073/pnas.1115485109.
10. Hall MP, Unch J, Binkowski BF, et al. Engineered luciferase reporter from a deep sea shrimp utilizing a novel imidazopyrazinone substrate. *ACS Chem Biol*. 2012;7(11):1848-1857. doi:10.1021/cb3002478.
11. Mezzanotte L, van 't Root M, Karatas H, Goun EA, Löwik CWGM. In Vivo Molecular Bioluminescence Imaging: New Tools and Applications. *Trends Biotechnol*. 2017;35(7):640-652. doi:10.1016/j.tibtech.2017.03.012.

Chapter 1

Chapter 1: A synthetic ribosome display-selectable nanobody library matching the complexity of the natural camelid heavy-chain antibody repertoire

1. Introduction

Since the discovery of camelid heavy-chain antibodies[1], their single-domain antigen-binding fragments, known as VHHs or nanobodies (Nb), have received great interest as robust bio-reagents for a variety of diagnostic (including basic research) and therapeutic applications.

Nbs usually display binding affinities similar to those of conventional antibodies but with a number of unique favorable features compared, for example, to monoclonal antibodies. These include: i) an extremely small size of ~15 kDa, which is considerably lower than that of conventional antibodies (~150 kDa) and their Fab (~50 kDa) and scFv (~25 kDa) derivatives as well[2–4]; ii) a generally higher thermal stability and ease of expression in bacterial hosts, afforded by their single-domain nature and strict monomeric behavior[5]; iii) an intrinsically high degree of humanization and a concomitantly reduced reactogenicity in humans due to the high amino acid sequence identity shared with the human type III VH domain (VH_3)[3]; iv) the ability, due to their small size and preference for concave-shaped epitopes (e.g., the catalytic sites of enzymes), to recognize and interact with antigen surfaces that are largely inaccessible to conventional antibodies[6,7].

Nbs are being increasingly employed for various *in vivo* imaging applications as radionuclide-labeled, optical or ultrasound probes. Thanks to their high binding specificity and small size, Nb-based probes can produce very high-contrast images of target antigen expressing tissues in various disease models[8]. Cytotoxic compound- (or otherwise) conjugated Nb derivatives are also being employed as anti-cancer therapeutics by exploiting their ability to bind tumor antigens with high affinity and specificity, coupled to the rapid clearance of the unbound species via renal elimination[2,3,8,9]. Similar to monoclonal antibodies, several VHHs are indeed being developed as new magic bullets for cancer therapy and some of them are currently being evaluated in phase I and II clinical trials[10]. Nbs are also being increasingly utilized as key reagents for basic research. For example, in assisting the crystallization of difficult proteins by limiting domain/loop mobility, by stabilizing protein-conjugated polysaccharides and/or increasing protein solubility as well as by providing crystallization-promoting intermolecular contacts to otherwise difficult to handle membrane proteins[11].

Nb isolation and production normally starts from immunization of a camelid, most often small camelids such as llamas (*Lama glama*) due to their relatively small size, ease of breeding and vaccination. Immunization usually requires two months of weekly antigen administrations, followed by blood sample collection and lymphocyte isolation. Lymphocyte total RNA is then extracted, reverse-transcribed, and the resulting cDNA, amplified by PCR, is cloned into a phage display vector, typically leading to a Nb library complexity of approximately 10^7-10^9 independent clones[12]. Three to four rounds of phage display are usually sufficient to isolate tens of individual candidate clones which are then randomly analyzed (and scored) by ELISA and other techniques with regard to their target binding affinity and specificity. The whole selection process thus takes approximately 3-4 months altogether and is usually quite expensive. In some extreme cases, this kind of *in vivo*-generated immune Nb library cannot be obtained, for instance when animal immunization is precluded by strong antigen toxicity or pathogenicity[12–15].

Animal immunization can be avoided through the implementation of naïve or synthetic libraries. However, with the most common selection techniques such as phage display, library size is almost always limited by transformation efficiency (no more than ~10^9 independent transformants), thus leading to a final complexity about three orders of magnitude lower than the estimated natural Nb diversity (~10^{12})[16–18]. Due to this limited library size, the target affinity of the Nbs retrieved from multiple panning steps may be insufficient for some applications, and additional time-consuming steps, such as the creation of sub-libraries via CDR codon randomization, have to be performed in order to improve binding affinity[19].

At variance with the above *in vivo* selection approaches, ribosome display (RD) is a potent, completely *in vitro* technique, capable of selecting (and evolving) proteins/peptides from naïve libraries of very high complexity based on their ability to bind to any target of interest[20,21]. The starting library can thus contain more than 10^{12} different DNA molecules in the form of PCR fragments, but what further distinguishes RD from other selection technologies is that it includes a PCR amplification step, thus allowing for additional sequence variation and a further increase of the actual size of the library[22]. This additional randomization step can be achieved at each selection cycle via DNA shuffling and/or error-prone PCR, in a process that resembles antibody affinity maturation. Another advantage of RD-based selection is that by relying on a linear DNA library generated by PCR, it avoids the time-consuming and often not fully efficient vector ligation and bacterial transformation steps. Accordingly, a complete RD selection (3-4 cycles) can be performed in 2-3 weeks compared to the 3-4 months required by conventional selection approaches starting from animal immunization.

Here, we report the design, construction and validation of a large DNA library (>10^{12} individual members) suitable for ribosome display, based on consensus Nb framework sequence as scaffold. Chimeric Nbs obtained by grafting CDRs from natural Nbs into the designed framework are well expressed in *E. coli* as soluble intracellular proteins with a target-binding affinity nearly identical to that of the donor Nbs. The constructed combinatorial library has the expected complexity and is suitable for RD selection, as highlighted by the identification of new maltose binding protein (MBP) binders.

2. Materials and methods

2.1 Molecular biology reagents

Standard protocols[23] were used for all basic recombinant DNA procedures. Enzymes were from Takara Bio Europe (Saint-Germain-en Laye, France), New England Biolabs (Ipswich, MA, USA) and Fermentas (Thermo Fisher Scientific, Waltham, MA, USA). Molecular cloning and recombinant protein expression were carried out in XL1-Blue and BL21 *E. coli* strains (Stratagene; La Jolla, CA, USA), using the pRDV (GenBank accession code AY327136), pET28 (Merck Millipore, Darmstadt, Germany) and pGEX-4T-2 (GenBank accession code U13854.1) plasmids. Following appropriate design (see below), synthesis of the GFPwt, Gcons and Lcons Nbs-encoding sequences was performed by Eurofins Genomicss (Ebersberg, Germany), all protein-encoding sequences were optimized with respect to the *E. coli* codon usage. An *Nco*I site at the 5' end and a *Hind*III site at the 3' end were introduced in both pRDV and pET28 in order to achieve directional cloning (see **Table 1**).

Name	**Sequence**[1]
Gwt	QVQLVESGGALVQPGGSLRLSCAASG**FPVNRYSMRWY**RQAP GKERE**W**VA**GMSSAGDRSS**YEDSVKGRFTISRDDARNTVYLQ MNSLKPEDTAVYYCNV**NVGFE**YWGQGTQVTVSS
Gcons	QVQLQESGGGLVQAGGSLRLSCAASG**FPVNRYSMRWY**RQAP GKERE**F**VA**GMSSAGDRSS**YADSVKGRFTISRDNAKNTVYLQ MNSLKPEDTAVYYCAA**NVGFE**YWGQGTQVTVSS
Lcons[2]	QVQLQESGGGLVQAGGSLRLSCAASG**YIASINYLGWF**RQAP GKERE**F**VA**AVSPAGGTPY**YADSVKGRFTISRDNAKNTVYLQ MNSLKPEDTAVYYCAA**ARQGWYIPLNSYGYN**YWGQGTQVTV SS

Table 1 Amino acid sequences of the synthetic chimeric Nbs produced and characterized in this chapter.
[1] CDR sequences are shown in blue.
[2] Structurally critical amino acid residue 47 is shown in red. Phe47 was mutated to Gly in the LconsBM construct.

Maltose binding protein sequence was PCR-amplified from pMAL (New England Biolabs, Ipswich, MA, USA) plasmid introducing *EcoRI* sites at 5' and 3' ends (see **Table 2**).

Name	**Sequence**[1,2]
MBP-plus	tccgcgtggatccccagGAATTCcaATGAAAATAAAAACAGGTGCAC
MBP-minus	cgctcgagtcgacccggGAATTCTCAAGTCTGCGCGTCTTTCA

Table 2 Primers used for amplification of maltose binding protein (MBP) nucleotide sequence from pMAL plasmid.

[1] *EcoRI* sites are shown in blue, stop codon is shown in red

[2] Uppercase letters indicate pMAL annealing sites

PCR was performed with 1 unit Phusion DNA Polymerase (New England Biolabs, Ipswich, MA, USA) in presence of the oligonucleotides (4 nM each), plus dNTPs (0.8 mM), 1x PCR buffer and 10 ng pMAL in a final volume of 50 µl: initial denaturation 98°C, 1 min; 25 cycles of 10 s at 98°C, 30 s at 58°C, and 90 s at 72°C; additional extension 72°C, 7 min. Ligation of MBP encoding sequence in the pGEX plasmid was performed following standard protocols[23].

2.2 Bioinformatic analysis

Llama Nb sequences, retrieved from the ABVDDB database (http://swift.cmbi.ru.nl/mcsis/systems/ABVDDB/), were aligned with MEGA (http://www.megasoftware.net/) and amino acid frequencies at any given position were determined and visualized with the GeneDoc software (http://genedoc.software.informer.com/2.7/). Logo representation of the amino acid consensus sequence was made with the WebLogo 3 software (http://weblogo.berkeley.edu/logo.cgi). Statistical significance of amino acid distributions at randomized positions of individual library members was assessed with the χ^2-test.

2.3 Recombinant protein expression and purification

Standard procedures were used for recombinant Nb expression. Briefly, 10 ml of stationary overnight cultures (LB, 100 mg/l of ampicillin or 50 mg/l of kanamycin at 37 °C) were inoculated into 1 l cultures of the same media. After reaching an A_{600} value of 0.5-0.7, cultures were induced with 1 mM IPTG and further incubated for 3-4 hours at 37°C, except for library-derived Nbs whose expression was performed at 20°C overnight. Following centrifugation (8000 g, 15 min), bacterial cell pellets were recovered, resuspended in 100 ml of Tris-buffered saline (TBS, pH 9.0, freshly supplemented with protease inhibitors), and lysed by sonication (20 min total sonication time performed with

3 sec bursts alternated with 6 sec resting on ice) carried out at constant power (4W/cm^2; Sonicator 3000, Misonix). Lysates were then centrifuged (10000 g, 20 min) and the resulting supernatants were used as starting material for metal-affinity purification using a built-in 6xHis-tag and a His-select cobalt affinity resin (Sigma-Aldrich, Saint Louis, MO, USA) as per manufacturer's instructions. Bacterial lysates and individual metal-affinity chromatography fractions were analyzed by SDS-PAGE on 14% polyacrylamide gels.
Recombinant GST-MBP used in this work was expressed following the protocol described above for library-derived Nbs and purified using MBPTrap HP (GE Healthcare, Little Chalfont, UK) as per manufacturer's instructions. Bacterial lysates and individual eluted fractions were analyzed by SDS-PAGE on 11% polyacrylamide gels.
Recombinant green fluorescent protein (GFP) used in this work is enhanced GFP[24]. Biotinylated GFP, maltose binding protein (MBP) and thioredoxin (Trx) for RD tests were produced *in vivo* by cloning the corresponding genes into the pAT222 vector (GenBan accession number AY327138)[25], followed by co-transformation with the biotinylating enzyme (BirA)-encoding plasmid pBirAcm (Avidity) and metal-affinity purification of the resulting proteins as above. Chicken egg white lysozyme was biotinylated *in vitro* with the biotin-N-hydroxysuccinimide ester reagent (Sigma-Aldrich) as per manufacturer's instructions.

2.4 Synthesis of the RD-selectable nanobody library

The Nb library was generated by multiple steps of assembly PCR using the PAGE-purified oligonucleotides (Microsynth, Balgach, Switzerland) listed in **Table 3** and the Phusion DNA polymerase New England Biolabs (Ipswich, MA, USA); individual PCR products were agarose gel-purified using a Macherey-Nagel kit (Düren, Germany).
PCR1: the oligonucleotides T7b and FR1-RE were used to amplify the pRDV-cloned Gcons gene (Initial denaturation 98°C, 20 s; 28 cycles of 10 s at 98°C, 30 s at 55°C, and 30 s at 72°C; additional extension 72°C, 5 min), to generate a final product containing FR1 preceded by a T7 promoter and a RBS.

Name	Sequence[1]
T7B	ATACGAAATTAATACGACTCACTATAGGGAGACCACAACGG
FR1-RE	ACCTGACGCTGCACATGAC
CDR1-FW[2]	GTCATGTGCAGCGTCAGGTMGTAYTTTTTCGRDTWATRCTATKGSTTGGTWTCGTCAAG CACCAGGGAAAG
FR2-RE	AATGGCGGCCACAAACTCGCGTTCTTTCCCTGGTGCTTGACG
CDR2-FW[2]	CGAGTTTGTGGCCGCCATTAVTWSGRGTGRTGRTAVKACCTATTATGCGGATTCCGTGA AAGGA
FR3-RE	CGCAGCGCAATAGTAGACAG
CDR3-FW[2]	CTGTCTACTATTGCGCTGCGSVTMSTVGTNHYNHYVGTNHYNHYYHTWMTVNTBCTVNT RVKTWTRRTTATTGGGGCCAGGGTACTC
tolAkurz	CCGCACACCAGTAAGGTGTGCGGTTTCAGTTGCCGCTTTCTTTCT
pRDV_NcoI_for	GTTTAACTTTAAGAAGGAGATATATCCATGG
JSCRDir2	ATCTGCTTCGGCCTTCGCTTTAGCATCTGCCGCCGCTTTCG

Table 3 Oligonucleotides utilized in this chapter.

[1]Sequences are shown in a standard 5'-3' orientation.

[2]The standard one-letter abbreviation nomenclature for specific subsets of nucleotides is used, where: M represents A, or C; Y represents C or T; R represents A, or G; D represents A, G or T; W represents A, or T; K represents G or T; S represents C or G; V represents A, C or G; H represents A, C or T; B represents C, G or T; and N represents any of the four nucleotides.

PCR2: the oligonucleotides CDR1 and FR2-RE (4 nM each), plus dNTPs (0.8 mM), 1x PCR buffer and 1 unit of Phusion DNA polymerase in a final volume of 50 µl, were fused together by PCR (condition as PCR1 except 20 cycles and no additional extension). The purified PCR1 product (100 ng) was then added, together with DNA polymerase (0.5 units) and dNTPs (0.4 mM), and another 20 cycles of PCR amplification were performed. This was followed by the addition of oligonucleotides T7b and FR2-RE (0.5 µM each) plus DNA polymerase and dNTPs as above, and a further round of PCR amplification (condition as PCR1) to generate a final product containing FR1, CDR1 and FR2, flanked by a T7 promoter and RBS.

PCR3: the oligonucleotides CDR2-FW and FR3-RE were used to PCR-amplify the pRDV-cloned Gcons gene (condition as PCR1) and to generate an amplicon bearing the CDR2 and the FR3.

PCR4: the oligonucleotides CDR3-FW and tolAkurz were used to amplify the pRDV-cloned Gcons gene (condition as PCR1) and to generate a final product containing the CDR3, FR4 and spacer present in the RD construct.

PCR5: 40 ng and 30 ng of the purified PCR2 and PCR3 products, respectively, were fused together by PCR (condition as PCR1 except for 20 cycles and no additional extension) carried out in the presence of dNTPs (0.8 mM), 1x PCR buffer, and 1 unit of DNA polymerase in a final volume of 50 µl. The fused product upon supplementation of oligonucleotides T7b and FR3-RE (0.5 µM each), dNTPs (0.4 mM) and 0.5 units of DNA

polymerase was PCR amplified (condition as PCR1 except 60 s of the cycle extension time). The final product contains FR1, CDR1, FR2, CDR2 and FR3, flanked by a T7 promoter and RBS.

PCR6: the purified PCR4 and PCR5 products (50 ng each) were fused together by 25 cycles of PCR amplification (condition as PCR1 except 60 s of the cycle extension time and no additional extension) carried out in the presence of dNTPs (0.8 mM), 1x PCR buffer, and 1 unit of DNA polymerase in a final volume of 50 µl. This was followed by addition of oligonucleotides T7b and tolAkurz (0.5 µM each), dNTPs (0.4 mM) and DNA polymerase (0.5 units), and amplification of the fused product (condition as PCR1 except 60 s of the cycle extension time) to generate the complete RD-library. PCR6 was repeated 12 times in order reach a library complexity of approximately 10^{12}.

2.5 Ribosome display

The synthetic Nb genes were amplified by PCR using oligonucleotides T7b and tolAkurz as primers (oligonucleotides (4 nM each), plus dNTPs (0.8 mM), 1x PCR buffer, 1 unit Vent DNA polymerase (New England Biolabs, Ipswich, MA, USA) 100 ng of library in a final volume of 50 µl: initial denaturation 95°C, 3 min; 25 cycles of 30 s at 95°C, 30 s at 55°C, and 45 s at 72°C; additional extension 72°C, 5 min). The amplified DNA was transcribed and RD selection was performed as described previously[26–28]. For each round of ribosome display, polystyrene 96 wells microtiter plates (SpectraPlate-96 HB; Perkin Elmer, Waltham, MA, USA) were coated with 66 nM neutravidin (Pierce, Waltham, MA, USA; 100 µl/well) dissolved in TBS for 1 hr at room temperature; the wells were then blocked with 0.5% (w/v) BSA in TBS for 1 hr at 4°C shaking the plate at 600 rpm, followed by the addition and immobilization of the biotinylated target (500 nM) by incubation for 1 hour at 4°C shaking the plate at 600 rpm. The Nb transcripts generated above were used as templates to assemble an *in vitro* translation reaction, which after 20 minutes at 37°C, was stopped by the addition of stop solution[28], transferred to the microtiter plate wells and incubated for another 1 hr at 4°C shaking the plate at 600 rpm. The *in vitro* translation reaction mixture solution was then removed and the wells were washed 6 times with washing buffer[28]. After elution of the bound complexes with elution buffer[28], the mRNA was reverse transcribed (Affinity Script reverse transcriptase; Stratagene), using the JSCRDir2 oligonucleotide as primer. The resulting cDNA was amplified by PCR as above using the pRDV_NcoI_for and JSCRDir2 oligonucleotide primers (see **Table 3**), which anneal on the pRDV vector at external positions with respect to the NcoI and HindIII restriction sites, located, respectively, upstream and downstream to the Nb coding sequence. The PCR-amplified fragments codifying for library Nbs were digested with NcoI and HindIII enzymes and ligated in pRDV vector. Second round and third rounds of

panning were performed following the protocol described above but increasing selection stringency: 66 nM of streptavidin or magnetic streptavidin beads (New England Biolabs, Ipswich, MA, USA) were used as target-capturing agents; 100/50 nM of target proteins were bound to streptavidin, and volume and extent of washing steps were increased. Furthermore, pre-panning steps were carried out as follow: translation stopped reactions were incubated for 1h at 4°C shaking the plate at 600 rpm in only-streptavidin coated wells/beads before incubation of the ternary complexes with the target protein.

2.6 Analysis of RD-selected single clones

Nucleotide sequences codifying for putative Nb binders obtained after the third round of panning were digested with NcoI and HindIII enzymes and cloned in pET28 vector following standard procedures[23]. 192 clones were analyzed for target binding using the following protocol: 10 µl of stationary overnight cultures (LB, 50 mg/l of kanamycin at 37 °C) were inoculated into 1 ml cultures of the same media in 96-well deep well plates (Radnor, PA, USA). After reaching an A_{600} value of 0.5-0.7, cultures were induced with 1 mM IPTG and further incubated overnight at 20°C. Following centrifugation (400 g, 10 min), bacterial cell pellets were recovered, suspended in 900 ml of Tris-buffered saline (TBS, pH 8.0, freshly supplemented with protease inhibitors), and lysed adding 100 µl of FastBreak detergent (Promega, Fitchburg, US) and shaking the plate for 30 min at 500 pm. Lysates were then centrifuged (400 g, 10 min) and the resulting supernatants were used as starting material for ELISA tests.

Polystyrene 96-wells microtiter plates were coated overnight at 4°C with casein-glutathione (prepared and used as previously described[29]) dissolved in carbonate buffer (1 vol. 0.5 M Na_2CO_3 : 4 vol. 0.5 M $NaHCO_3$ pH 9.6). Blocking was performed by incubation for 1 hr at room temperature with PBSC (Phosphate-buffered saline (PBS) pH 7.4 + 0.2% casein), followed by a 1 hr incubation at room temperature with the purified GST-tagged proteins in PBSC (800 nM each). The supernatants deriving from cell lysis were then added and incubated for 1 hr at RT. After incubation with an anti-histidine-tagged protein mouse mAb (Merck Millipore) diluted 1:1000 in PBSC, for 1 hr, a peroxidase-conjugated anti-mouse IgG (whole molecule) goat antibody (Sigma-Aldrich) diluted 1:5000 in PBSC was added. Following an additional 1 hr incubation at RT, wells were filled with the 2,2'-azino-di-[3-ethylbenzthiazoline sulfonate (ABTS) substrate (KPL, Gaithersburg, MD, USA) and absorbance was measured at 415 nm with a microplate reader (iMark, Biorad). Wells were washed with PBS containing 0.3% (v/v) Tween20 after each incubation step.

2.7 Surface plasmon resonance

All experiments were performed on a ProteOn XPR 36 instrument (Biorad, Hercules, California, U.S.A) in phosphate buffer saline (PBS) containing 0.005% Tween 20. Four hundred (for Gcons) and 150 (for Gwt) response units (RU) of *in vivo* biotinylated GFP were immobilized on two lanes of a neutravidin sensor chip, the sensor surface for the Gwt Nb was additionally blocked with Amine-PEG_2-biotin (Thermo Scientific). 16, 4, 1, 0.25 and 0.063 nM of Gcons and 9, 3, 1, 0.33 and 0.11 nM of the Gwt Nb were injected for 300s. Biotinylated lysozyme was immobilized at a surface density of 290 RU, and 300, 100, 33, 11, 3.7 and 1.2 nM of Lcons was injected for 300s. Dissociation times were varied depending on the off-rates between 300 s and 2200s. All data were double-referenced and fit to a 1:1 Langmuir model using the ProteOn Manger software (http://www.bio-rad.com/en-us/product/proteon-manager-software).

2.8 Other procedures

The Ellman reagent [5,5-dithiobis-(2-nitrobenzoic acid), DTNB; Sigma Aldrich; $\varepsilon_{(412\ nm)}$ = 14150 M^{-1} cm^{-1}] was used to quantify free SH groups. The assay was conducted in a final volume of 150 µl containing 0.1 mM DTNB and 2% SDS in 50 mM PBS (pH 8.0); a calibration curve was constructed with increasing concentrations of N-acetylcysteine (Sigma-Aldrich). The number of free cysteine residues/protein molecule was determined by dividing the concentration of DTNB-reactive SH groups by the concentration of protein utilized for the assay.

Biotinylated Lysozyme and GFP (see above) were used as capture proteins for ELISAs. Polystyrene 96-wells microtiter plates were coated overnight at 4°C with 66 nM neutravidin dissolved in TBS pH 7.5. Blocking was performed by incubation for 1 hr at room temperature with 0.5% BSA in TBS, followed by a 1 hr incubation at 4°C with the purified biotinylated proteins in TBS (1 µM each). The Nbs (1 µM each) dissolved in TBS were then added and incubated for 1 hr. After incubation with an anti-histidine-tagged protein mouse mAb (Merck Millipore) diluted 1:50 in PBS for 45 min., a peroxidase-conjugated anti-mouse IgG (whole molecule) goat antibody (Sigma-Aldrich) diluted 1:2000 in PBS was added. Following an additional 45 min. incubation at RT, wells were filled with the 2,2'-azino-di-[3-ethylbenzthiazoline sulfonate (ABTS) substrate (KPL, Gaithersburg, MD, USA) and absorbance was measured at 415 nm with a microplate reader (iMark, Biorad). Wells were washed with TBS containing 0.5% (v/v) Tween20 after each incubation step.

After single clones analysis, investigation of putative binders was performed through ELISA test using positive Nbs purified as described above. Following the protocol

described in 2.6 section, 800 nM of purified Nbs were used in place of bacterial crude extracts.

Reverse ELISA was performed using the following protocol: polystyrene 96-wells microtiter plates were coated overnight at 4°C with 800 nM of purified Nbs dissolved in PBS pH 7.4. Blocking was performed by incubation for 1 hr at RT with PBSC, followed by a 1 hr incubation at 4°C with serial 1:2 dilution of purified GST-tagged proteins in PBSC (starting from 800 nM each). After incubation with an anti-GST protein rabbit mAb (kindly provided by Dr. Barbara Montanini) diluted 1:2000 in PBSC for 1hr., a peroxidase-conjugated anti-rabbit IgG (whole molecule) goat antibody (Sigma-Aldrich) diluted 1:20000 in PBSC was added. Following an additional 1hr incubation at RT, wells were filled with the 2,2'-azino-di-[3-ethylbenzthiazoline sulfonate (ABTS) substrate (KPL, Gaithersburg, MD, USA) and absorbance was measured at 415 nm with a microplate reader (iMark, Biorad). Wells were washed with PBS containing 0.3% (v/v) Tween20 after each incubation step. ELISA tests were triplicated and analyzed with Student's T test (two-tailed, heteroscedastic).

3. Results

3.1 Consensus sequence library design

The first step in the design of our Nb consensus sequence library relied on the ABVDDB database (http://swift.cmbi.ru.nl/mcsis/systems/ABVDDB/), a well-annotated and extensive dataset that provides a large number of proprietary and public Nb sequences from camel (424), llama (1152) and other camelid species (92 sequences). Because of its larger size and the predominant presence of only one S-S bridge[30], the llama sequence dataset was chosen as primary reference, and following manual filtration to remove redundant and truncated entries, it was reduced to a final size of 783 unique sequences.

As shown by the logo representation in **Figure 1A**, the alignment of this Nb sequence dataset with ClustalW revealed the presence of four conserved framework regions (FR1-4) and three hypervariable regions (CDR1-3) resulting from somatic DNA recombination of different gene segments (V, D and J) as well as somatic hypermutation at some restricted sites. Using a consensus criterion, the most represented amino acids at individual FR positions (see **Figure 1B**) were selected as constituents of the invariable portion of the artificial polypeptide (designated as "consensus framework", CFW) to be used as scaffold for our synthetic Nb library.

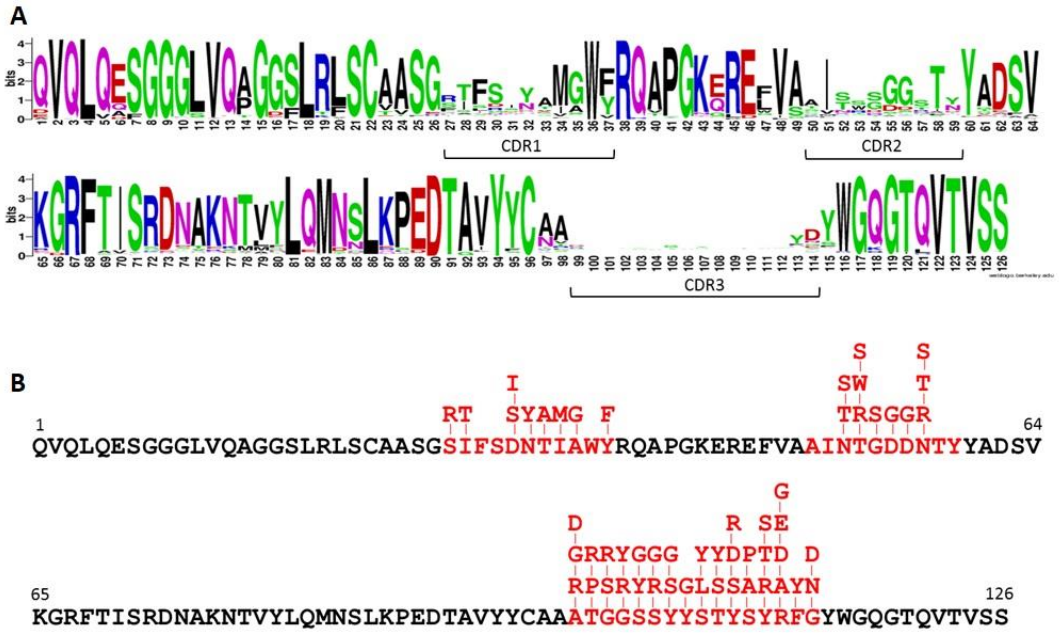

Figure 1 A: Logo representation of amino acid multiple sequence alignment of Llama VHH from the ABVDDB database. The height of symbols indicates the relative frequency of each amino acid at that position. B: Llama VHH consensus sequence, with framework regions and CDRs written in black and red, respectively. Within the CDRs, all amino acids with a frequency of occurrence higher than 10% are shown.

3.2 Consensus framework validation

To test the reliability and ease of recombinant production afforded by the CFW scaffold, we first determined the *E. coli* expression levels and solubility of two *ad hoc* generated chimeric Nbs bearing the CFW sequence grafted with complementarity determining regions (CDRs) of two natural Nbs of known 3D structure, recognizing, respectively, GFP ([31]; pdb ID: 3K1K) and lysozyme ([7]; pdb ID: 1ZVH). These particular CDRs were chosen because of the very different lengths of their CDR3 regions (5 and 15 residues, respectively, for the GFP- and the lysozyme-binding VHHs) and the broad availability of their targets. A total of nine amino acid substitutions distinguish the wild-type GFP-binding Nb (hereafter designated as Gwt) from the consensus GFP binding Nb (Gcons), whereas the wild-type lysozyme-binding Nb (Lwt) differs from its consensus counterpart (Lcons) at seven positions. Despite the lower overall deviation of Lcons from the Lwt sequence, we note that a non-conservative (Gly→Phe) substitution is present within the structurally critical framework region 2 of the Lcons Nb at position 47, whereas a conservative (Trp→Phe) replacement occurs at the same position of the Gcons Nb (see **Table 1**).

Chemically synthesized DNA sequences coding for Gcons and Lcons were cloned into the pET28 vector for bacterial expression and the resulting recombinant proteins were purified by metal-affinity chromatography using the vector-provided poly-histidine tag (see 'Material and methods' for details). Both Gcons and Lcons polypeptides were well expressed (**Figure 2**) with a final yield of approximately 15 and 10 mg of pure protein/L of bacterial culture for Gcons and Lcons, respectively. The lower yield of the Lcons Nb was likely due to its lower (~60%) solubility compared to the nearly complete solubility of Gcons. In contrast, no more than 3-4 mg of pure protein/L of bacterial culture were obtained with the wild type versions of the two Nbs, even when expressed in the bacterial periplasm[7,31]. For a closer comparison (i.e., both Gcons and Gwt expressed intracellularly), a synthetic version of the Gwt gene was cloned into the intracellular expression vector pET28, but also under these conditions the yield of pure protein was 5-fold lower than that obtained with the Gcons Nb (**Figure 2**).

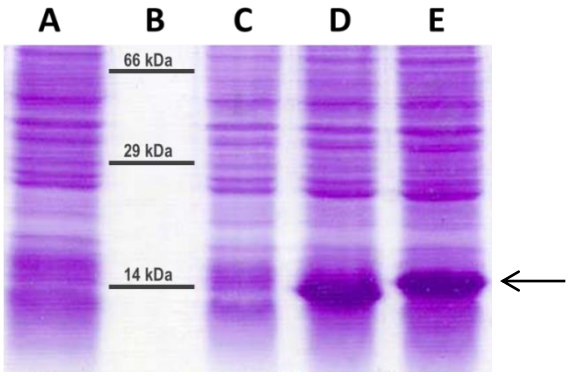

Figure 2 SDS-PAGE analysis of total *E. coli* lysates. A: uninduced cells; B: migration positions of molecular mass markers; C: IPTG-induced Gwt-expressing cells; D: IPTG-induced Gcons-expressing cells E: IPTG-induced Lcons-expressing cells. The arrow indicates the expected migration position of the three recombinant Nbs.

Since the CFW sequence harbors two disulfide-bondable cysteines, we titrated the purified Gcons and Lcons proteins with DTNB in order to examine the oxidation (S-S) state of these amino acids. No free SH-group was detected, thus suggesting a properly folded and disulfide-bonded state of the two synthetic Nbs despite expression in the reducing conditions of the bacterial intracellular environment (data not shown).

Although it was not the main purpose of framework validation, we also wished to assess the target-binding affinity of the two chimeric consensus Nbs. As noted above, one of the amino acid substitutions that distinguish Lcons from its Lwt counterpart is the replacement of Gly47 by a Phe residue within FR2 (see **Table 1**), and the non-conservative replacement of this residue in long CDR3 Nbs such as the anti-lysozyme Nb has previously been shown to cause a disproportionate increase of the off-rate binding constant, thus ultimately impairing target-binding affinity[32]. To gain direct insight on the functional consequences of this particular amino acid substitution, a back-mutated derivative of the Lcons Nb (hereafter designated as LconsBM), bearing a Gly residue at position 47 as in the natural Lwt donor Nb, was also produced.

The affinity of the Gcons Nb for GFP was initially tested spectrophotometrically. As shown in **Figure 3**, upon mixing GFP (4 µM) with the Gcons Nb or its wild type counterpart (Gwt), both at a 4 µM final concentration, there was an increase in GFP absorbance and a shift toward an absorption maximum at 475 nm, which are both diagnostic of Nb-GFP interaction[31]. Under identical experimental conditions, no spectral change was observed after mixing GFP with either the Lcons or the LconsBM Nbs (**Figure 3**). To further assess the GFP binding specificity of Gcons (1 µM), we used ELISAs, which yielded a signal diagnostic of GFP-Nb interaction upon incubation with immobilized biotinylated GFP but not lysozyme (data not shown). When using biotinylated lysozyme as target, instead, a specific ELISA signal was detected with LconsBM, but not Lcons (data not shown).

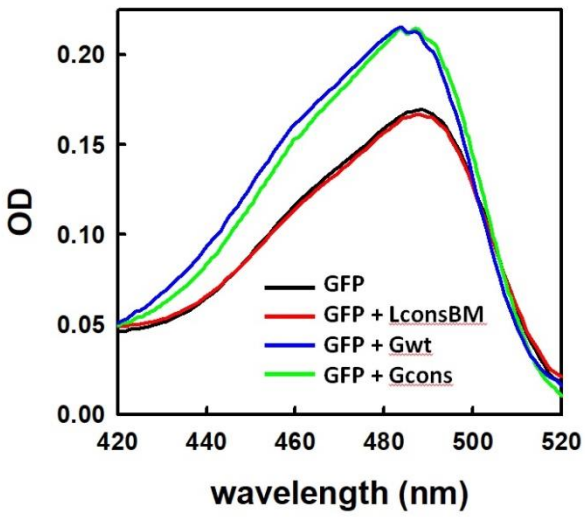

Figure 3 Nb-induced changes of GFP spectral properties. Absorption spectra of GFP only (black line), GFP plus the LconsBM Nb (red line), GFP plus the Gwt Nb (blue line), and GFP plus the Gcons Nb (green line) are shown. An equimolar concentration of GFP and of the indicated Nbs (4 µM each) was present in all samples (see 'Materials and Methods' for details).

The kinetic binding parameters of the Gwt, Gcons, Lcons and LconsBM Nbs for their respective targets were then quantitatively evaluated by Surface Plasmon Resonance (SPR) (**Figure 4**). Dissociation constants (K_d) of 159 and 35 pM were obtained for the Gcons Nb and its wild-type counterpart (Gwt), which in our hands yielded a K_d approximately 17-fold lower than the published (590 pM) K_d value[31]. While the latter discrepancy might be explained by different instrumentation and experimental set-up, the 4.5-fold lower affinity of Gcons compared to Gwt likely reflects framework sequence differences (a total of 9 amino acid substitutions) between the two proteins. In contrast, the calculated K_d of the LconsBM Nb (66 nM) was very similar to the published 77 nM K_d value of its wild type counterpart. As expected, the unmodified Lcons Nb yielded a very high K_d value (~3.5 µM) indicating once again the requirement of Gly47 for high-affinity target binding.

3.3 Ribosome display on synthetic chimeric nanobodies

The DNA sequences coding for the Gcons and LconsBM synthetic Nbs were cloned into the pRDV vector, amplified using the T7b and tolAkurz primers[28], *in vitro* transcribed, and the resulting RNAs were used for a single round of RD selection[26,27], carried out as described in "Materials and Methods". The RD selection targets, GFP and lysozyme, were immobilized on microtiter plates through a biotin tag and utilized as capture antigens in parallel with biotinylated *E. coli* maltose binding protein (MBP) and thioredoxin (Trx), which served as further negative controls. The purified RNAs were *in vitro* translated in order to form ternary complexes comprising the ribosome, the RNA and the corresponding Nb-containing polypeptide. These were added to the wells of microtiter plates containing the target (GFP or Lysozyme) and three control proteins: MBP, Trx and GFP when lysozyme was the target, or MBP, Trx and lysozyme when GFP was the target. After a stringent washing, the target-bound RNA was recovered by elution with a high concentration of EDTA and reverse-transcribed into DNA, which was then amplified by PCR.

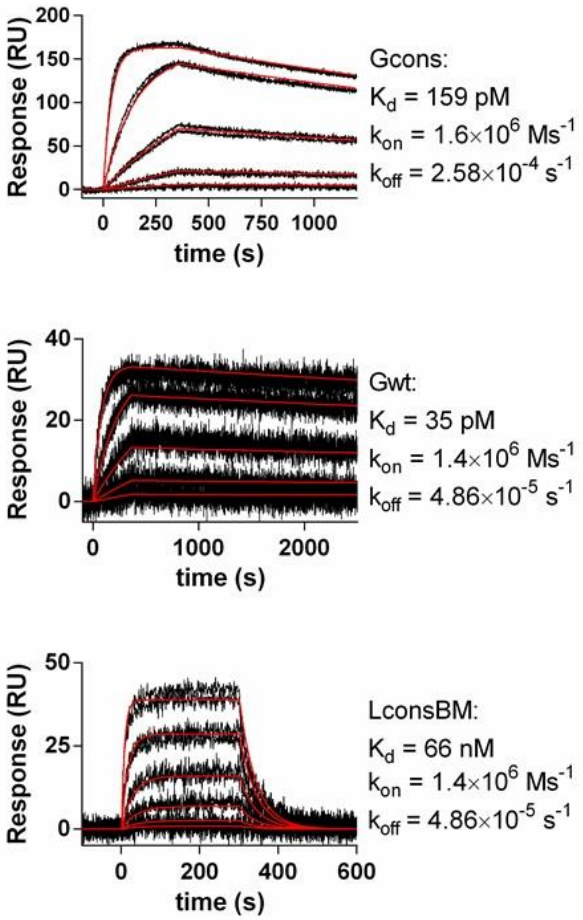

Figure 4 Surface plasmon resonance analysis of the following Nb-target interactions: Gcons-GFP (top), Gwt-GFP (middle), LconsBM-lysozyme (bottom). For each Nb-target pair, the estimated K_d, k_{on} and k_{off} values are indicated; duplicate tracings recorded for each Nb are shown in black and fits to a Langmuir binding-model in red (see "Materials and Methods" for details).

In the presence of ternary complexes bearing the Gcons mRNA, only GFP-containing wells yielded an RT-PCR product of the expected size, while no amplicon was detected in parallel wells containing lysozyme as an unrelated target control, thus pointing to a specific binding of GFP by the Gcons Nb. Conversely, when the LconsBM mRNA was used

as template for *in vitro* translation, an amplicon of the expected size was retrieved from lysozyme- but not GFP-containing wells. In keeping with the previously documented key role of Gly47, no specific binding was detected, also in this case, in the presence of the unmodified Lcons mRNA. Similarly, no Nb-coding amplicon was retrieved with neither of the two additional control proteins (MBP and Trx) (data not shown). These findings indicate that the synthetic anti-GFP and anti-lysozyme CF Nbs are also functional when produced *in vitro* under RD conditions, allowing the recovery of the corresponding mRNAs from a full selection cycle.

3.4 Construction and validation of the nanobody RD-library

Having demonstrated the robustness of our consensus framework as a potentially universal scaffold for the construction of an RD-selectable Nb library, we next designed the variable regions (CDR1, 2 and 3) as partially randomized sequences. To reduce the complexity of the library to a size compatible with its *in vitro* assembly and RD selection, at any given position within the CDRs we selected amino acids present with a frequency higher than 10% in the reference natural Nb sequence dataset (see the multiple sequence alignment in **Figure 1B**). While CDR1 and CDR2 display a nearly constant length due to a reduced variability among all possible V genes, the CDR3 regions have a more variable length caused by DNA recombination events and range in size from 2 to 16 amino acids. Given this size heterogeneity, we decided to use a fixed length of 16 amino acids, which is the most frequently represented among the CDR3s of natural llama Nbs (**Figure 1B**).

A unique, *E. coli* codon usage optimized sequence was used for the design of the CFW region, whereas partially degenerate codons, used for the CDRs, were based on the following restrictions: i) no stop codon should be present; ii) the degenerate nucleotide triplets present at any given position should not encode cysteine, which might form unwanted disulfide bonds; iii) as mentioned above, the chosen codons must code for amino acids with an overall frequency of occurrence in the reference sequence dataset higher than 10%. Because of the restrictions imposed by genetic code degeneration, these led to the exclusion of glycine at positions 103, 105 and 106, and tyrosine at position 109 (even though their frequencies were slightly higher than 10%) and to the incorporation of amino acid residues with a frequency lower than 10% at some other positions. Based on the above design and associated restrictions, the theoretical amino acid composition diversities of the CDR1 and CDR2 sequences are 768 and 576, respectively, whereas a much higher diversity of 1.8×10^{13} applies to the CDR3 sequence. Altogether, the theoretical overall complexity of the resulting combinatorial library thus corresponds to approximately 10^{18} different polypeptide sequences.

As a first step toward library construction, eight oligonucleotides, three of which containing partially degenerate nucleotide sequences corresponding to the three CDRs, were used to amplify four overlapping PCR products (see “Materials and Methods” for details). The resulting amplicons were fused together one by one starting from the 5’ end, in order to produce a final 815 bp Nb-encoding DNA fragment. Each member of the RD-selectable library thus generated contains a T7 RNA polymerase promoter and a consensus RBS (AAGGAG) at the 5’-end, followed by the Nb gene and a sequence coding for a spacer that is needed to fill the ribosome tunnel upon translational ternary complex formation during the RD-selection process[28].

Correct assembly of the RD-library and the presence of the designed constant regions-encoding sequences were both verified by sequencing a sample of the library-derived amplicon. Sequence variability within the CDRs was subsequently evaluated by cloning the library Nb-coding sequences into the pET28 vector and sequencing of 96 randomly picked clones. Over 75% of the clones turned out to be correct, while the remaining ones harbored single or multiple (up to three) nucleotide deletions. The missing nucleotides always mapped within the regions corresponding to the partially degenerate oligonucleotides used for library construction and likely reflect chemical synthesis errors present in a small fraction of the PAGE-purified primers. Sequence analysis of the correct clones revealed a redundancy for the CDR1 and CDR2 regions statistically consistent with our estimates. In keeping with the much higher complexity expected for the CDR3, no sequence recurrence was observed in this region. Also, no statistically significant difference emerged from the comparison of the observed and the expected amino acid distributions present at each randomized position (see “Materials and Methods”).

Several randomly picked pET28-Nb clones were tested for Nb expression efficiency and solubility in bacterial cells. As expected, approximately 75% of the tested clones led to the IPTG-inducible production of well detectable polypeptides of the expected size, most of which turned out to be soluble (data not shown).

For testing the selectable Nb library, an RD selection using biotinylated MBP as target has been performed. MBP was chosen for its broad availability, easy expression and despite its widespread use as solubilizing/tag protein, no Nb against MBP is currently reported. Three rounds of panning were performed gradually increasing stringency in order to obtain high-affinity binders. Furthermore, neutravidin and streptavidin were alternated as well-coating agents during panning steps in order to avoid selection of off-target binders.

The cDNA recovered at the end of the third panning was cloned in pET28 and 192 randomly picked single clones were analysed. After inducing protein expression in 96 deep well plates and subsequent cell lysis, supernatants containing soluble putative binders were used for an ELISA assay as described in “Materials and Methods”.

During ELISA further changes in coating (from Streptavidin to Gluthatione-Casein), blocking (from BSA to Casein) and target-Tag (from Biotin to GST) components were performed to reveal only MBP specific binders and to prevent off-target Nbs detection. 8 clones showed MBP binding capacity and the corresponding Nbs were expressed and purified with a yield of expression ranging from 1 to 24 mg per liter of culture (data not shown).

MBP binding of the 8 positive clones was corroborated carrying out reverse ELISA tests with purified Nbs (as described in "Materials and Methods") and 4 clones confirmed their binding ability (**Figure 5**).

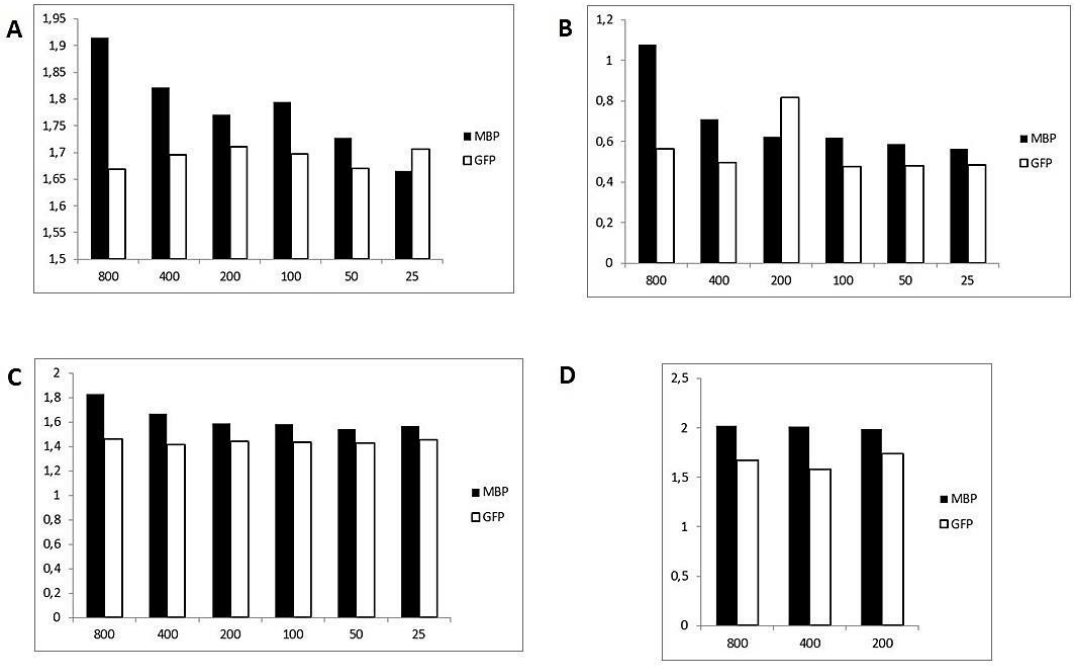

Figure 5 Histograms presenting the results of reverse ELISA tests with purified Nbs: ordinates present the final absorbance value at 415 nm and abscissas the serial tested dilutions of the target starting from 800 nM. Nbs were tested for their MBP (black columns) and GFP (white columns) binding capacity. A: D1 clone; B: F9 clone; C: H10 clone; D: E2 clone.

In particular, F9 clone showed the highest MBP binding specificity compared to the negative control (**Figure 6A**), in addition to a very high yield of expression (24 mg per liter of culture). Thus its sequence was analysed and its belongings to starting Nb library confirmed (**Figure 6B**).

A

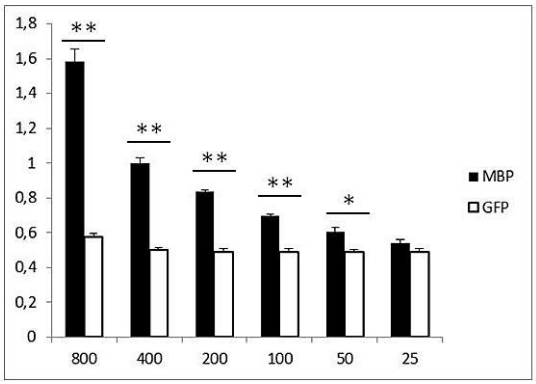

B

1 64
QVQLQESGGGLVQAGGSLRLSCAASGSIFSVYTIAWYRQAPGKEREFVAAISSGGGTTYYADSV
65 126
KGRFTISRDNAKNTVYLQMNSLKPEDTAVYYCAVGPRYLLGFHNDAVGFGYWGQGTQVTVSS

Figure 6 Final analysis of F9 clone. A) Histogram presenting the merge of three ELISA analysis results with standard errors: ordinates present the final 415 nm absorbance value and abscissas the serial tested dilutions of targets starting from 800 nM (MBP in black and GFP in withe). ** indicates $p < 0.01$, * indicates $p < 0.05$ of the difference between MBP and negative control signals (see "Materials and Methods" for details); B) Sequence of F9 clone, CDRs are in red, introduced PCR mutation is in green.

4. Discussion

Proper folding of Nbs depends on the formation of at least one disulfide bridge, and for this reason they are usually expressed in the oxidizing environment of the bacterial periplasm[33]. Nbs built on our CFW are expressed in good amounts (1-24 mg of pure protein/liter of bacterial culture) even intracellularly, thus further corroborating the robustness of our designed scaffold. Having been derived from a large set of natural Nb sequences, this scaffold corresponds to the most frequently occurring llama VHH subfamily polypeptide.

Grafting of CDR loops from natural Nbs into a CFW sequence may negatively impact on Nb function, especially when specific amino acid substitutions are located in structurally critical regions such as FR2[32,34,35]. This was the case of our Lcons Nb, which required a specific G47F back-mutation in the FR2 (restoring the amino acid residue present in the original donor Nb) in order to re-gain target-binding competence. No such problem, and a target-binding affinity similar to that of the parent anti-GFP Nb, was observed, instead, with the Gcons Nb, which sports a conservative (Trp→Phe) amino acid substitution at position 47 of FR2.

This, together with the high complexity achieved with the constructed Nb library and the screening power of ribosome display selection, which allowed the identification of new MBP binders (even if the K_d of the new Nbs remains to be assessed), makes us believe that functionally competent FR-CDR combinations can be isolated for any given target. Furthermore, the peculiar single point mutation in FR2 of our scaffold observed in F9 clone (**Figure 6A**) underlines the library complexity increase that RD technique enables, boosting the possibility of new binders identification. It should also be noted that although designed for ribosome display selection, this Nb library is readily transferable to more conventional selection formats such as phage display.

In synthetic antibody combinatorial libraries, a high CDR diversity is usually achieved through the use of scrambled codons such as NNK, VNN or MNN, where K, V and M represent, respectively, G or T; A, C or G; A or C; and N corresponds to any base[36,37]. In our approach, instead, nucleotide triplet degeneration was restricted to codons corresponding to the amino acid residues most represented in the natural llama VHH repertoire. Even if a similar approach was reported[18], only avoiding cloning procedure a high complexity library similar to llama natural repertoire can be archived; in this way we generated a sort of naïve library matching the sequence variability that in the natural context is achieved via somatic DNA recombination and hypermutation at some specific sites. Construction of a library of similar complexity starting from lymphocytes derived from naïve animals would be much more labor intensive.

Although PAGE-purified oligonucleotides have been used for library synthesis, only about 75% of the synthetic oligo products turned out to be correct. A great improvement in RD-library quality might be obtained by constructing the three CDRs, or at least CDR3, using trinucleotide preassembled oligos as starting material[38]. This would not only reduce deletions caused by unavoidable synthesis errors, but would also afford full control on the presence and distribution of the desired amino acids, while avoiding stop codons. Given the flexibility inherent to the RD selection platform, which relies on a linear DNA library, this improvement as well as other modifications of the CDR3 (e.g., length and/or triplet composition) can be introduced with the use of just two assembly PCR steps and a single degenerate oligonucleotide (CDR3-FW) coding for a CDR3 bearing the desired changes.

5. Bibliography

1. Hamers-Casterman C, Atarhouch T, Muyldermans S, et al. Naturally occurring antibodies devoid of light chains. *Nature*. 1993;363(6428):446-448. doi:10.1038/363446a0.
2. Oliveira S, Heukers R, Sornkom J, Kok RJ, Van Bergen En Henegouwen PMP. Targeting tumors with nanobodies for cancer imaging and therapy. *J Control Release*. 2013. doi:10.1016/j.jconrel.2013.08.298.
3. Smolarek D, Bertrand O, Czerwinski M. Variable fragments of heavy chain antibodies (VHHs): A new magic bullet molecule of medicine? *Postepy Hig Med Dosw*. 2012;66:348-358. doi:10.5604/17322693.1000334.
4. Muyldermans S, Baral TN, Retamozzo VC, et al. Camelid immunoglobulins and nanobody technology. *Vet Immunol Immunopathol*. 2009. doi:10.1016/j.vetimm.2008.10.299.
5. Harmsen MM, De Haard HJ. Properties, production, and applications of camelid single-domain antibody fragments. *Appl Microbiol Biotechnol*. 2007. doi:10.1007/s00253-007-1142-2.
6. Lauwereys M, Ghahroudi MA, Desmyter A, Genst E De, Wyns L, Muyldermans S. Potent enzyme inhibitors derived from dromedary heavy-chain antibodies. 1998;17(13):3512-3520.
7. De Genst E, Silence K, Decanniere K, et al. Molecular basis for the preferential cleft recognition by dromedary heavy-chain antibodies. *Proc Natl Acad Sci*. 2006;103(12):4586-4591. doi:10.1073/pnas.0505379103.
8. Chakravarty R, Goel S, Cai W. Nanobody: The “magic bullet” for molecular imaging? *Theranostics*. 2014. doi:10.7150/thno.8006.
9. Hassanzadeh-Ghassabeh G, Devoogdt N, De Pauw P, Vincke C, Muyldermans S. Nanobodies and their potential applications. *Nanomedicine*. 2013. doi:10.2217/nnm.13.86.
10. De Meyer T, Muyldermans S, Depicker A. Nanobody-based products as research and diagnostic tools. *Trends Biotechnol*. 2014. doi:10.1016/j.tibtech.2014.03.001.
11. Desmyter A, Spinelli S, Roussel A, Cambillau C. Camelid nanobodies: Killing two birds with one stone. *Curr Opin Struct Biol*. 2015;32:1-8. doi:10.1016/j.sbi.2015.01.001.
12. Olichon A, De Marco A. Preparation of a naïve library of camelid single domain antibodies. *Methods Mol Biol*. 2012. doi:10.1007/978-1-61779-968-6_5.
13. Pardon E, Laeremans T, Triest S, et al. A general protocol for the generation of Nanobodies for structural biology. *Nat Protoc*. 2014. doi:10.1038/nprot.2014.039.
14. Verheesen P, Roussis A, de Haard HJ, et al. Reliable and controllable antibody fragment selections from Camelid non-immune libraries for target validation. *Biochim Biophys Acta - Proteins Proteomics*. 2006. doi:10.1016/j.bbapap.2006.05.011.
15. Monegal A, Ami D, Martinelli C, et al. Immunological applications of single-domain llama recombinant antibodies isolated from a naïve library. *Protein Eng Des Sel*. 2009. doi:10.1093/protein/gzp002.
16. Kehoe JW, Kay BK. Filamentous phage display in the new millennium. *Chem Rev*. 2005. doi:10.1021/cr000261r.
17. Moutel S, Bery N, Bernard V, et al. NaLi-H1: A universal synthetic library of humanized nanobodies providing highly functional antibodies and intrabodies. *Elife*. 2016;5(JULY):1-31. doi:10.7554/eLife.16228.
18. McMahon C, Baier AS, Pascolutti R, et al. Yeast surface display platform for rapid discovery of conformationally selective nanobodies. *Nat Struct Mol Biol*. 2018;25(3):289-296. doi:10.1038/s41594-018-0028-6.
19. Koide A, Tereshko V, Uysal S, Margalef K, Kossiakoff AA, Koide S. Exploring the Capacity of Minimalist Protein Interfaces: Interface Energetics and Affinity Maturation to Picomolar KD of a Single-domain Antibody with a Flat Paratope. *J Mol Biol*. 2007. doi:10.1016/j.jmb.2007.08.027.
20. Plückthun A. Ribosome display: A perspective. *Methods Mol Biol*. 2012. doi:10.1007/978-1-61779-379-0_1.
21. Yau KYF, Groves MAT, Li S, et al. Selection of hapten-specific single-domain antibodies from a non-immunized llama ribosome display library. *J Immunol Methods*. 2003;281(1-2):161-175.

doi:10.1016/j.jim.2003.07.011.
22. Schaffitzel C, Hanes J, Jermutus L, Plückthun A. Ribosome display: An in vitro method for selection and evolution of antibodies from libraries. *J Immunol Methods*. 1999. doi:10.1016/S0022-1759(99)00149-0.
23. Sambrook J, W Russell D. Molecular Cloning: A Laboratory Manual. *Cold Spring Harb Lab Press Cold Spring Harb NY*. 2001. doi:10.1016/0092-8674(90)90210-6.
24. Crameri A, Whitehorn EA, Tate E, Stemmer WPC. Improved Green Fluorescent Protein by Molecular Evolution Using DNA Shuffling. *Nat Biotechnol*. 1996. doi:10.1038/nbt0396-315.
25. Amstutz P, Binz HK, Parizek P, et al. Intracellular kinase inhibitors selected from combinatorial libraries of designed ankyrin repeat proteins. *J Biol Chem*. 2005. doi:10.1074/jbc.M501746200.
26. Hanes J, Plückthun A. In vitro selection and evolution of functional proteins by using ribosome display. *Proc Natl Acad Sci U S A*. 1997. doi:10.1073/pnas.94.10.4937.
27. Huber T, Steiner D, Röthlisberger D, Plückthun A. In vitro selection and characterization of DARPins and Fab fragments for the co-crystallization of membrane proteins: The Na+-citrate symporter CitS as an example. *J Struct Biol*. 2007. doi:10.1016/j.jsb.2007.01.013.
28. Zahnd C, Amstutz P, Plückthun A. Ribosome display: Selecting and evolving proteins in vitro that specifically bind to a target. *Nat Methods*. 2007. doi:10.1038/nmeth1003.
29. Sehr P, Zumbach K, Pawlita M. A generic capture ELISA for recombinant proteins fused to glutathione S-transferase: Validation for HPV serology. *J Immunol Methods*. 2001;253(1-2):153-162. doi:10.1016/S0022-1759(01)00376-3.
30. Muyldermans S. Nanobodies : Natural Single-Domain Antibodies. 2013. doi:10.1146/annurev-biochem-063011-092449.
31. Kirchhofer A, Helma J, Schmidthals K, et al. Modulation of protein properties in living cells using nanobodies. *Nat Struct Mol Biol*. 2010. doi:10.1038/nsmb.1727.
32. Vincke C, Loris R, Saerens D, Martinez-Rodriguez S, Muyldermans S, Conrath K. General strategy to humanize a camelid single-domain antibody and identification of a universal humanized nanobody scaffold. *J Biol Chem*. 2009;284(5):3273-3284. doi:10.1074/jbc.M806889200.
33. Liu JL, Goldman ER, Zabetakis D, et al. Enhanced production of a single domain antibody with an engineered stabilizing extra disulfide bond. *Microb Cell Fact*. 2015. doi:10.1186/s12934-015-0340-3.
34. Saerens D, Pellis M, Loris R, et al. Identification of a universal VHH framework to graft non-canonical antigen-binding loops of camel single-domain antibodies. *J Mol Biol*. 2005;352(3):597-607. doi:10.1016/j.jmb.2005.07.038.
35. Mitchell LS, Colwell LJ. Analysis of nanobody paratopes reveals greater diversity than classical antibodies. *Protein Eng Des Sel*. 2018;(July):1-9. doi:10.1093/protein/gzy017.
36. Yan J, Li G, Hu Y, Ou W, Wan Y. Construction of a synthetic phage-displayed Nanobody library with CDR3 regions randomized by trinucleotide cassettes for diagnostic applications. *J Transl Med*. 2014. doi:10.1186/s12967-014-0343-6.
37. Yang HY, Kang KJ, Chung JE, Shim H. Construction of a large synthetic human scFv library with six diversified CDRs and high functional diversity. *Mol Cells*. 2009. doi:10.1007/s10059-009-0028-9.
38. Virnekas B, Ge L, Plukthun A, Schneider KC, Wellnhofer G, Moroney SE. Trinucleotide phosphoramidites: Ideal reagents for the synthesis of mixed oligonucleotides for random mutagenesis. *Nucleic Acids Res*. 1994. doi:10.1093/nar/22.25.5600.

Chapter 2

Chapter 2: A humanized artificial semi-random nanobody library suitable for speeded up phage display selection

1. Introduction

Antibodies are a novel frontier in therapeutic area and their rapid diffusion increases the demand for new efficient binders[1]. During the research of faster and cheaper therapies, molecular engineering was applied to antibody production and now modified antibodies and antibody-derivatives are available on the market. One of the fundamental goals that extended antibody applications was humanization: a lot of strategies (i.e. grafting ectopic CDRs in human antibodies, mice that produce human antibodies) were developed to render animal antibodies as similar as possible to human ones. Humanization techniques decrease the immunogenicity of novel therapeutic molecules, thus humanized mAb, like Rituximab and Cetuximab, are now applied during treatments[2,3].

The use of small variable antibody domains (like Fab and scFv fragments) instead of entire immunoglobulins reduced treatment immunogenicity and thus the discovery of heavy chain only antibodies (hcAb) in camelids sera in 1993 elicited great curiosity[4]. HcAbs are able to bind their target with a single variable heavy domain called VHH or nanobody (Nb) which, in addition with a plethora of advantages (i.e. small size, high solubility, specific binding capacity), can be singularly expressed maintaining the binding capacity of the entire immunoglobulin[5]. Like every variable domain, Nbs are naturally low immunogenic[6] and furthermore they share a high identity score with human VH III subfamily reducing the risk of immune rejection in case of human subministration[7]. However, despite their intrinsic immune tolerance, Nbs differ from human IgG VH III domains in about 10 amino acids, and therefore therapeutic Nbs have to be humanized to further reduce the risk of immune response elicitation in patients[8,9] (as demonstrated by humanized approved Nb Caplacizumab[10,11]). Different Nb humanization strategies are described in the literature but most of them reported a loss of Nb affinity after framework regions (FRs) mutation, probably because these regions might be involved in target binding or their modification could lead to different CDRs exposure[12,13].

The construction of already humanized Nb libraries seems to be an interesting strategy to resolve Nb humanization problems because ready-to-use Nbs can be selected avoiding post-selection humanization procedures. Contrary to immune or naïve libraries, which are built with natural Nbs[14–16], artificial ones can derive from validated scaffolds, already humanized, randomizing only the CDRs[17–19]. Compared to immune libraries, these types

of libraries, obtained by *in vitro* assembly[20], must have a larger diversity but have the advantage that they can be used for selections against toxic or not immunogenic targets[21,22].

Despite different selection strategies have been developed through years, phage display remains the easiest and most widespread method for the identification of new antibodies[23]. Functional library components are exposed on the surface of M13 phages fused in frame to pIII phage protein and binders of interest during panning steps can be selected. Engineered pIII surface protein is provided by a phagemid vector which is not able to independently produce complete M13 phages because it lacks the necessary components for functional phage assembly. Thus after every panning step infection of selected phages leads to antibiotic resistant *Escherichia coli* cells that contain Nbs encoding phagemids and in order to produce complete phages for the next panning an infection with a helper phage and subsequent phage collection are required. For these reasons, a single panning step takes up to 3/4 days[24].

Here we present the humanization of a llama VHH consensus framework to be used as a scaffold for Nb production and for the construction of a humanized artificial Nb library in a novel vector for phage display selection. Previously we reported the design and production of a consensus framework scaffold (CFW) suitable for Nb production (see Chapter 1 for details) which derived from the alignment of more than 750 llama Nbs. After grafting of CDRs from natural known VHH, the scaffold was able to produce soluble and functional Nbs and a high-complex library suitable for ribosome display selection was produced. Here we introduced 12 point mutations in the FRs of our scaffold rendering them identical to the FRs of a human IgG VH III domain. The ability of this complete humanized scaffold (hCFW) to expose correctly CDRs was confirmed and a high-complex artificial humanized Nb library was built.

In order to speed up phage display steps, we produced a novel phage vector: introducing engineered pIII protein gene, derived for a phagemid, into the M13 complete genome (M13mp8), a novel phage vector suitable for phage display selection was produced (M13-flash). The vector was able to produce functional phages which exposed Nbs on their surface, so that the single selection step took only one day. The humanized artificial Nb library is now ready to be cloned in this new vector using among different cloning strategies the one that it will allow us to obtain the highest complex library.

2. Materials and Methods

2.1. Molecular biology reagents and cloning procedures

Standard protocols[25] were used for all basic recombinant DNA procedures. Enzymes were from Takara Bio Europe (Saint-Germain-en Laye, France) and New England Biolabs (Ipswich, MA, USA). Molecular cloning and recombinant protein expression were carried out in BL21 codon plus *E. coli* strains (Stratagene; La Jolla, CA, USA), using pET28 (Merck Millipore, Darmstadt, Germany) and pIT2 (http://www.geneservice.co.uk/products/proteomic/datasheets/tomlinsonIJ.pdf) plasmids. Following appropriate design, synthesis of hGcons and hG09cons encoding sequences were performed by Eurofins Genomics (Ebersberg, Germany), all protein-encoding sequences were optimized with respect to the *E. coli* codon usage (**Table 1**).

Name	Sequence
E.coli codon optimized hGcons gene	ccATGGgcGAGgtacagctgCTTgaatcgggtggtggcctggttcaaCCAgg cggcagtttacgcctgtcatgtgcagcgtcaggtCGCAATGTGGAGAATCAG GCAATGGGCTGGTTTCGTCAaGCACCAGGgAAAGGCCTGGAGTGGGTGTCGA CAATCAGCTATAGCGGGGTTACGACCTACtatgcggattccgtgaaaggacg cttcaccatttctcgggacaatTCGaagaacaccCTGtatttgcagatgaac tccctgCGTGCGgaagatacggctgtctactattgcgctgcgCATCGTGGTA CAGCTCTGACCATGAGTCGTGCCTCGCCTGCGGACTTTGGCTCAtggggcca gggtactCTGgtcaccgtaagcagcAAgCTt
E.coli codon optimized hG09cons gene	catatgGGTCGTCGTCGTCGCCGTTCATCcatgggccaggtacagctggtag aatcgggtggtggcctggttcaaccgggcggcagtttacgcctgtcatgtgc agcgtcaggttttccggtgaatcggtactctatgcgctgggtgcgtcaagca ccagggaaagggctggagtgggtggccggcatgtctagtgccggtgatcgct caagctatgcggattccgtgaaaggacgcttcaccatttctcgggacaattc taagaacaccctgtatttgcagatgaactccctgcgcgcggaagatacggct gtctactattgcgctgcgaatgtgggcttcgagtattggggccagggtactc tggtcaccgtaagcagcgcggccgc

Table 1 Nucleotide sequences of the synthetic genes used in this chapter. Sequences are shown in standard 5'-3' orientation.

Ligations of hGcons and hG09cons (using NcoI and HindIII cloning sites) in pET28 plasmids were performed following standard protocols[25].
Ligations of Gcons and hG09cons nucleotide sequences (using NcoI and NotI cloning sites) in pIT2 plasmid were performed following standard protocols[25].

2.2. Recombinant protein expression and purification

Standard procedures were used for recombinant hGcons and hG09cons expression. Briefly, 10 ml of stationary overnight cultures (LB, 50 mg/l of kanamycin and 34 mg/l of chloramphenicol at 37 °C) were inoculated into 1 l cultures of the same media. After reaching an A_{600} value of 0.4-0.6, cultures were induced with 1 mM IPTG and further incubated for overnight at 20°C. Following centrifugation (5000 rpm, 15 min), bacterial

cell pellets were recovered, suspended in 200 ml of Tris 10 mM pH 8.0 and centrifuged in the same conditions. Bacterial pellets were suspended in 50 ml of Tris-buffered saline (25 mM Tris pH 8.0, 0.3 M NaCl, freshly supplemented with protease inhibitors), and lysed by sonication (20 min total sonication time performed with 3 sec bursts alternated with 6 sec resting on ice) carried out at constant power (4W/cm2; Sonicator 3000, Misonix). Lysates were then centrifuged (10000 rpm, 30 min) and the resulting supernatants were used as starting material for metal-affinity purification using a built-in 6xHis-tag and a His-select cobalt affinity resin (Sigma-Aldrich, Saint Louis, MO, USA) as per manufacturer's instructions. Bacterial lysates and individual metal-affinity chromatography fractions were analyzed by SDS-PAGE on 15% polyacrylamide gels.

Expression of Gcons protein is described in detail in Chapter 1, expression of GconsMuFc protein is described in detail in Chapter 3, expression of G09cons protein is described in detail in Chapter 4.

Recombinant green fluorescent protein (GFP) used in this work is enhanced GFP. GST-GFP, GFP and E2 Crimson were gently provided by collaborators.

2.3. ELISA tests procedure

GST-ELISA tests to verify compared Gcons and hGcons activity were carried out using the following protocol: polystyrene 96-wells microtiter plates were coated overnight at 4°C with casein-glutathione (prepared and used as previously described[26]) dissolved in carbonate buffer (1 vol. 0.5 M Na_2CO_3 : 4 vol. 0.5 M $NaHCO_3$ pH 9.6). Blocking was performed by incubation for 1 hr at room temperature with 0.2% casein in Phosphate-buffered saline (PBS, pH 7.4), followed by a 1 hr incubation at room temperature with the purified GST-tagged protein in PBS (800 nM each). After incubation with serial 1:3 dilutions of hGcons and Gcons (starting from 800 nM) for 1 hr at room temperature, an anti-histidine-tagged protein mouse mAb (Merck Millipore) diluted 1:1000 in PBS+0.2% casein was added and incubated for 1 hr. Then a peroxidase-conjugated anti-mouse IgG (whole molecule) goat antibody (Sigma-Aldrich) diluted 1:5000 in PBS+0.2% casein was added. Following an additional 1 hr incubation at RT, wells were filled with the 2,2'-azino-di-[3-ethylbenzthiazoline sulfonate (ABTS) substrate (KPL, Gaithersburg, MD, USA) and absorbance was measured at 415 nm with a microplate reader (iMark, Biorad). Wells were washed with PBS containing 0.3% (v/v) Tween20 after each incubation step.

ELISA performed with hG09cons and G09cons proteins to compare their activity was executed using the following protocol: polystyrene 96-wells microtiter plates were coated overnight at 4°C with casein-glutathione dissolved in carbonate buffer (1 vol. 0.5 M Na_2CO_3 : 4 vol. 0.5 M $NaHCO_3$ pH 9.6). Blocking was performed by incubation for 1 hr at room temperature with 0.2% casein in Phosphate-buffered saline (PBS, pH 7.4), followed

by a 1 hr incubation at room temperature with the purified GST-GFP protein in PBS (800 nM each). 800 nM of GconsMuFc were then added and incubated for 1 hr at RT. After incubation serial 1:3 dilutions of G09cons were added and incubated for 1 hr at room temperature. After incubation with an anti-histidine-tagged protein mouse mAb (Merck Millipore) diluted 1:1000 in PBS+0.2% casein for 1 hr, a peroxidase-conjugated anti-mouse IgG (whole molecule) goat antibody (Sigma-Aldrich) diluted 1:5000 in PBS+0.2% casein was added. Following an additional 1 hr incubation at RT, wells were filled with the 2,2'-azino-di-[3-ethylbenzthiazoline sulfonate (ABTS) substrate (KPL, Gaithersburg, MD, USA) and absorbance was measured at 415 nm with a microplate reader (iMark, Biorad). Wells were washed with PBS containing 0.3% (v/v) Tween20 after each incubation step.

2.4 Synthesis of the humanized nanobody library

The Nb library was generated by multiple steps of assembly PCR using the PAGE-purified oligonucleotides (Microsynth, Balgach, Switzerland) listed in **Table 2** and the Phusion DNA polymerase New England Biolabs (Ipswich, MA, USA); individual PCR products were agarose gel-purified using a Macherey-Nagel kit (Düren, Germany).

Name	Sequence
nLMB3	CACAGGAAACAGCTATGACCATG
pHEN	CTATGCGGCCCCATTCA
FR1-RE	ACCTGACGCTGCACATGAC
FR3-RE	CGCAGCGCAATAGTAGACAG
hCDR1-FW	GTCATGTGCAGCGTCAGGTTYCAYTTTTTCGRDTWATRCTATKGSTTGGKWCCGTCAAGCACCAGGGAAAG
hFR2-RE	AATGGCCGACACCCACTCCAGGCCTTTCCCTGGTGCTTGACG
hCDR2-FW	GGAGTGGGTGTCGGCCATTAVTWSGRGTGRTGRTAVKACCTACTATGCGGATTCCGTGAAAGGA
hCDR3-FW	CTGTCTACTATTGCGCTGCGSVTMSTVGTNHYNHYVGTNHYNHYYHTWMTVNTBCTVNTRVKTWTRRTTATTGGGGCCAGGGTACTC

Table 2 Oligonucleotides utilized for assembling PCR steps. Sequences are shown in a standard 5'-3' orientation. The standard one-letter abbreviation nomenclature for specific subsets of nucleotides is used, where: M represents A, or C; Y represents C or T; R represents A, or G; D represents A, G or T; W represents A, or T; K represents G or T; S represents C or G; V represents A, C or G; H represents A, C or T; B represents C, G or T; and N represents any of the four nucleotides.

PCR1: the oligonucleotides nLMB3 and FR1-RE were used to amplify the pIT2 hG09 gene (Initial denaturation 98°C, 20 s; 28 cycles of 10 s at 98°C, 30 s at 65°C, and 30 s at 72°C; additional extension 72°C, 5 min), to generate a final product containing FR1 preceded by a NcoI cloning site.

PCR2: the oligonucleotides hCDR1-FW and hFR2-RE (4 nM each), plus dNTPs (0.8 mM), 1x PCR buffer and 1 unit of Phusion DNA polymerase in a final volume of 50 µl, were fused together by PCR (condition as PCR1 except 20 cycles, 66°C annealing temperature and no additional extension). The purified PCR1 product (100 ng) was then added, together with

DNA polymerase (0.5 units) and dNTPs (0.4 mM), and another 20 cycles of PCR amplification were performed. This was followed by the addition of oligonucleotides nLMB3 and hFR2-RE (0.5 µM each) plus DNA polymerase and dNTPs as above, and a further round of PCR amplification (condition as PCR1 except 20 cycles, 66°C annealing temperature and no additional extension) to generate a final product containing FR1, CDR1 and FR2, flanked by a NcoI restriction site.
PCR3: the oligonucleotides hCDR2-FW and FR3-RE were used to PCR-amplify the pIT2 hG09 gene (condition as PCR1 except 64°C annealing temperature) and to generate an amplicon bearing the CDR2 and the FR3.
PCR4: the oligonucleotides hCDR3-FW and pHEN were used to amplify the pIT2 hG09 gene (condition as PCR1 except 62°C annealing temperature) and to generate a final product containing the CDR3, FR4 and NotI restriction site.
PCR5: 40 ng and 30 ng of the purified PCR2 and PCR3 products, respectively, were fused together by PCR (condition as PCR1 except for 20 cycles, 70°C annealing temperature and no additional extension) carried out in the presence of dNTPs (0.8 mM), 1x PCR buffer, and 1 unit of DNA polymerase in a final volume of 50 µl. The fused product upon supplementation of oligonucleotides nLMB3 and FR3-RE (0.5 µM each), dNTPs (0.4 mM) and 0.5 units of DNA polymerase was PCR amplified (condition as PCR1 except 70°C annealing temperature and 60 s of the cycle extension time). The final product contains FR1, CDR1, FR2, CDR2 and FR3, flanked by a NcoI restriction site.
PCR6: the purified PCR4 and PCR5 products (50 ng each) were fused together by 25 cycles of PCR amplification (condition as PCR1 except 64°C annealing temperature, 60 s of the cycle extension time and no additional extension) carried out in the presence of dNTPs (0.8 mM), 1x PCR buffer, and 1 unit of DNA polymerase in a final volume of 50 µl. This was followed by addition of oligonucleotides nLMB3 and pHEN (0.5 µM each), dNTPs (0.4 mM) and DNA polymerase (0.5 units), and amplification of the fused product (condition as PCR1 except 64°C annealing temperature and 60 s of the cycle extension time) to generate the complete humanized Nb library. PCR6 was repeated 10 times in order reach a library complexity of approximately 10^{10}.

2.5. Assembly of the novel vector suitable for Phage Display selection

Trypsin sensitive pIII encoding gene was amplified from KM13 Helper phage genome adding at 5' and 3' ends sequences overlapping destination vector cloning site. PCR was performed with 1 unit Phusion DNA Polymerase (New England Biolabs, Ipswich, MA, USA) in presence of the M13-P3(helper)-FW and M13-P3(helper)-RE (see **Table 3**) oligonucleotides (4 nM each), plus dNTPs (0.8 mM), 1x PCR buffer and 75 ng KM13

genome in a final volume of 50 µl: initial denaturation 98°C 3 min; 25 cycles of 30 s at 98°C, 30 s at 60°C, and 60 s at 72°C; additional extension 72°C 7 min.
M13mp8 phage genome was PCR amplified in order to exclude endogenous pIII protein and to introduce at 5' and 3' ends sequences overlapping pIII KM13 Helper phage amplicon. PCR was performed with 1 unit Phusion DNA Polymerase (New England Biolabs, Ipswich, MA, USA) in presence of the M18mp8del-noP3-FW and M18mp8del-noP3-RE (see **Table 3**) oligonucleotides (4 nM each), plus dNTPs (0.8 mM), 1x PCR buffer and 50 ng M13mp8 genome in a final volume of 50 µl: initial denaturation 98°C 3 min; 25 cycles of 30 s at 98°C, 30 s at 60°C, and 4 min at 72°C; additional extension 72°C 7 min.
pIII KM13 phage amplicon was fused to M12mp8 deleted genome using CPEC ligation system[27] and using the following protocol: 50 ng of pIII KM13 were mixed with 200 ng of deleted M13mp8 genome. PCR was performed with 1 unit Phusion DNA Polymerase (New England Biolabs, Ipswich, MA, USA) in presence of dNTPs (0.8 mM), 1x PCR buffer in a final volume of 50 µl: initial denaturation 98°C 5 min; 25 cycles of 20 s at 98°C and 4 min at 72°C; additional extension 72°C 10 min. This cloning step generated pIII trypsin sensitive M13mp8 (tsM13mp8)
pLac-pIII sequence was PCR amplified from pIT2 vector introducing EcoRI restriction site at 5' end and HindIII restriction site at 3' end. PCR was performed with 1 unit Phusion DNA Polymerase (New England Biolabs, Ipswich, MA, USA) in presence of the pIT2-EcoRI-FW and pIT2-HindIII-RE (see **Table 3**) oligonucleotides (4 nM each), plus dNTPs (0.8 mM), 1x PCR buffer and 100 ng pIT2 vector in a final volume of 50 µl: initial denaturation 98°C 3 min; 25 cycles of 30 s at 98°C, 30 s at 61°C, and 90 sec at 72°C; additional extension 72°C 10 min.
The tsM13mp8 genome was digested with EcoRI and HindIII restriction enzymes following standard protocol[25] and ligation of pLac-pIII sequence in tsM13mp8 genome was performed with InFusion HD cloning kit following user's manual instructions[28]. This cloning step generated the new M13 vector for phage display (M13-flash).

2.6. Cloning procedures in M13-flash vector

Gcons nucleotide sequence was PCR amplified from pIT2 Gcons vector introducing at 5' and 3' end sequences overlapping M13-flash vector cloning site. PCR was performed with 1 unit Phusion DNA Polymerase (New England Biolabs, Ipswich, MA, USA) in presence of the consNb-GFP-FW and consNb-GFP-RE (see **Table 3**) oligonucleotides (4 nM each), plus dNTPs (0.8 mM), 1x PCR buffer and 100 ng pIT2 Gcons vector in a final volume of 50 µl: initial denaturation 98°C 3 min; 25 cycles of 30 s at 98°C, 30 s at 57°C, and 30 sec at 72°C; additional extension 72°C 10 min.

M13-flash genome was digested with NcoI and NotI restriction enzymes following standard protocol[25] and ligation of Gcons nucleotide sequence in M13-flash genome was performed with InFusion HD cloning kit following user's manual instructions[28].

Name	Sequence
M13-P3(helper)-FW	gtgaaaaaattattattcgcaattcc
M13-P3(helper)-RE	ttaagactccttattacgcagtatg
M18mp8del-noP3-FW	ccacctttatgtatgtattttctacg
M18mp8del-noP3-RE	cggagtgagaatagaaaggaac
pIT2-EcoRI -FW	CCATGATTACGAATTGCTTGCATGCAAATTCTA
pIT2-HindIII-RE	ggccagtgccaagctTTATTAAGACTCCTTATTACGCAGTATG
consNb-GFP-FW	GCCCAGCCGGCCATGggccaggtac
consNb-GFP-RE	TGATGATGTGCGGCCgcgcttacggtgacctgaG
attR1-pDEST32-FW	cccagccggCCATGGcgaatcaaACAAGTTTGTACAAA
attR2-pDEST32RE	tgatgatgtGCGGCCGCccatAaaACCACTTTGTACAAG

Table 3 Oligonucleotides utilized in this chapter. Sequences are shown in a standard 5'-3' orientation.

Humanized Nb library was digested with NcoI and NotI restriction enzymes following standard protocol[25] and ligation of library nucleotide sequence (using NcoI and NotI cloning sites) in M13-flash genome was performed following standard protocols[25].
Gateway attP1-2 cassette nucleotide sequence was PCR amplified from pDEST32 vector introducing at 5' and 3' end sequences overlapping M13-flash vector cloning site. Touch-down PCR was performed with 1 unit Phusion DNA Polymerase (New England Biolabs, Ipswich, MA, USA) in presence of the attR1-pDEST32-FW and attR2-pDEST32RE (see **Table 3**) oligonucleotides (4 nM each), plus dNTPs (0.8 mM), 1x PCR buffer and 10 ng pDEST32 vector in a final volume of 50 µl: initial denaturation 98°C 3 min; 25 cycles of 30 s at 98°C, 30 s at 57 - 48°C, and 90 sec at 72°C; additional extension 72°C 10 min.
M13-flash genome was digested with NcoI and NotI restriction enzymes following standard protocol[25] and ligation of attP1-2 cassette nucleotide sequence in M13-flash genome was performed with InFusion HD cloning kit following user's manual instructions[28]. This cloning step generated a destination M13 vector derivative suitable for Gateway cloning system (Invitrogen, Carlsbad, California, USA): M13-flash-DEST.

2.7. Phage ELISA and phage display procedures

50 µl of stationary overnight culture of TG1 *E. coli* strain cells were inoculated into 5 ml of LB media and after reaching an A_{600} value of 0.5 were conserved at 4°C until use.
Panning steps were performed in polystyrene 96-wells microtiter plates using the following protocol: polystyrene 96-wells microtiter plates were coated overnight at 4°C with the purified GST-GFP and E2 Crimson protein in PBS (800 nM each). Blocking was performed by incubation for 1 hr at room temperature with 0.2% casein in Phosphate-

buffered saline (PBS, pH 7.4), followed by 2 hr incubation shaking at 700 rpm with 10^{11} phages in PBS+0.2% casein buffer. Wells were washed 15 times and 100 µl of prepared TG1 cells were added incubating 1 hr shaking at 700 rpm. 50 µl of incubated TG1 cells were added to 3 ml of TG1 A_{600} 0.5 cells and infection was performed for 30 min at 37°C. To infected TG1 cells, 7 ml of media were added and cells were incubated o/n at 30°C. The next day cells were centrifuged (5000 rpm, 15 min), the supernatant was filtered with 0.2 µm filters and used for subsequent panning step. Wells were washed with PBS containing 0.3% (v/v) Tween20 after each incubation step.

Phage ELISA tests were carried out using the following protocol: polystyrene 96-wells microtiter plates were coated overnight at 4°C with the purified GST-GFP and E2 Crimson protein in PBS (800 nM each). Blocking was performed by incubation for 1 hr at room temperature with 0.2% casein in Phosphate-buffered saline (PBS, pH 7.4), followed by a 1 hr incubation at room temperature shaking at 700 rpm with 100 µl of 10^9 phages diluted in PBS+0.2% casein. After incubation with an anti-pVIII M13 protein (GE Healthcare, Little Chalfont, USA) diluted 1:5000 in PBS+0.2% casein for 1 hr at room temperature, a peroxidase-conjugated anti-mouse IgG (whole molecule) goat antibody (Sigma-Aldrich) diluted 1:5000 in PBS+0.2% casein was added. Following an additional 1 hr incubation at RT, wells were filled with the 2,2'-azino-di-[3-ethylbenzthiazoline sulfonate (ABTS) substrate (KPL, Gaithersburg, MD, USA) and absorbance was measured at 415 nm with a microplate reader (iMark, Biorad). Wells were washed with PBS containing 0.3% (v/v) Tween20 after each incubation step.

3. Results

3.1. Humanization of the consensus framework scaffold

In order to humanize our CFW scaffold (see Chapter 1 for details), a consensus sequence of human IgG VH III subfamily was chosen as reference[29]. Nbs present high identity level with the chosen human subfamily, indeed only 12 different amino acids out of CDRs were identified (**Figure 1A**).

We decided to introduce all the highlighted differences in our sequence obtaining a humanized consensus framework (hCFW) scaffold that bears FRs identical to the human IgG VH III subfamily. The degree of humanization of hCFW is a bit higher than commercial humanized monoclonal antibodies. As an example, by aligning the hCFW scaffold with FRs of Trastuzumab (a FDA approved anti-HER2 humanized monoclonal antibody[30]), only five amino acids with different chemical-physical properties were identified (**Figure 1B**). Sharing a higher identity level with human variable domains, Nbs produced with our consensus scaffold were expected not to elicit any immune response in humans.

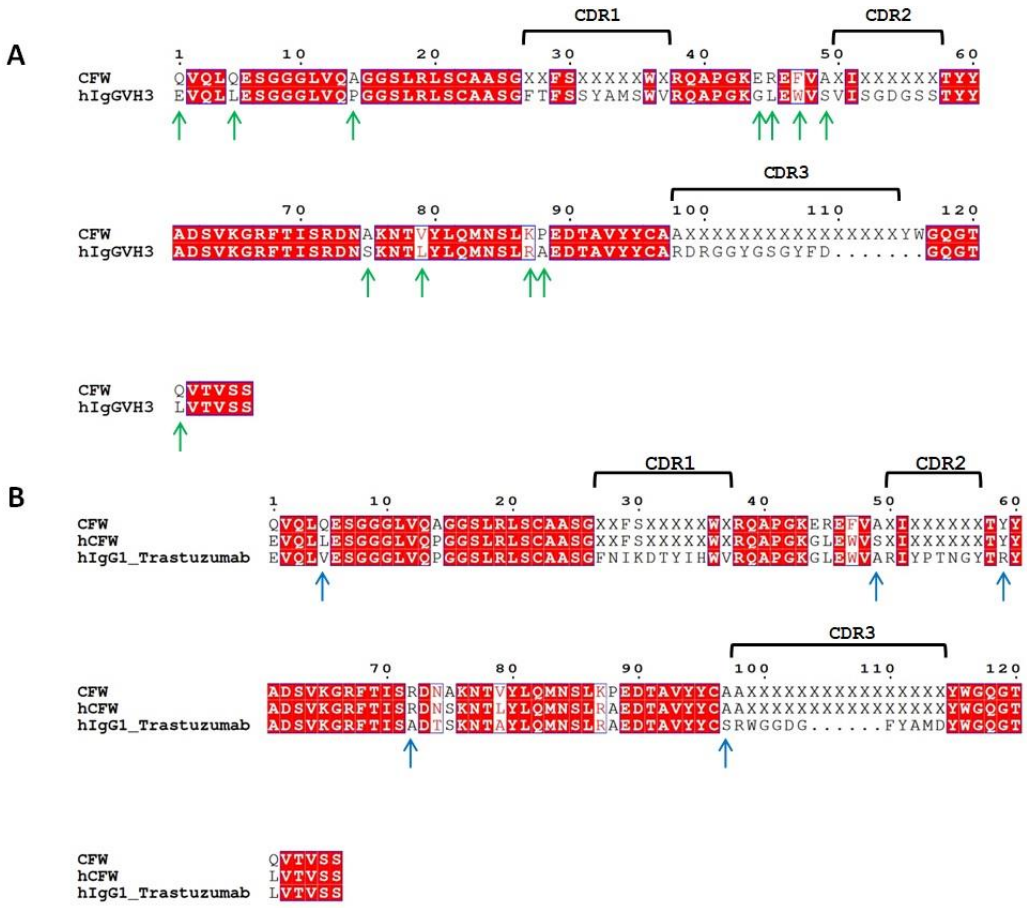

Figure 1 ESPript3 alignments (http://espript.ibcp.fr/ESPript/ESPript/). A) CFW amino acid sequence compared to human IgG VH III consensus sequence, differential amino acids are indicated by green arrows. B) CFW and hCFW amino acid sequences compared to Trastuzumab, amino acids with different chemical-physical properties between hCFW and Trastuzumab are highlighted by blue arrows.

3.2. Validation of the humanized consensus framework scaffold (hCFW)

3.2.1. Cloning and expression of humanized Gcons and G09cons nanobodies

To verify if after humanization our CFW scaffold was still able to stabilize and solubilize natural Nbs, while maintaining target-specific binding, CDRs of two VHHs were grafted into hCFW. As donors of CDRs, the Gcons (anti-GFP Nb, see Chapter 1 for details) and G09cons (anti-murine IgGs Nb, see Chapter 4 for details) were chosen for their high level of expression in *E. coli* and specific/strong target binding capacity obtaining humanized Gcons (hGcons) and G09cons (hG09cons) Nbs respectively.

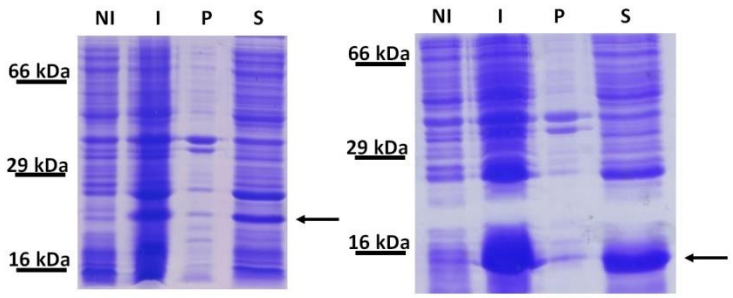

Figure 2 Expression and solubility analysis of hGcons (left) and hG09cons (right). NI: non-induced control; I: induced bacterial lysate; S: bacterial lysate supernatant; P: bacterial pellet. The arrows mark the polypeptide bands corresponding to the Nbs. Molecular size of the marker is indicated next to the figures (see "Materials and Methods" for details).

Artificial synthetized hGcons and hG09cons nucleotide sequences were cloned in pET28 vector and expressed in BL21 *E. coli* strain. After cells lysis both proteins were present in soluble fractions (**Figure 2**) and were purified by metal-affinity chromatography using the vector-provided poly-histidine tag (see "Materials and methods" for details) with a final yield of approximately 8 mg and 15 mg of pure protein/L of bacterial culture respectively. The high levels of expression of both proteins demonstrated that our hCFW is still able to produce high-expressing and soluble Nbs.

3.2.2. Analysis of hGcons and hG09cons target binding capacity

After CDRs grafting loss of Nbs target-binding capacity may occur because of CDRs incorrect exposure. To asses that hGcons and hG09cons were still able to bind their targets, ELISA tests comparing the humanized and not humanized Nbs (**Figure 3**) were carried out (see "Materials and Methods" for details).

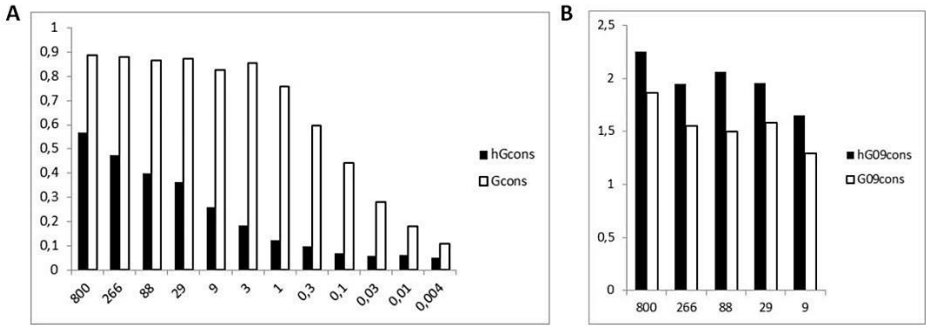

Figure 3 A) GST-ELISA testing of the hGcons/Gcons Nbs against GFP-GST. B) GST-ELISA testing of the hG09cons/G09cons Nbs against GconsMuFc. Bars represent absorbance measured at 415 nm after addition of the horseradish peroxidase (HRP) substrate, abscissa indicates the serial tested dilution of hGcons/Gcons and hG09cons/G09cons respectively (nM) (see "Materials and Methods" for details).

Results indicated that hG09cons Nb showed similar binding activity of G09cons, however, hGcons showed a decrease in target affinity if compared to the not humanized

counterpart. These outcomes demonstrated that hCFW exposed CDRs correctly although in some cases, especially when FRs contribute to target-binding, an alteration of amino acids within the framework might lead to a loss of Nb binding capacity.

3.3. Construction of the humanized artificial semi-random nanobody library

Once established the functionality of our humanized consensus scaffold, semi-random CDRs were introduced and a high-complex artificial Nb gene library was built. CDRs design and library assembly were performed as described in Chapter 1 (**Figure 4**, see "Materials and Methods" for details). Compare to the construction of ribosome display artificial library, the only difference was the modification of 12 different codons within CFW in order to introduce the 12 humanizing amino acids. The estimated complexity of this library was 10^{18} different Nb genes.

For verifying the correct assembly of the library, a small aliquot of the amplicon was cloned in pIT2 phagemid and 96 randomly picked clones were sequenced: more than 75% of the clones were correct, while the remaining Nb genes presented nucleotide deletions in the CDRs probably due to synthesis errors in PAGE-purified primers. Analysis of CDRs revealed that their amino acid composition at each randomized position corresponded to the expected one. Thus, this high complex Nb gene library now is ready to be cloned in a vector suitable for phage display selection.

Figure 4 Schematic representation of the humanized library construction by assembling PCR. Framework regions (grey) and complementarity determining regions (black) are shown. Arrows represent oligonucleotides used. See "Materials and Methods" for experimental detail and **Table 2** for the sequence of each oligonucleotide.

3.4. Production of a novel vector suitable for phage display selection

3.4.1. Assembly of a vector to speed up phage display procedure

For taking advantage of the phage display technology, usually gene libraries are cloned in frame with pIII M13 phage surface protein in expressing phagemid vectors. Since phagemids do not encode other phage proteins, for a correct phage assembly the presence of a helper vector, bearing all the necessary components, is required. This phagemid features render panning steps a long procedure. We decided to construct a novel vector for phage display which allowed us to speed up the selection steps.

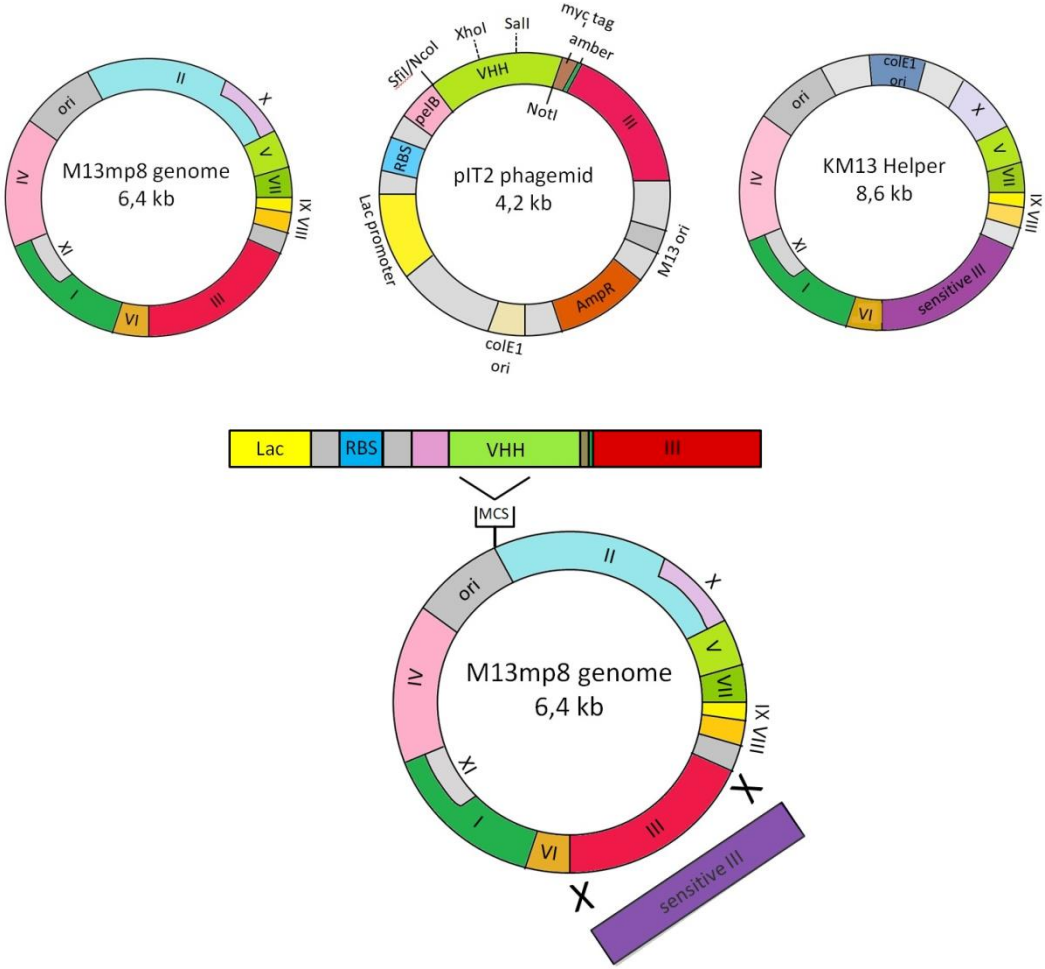

Figure 5 Schematic representation of M13mp8 genome, pIT2 phagemid and KM13 Helper phage. A schematic representation of M13mp8 genome modifications is also represented; RBS: ribosome binding site; MCS: multiple cloning site (see "Materials and Methods" for details).

Starting from an ancient M13 vector (M13mp8), first of all we wanted to modify endogenous pIII M13 to render it sensitive to trypsin digestion (necessary feature for phage recovery after selection). Exploiting CPEC cloning procedure, trypsin sensitive pIII gene from helper phage KM13 was introduced into the M13mp8 genome in place of the endogenous one (**Figure 5,** see "Materials and Methods" for details). This M13 modified vector (hereafter designated as tsM13mp8) was then further engineered by introducing the Lac-pIII sequence of pIT2 phagemid into its multiple cloning sites. The Lac-pIII sequence contains different genetic features such as a Lac inducible promoter, pelB secretion peptide encoding sequence, a multiple cloning sites (for cloning Nb sequences), His-Tag and Myc-Tag encoding sequences, followed by a wild type pIII gene. The presence of a stop codon just before pIII gene allows the expression of Nb-pIII fusion protein only in bacterial strain possessing an amber suppressor gene (e.g. TG1 strain) (**Figure 5**, see "Materials and Methods" for details).
In short, the newly constructed vector (called M13-flash) bears two pIII genes, one is from the helper phage KM13, while the other comes from pIT2 together with some phagemid features.
M13–flash vector can be used for the direct cloning of the Nb gene library since it should be able to produce complete phages, displaying Nb on their surface without the need of a helper phage.

3.4.2. Validation of M13-flash suitability for phage display selection

Once M13-flash vector was assembled, in order to validate its functionality during panning steps, a small aliquot of the humanized Nb library amplicons and anti-GFP Gcons Nb gene (see Chapter 1 for details) were cloned in frame with engineered pIII protein obtaining M13-flash Library and M13-flash Gcons vectors. The vectors were transformed in TG1 *E. coli* strain, selected and amplified in liquid medium. With both of them, high titers of phages (up to 10^{12} clones) have been produced, demonstrating the possibility to obtain complete phage assembly from M13-flash vector without helper phage infection. Before amplification, small aliquots of the transformed bacteria were plated to evaluate the library complexity and the rate of non-recombinant clones. The generated small humanized Nb library showed a complexity of about 10^6 independent clones with a frequency of less than 0.1 % of non-recombinant phages.
M13-flash derived phages were expected to expose Nbs on their surface because Nb-pIII engineered proteins, under the control of the leaky Lac promoter, might be expressed in association with the production of phage-derived pIII protein whose expression is controlled by an endogenous M13 promoter[31]. To demonstrated the correct exposure of Nbs on phages surface and to validate M13-flash functionality during phage display,

panning steps on an *ad hoc* pool of phages were performed: phages derived from M13-flash Gcons and the small M13-flash Library were mixed with a ratio of 1:10^6 respectively. Three panning steps following the protocol described in "Materials and Methods" against GFP protein and an unrelated protein (E2-Crimson) were performed in order to verify the selection of specific binders. At the end of the procedure, a phage ELISA test was performed in which phages, collected after every panning step, were analysed for their exposure of GFP or E2-Crimson binders.

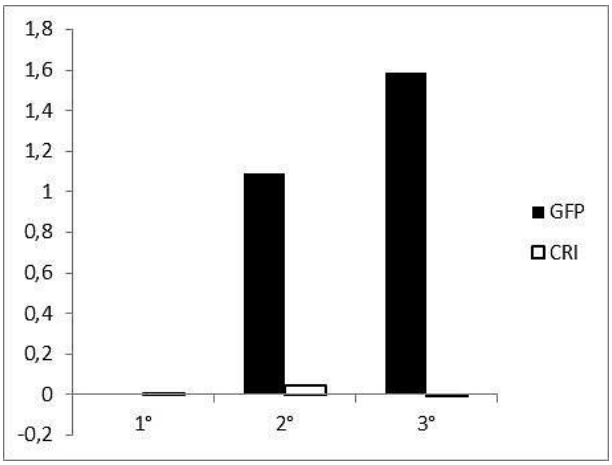

Figure 6 Phage ELISA testing of phages deriving from 1°, 2° and 3° panning steps against GFP or E2-Crimson (CRI). Bars represent absorbance measured at 415 nm after addition of the horseradish peroxidase (HRP) substrate, abscissa indicates the tested panning steps (see "Materials and Methods" for details).

As shown in **Figure 6**, after every panning step performed against GFP an increase in GFP binders titer was observed; the same result was not obtained in case of anti-E2 Crimson selection. 96 randomly picked clones from the enriched library derived from the third panning were individually submitted to phage ELISA test which showed the presence of 8 clones expressing GFP specific binders.

These results indicated that M13-flash phages are able to expose functional Nbs on their surface and the possibility to use successfully this vector in a speeded up phage display selection procedure.

3.5. Cloning of the humanized artificial semi-random nanobody library in M13-flash vector

Once established the complete functionality of M13-flash, different attempts to clone into this vector the humanized Nb library were performed. In order to obtain a final complexity of 10^9 different Nbs (the maximum complexity allowed by cloning techniques which require bacterial transformation) a classical ligation in NcoI-NotI cloning sites was accomplished but no more than 10^7 different clones were isolated. Other cloning procedures were followed like CPEC, InFusion HD and assembling PCR, but no one gave a library with higher complexity.

Currently, we are working on modifying M13-flash vector to render it suitable for Gateway cloning. This innovative cloning procedure is based on site-specific

recombination mediated by bacteriophage lambda proteins which guarantees high ligation efficiency in library construction. In particular, in a first reaction (BP reaction), the library will be transferred in a donor vector (pDONR222, Invitrogen, Carlsbad, California, USA) and subsequently, with a second reaction (LR reaction), in the destination vector[32]. M13-flash have been further engineered (see "Materials and methods" for details) in order to transform it a destination vector (M13-flash-DEST) and now it is ready to be tested in the Gateway cloning procedure.

4. Discussion

In order to render antibodies suitable for human applications humanization of their sequences is required; indeed rendering therapeutic antibodies as similar as possible to human antibodies decreases the risk of treatment immune rejection in patients[3]. Since humanization of a functional antibody can lead to loss of solubility and/or target binding capacity[12] the construction of humanized antibody library from which to mine new antibodies seems the most interesting strategy.

Here we present the construction of a humanized Nb library to be used in a phage display selection. This library is an evolution of a previously reported work in which a complex and functional artificial library for ribosome display selection was built (Chapter 1). Starting from our consensus framework scaffold (CFW), which derives from the alignment of more than 750 Nb llama sequences, we inserted 12 point mutations to generate a humanized version (hCFW) with which to construct an artificial humanized Nb library. The use of a humanized universal scaffold may bring some advantages: i) it helps in the standardisation of subsequent Nbs manipulation since VHHs bearing the same framework should present similar immunogenicity and stability[33], ii) the selection of already humanized Nbs avoids post-selection modification that could lead to loss of target affinity[12].

Despite humanized Nb libraries have been reported[13,20], our hCFW is the first scaffold, at our knowledge, identical to human IgG VH III consensus sequence; this similarity to the FRs of human antibody (**Figure 1B**) might reduce the risk of Nbs rejection in case of patients treatment with these molecules. Also the use of single human VH domains as binding units and the construction of human VH libraries have been previously reported[34,35], as well as attempts to solubilize and stabilize selected human VH domains through "camelization" of their sequence[36], but the lack of their VL domain counterpart[13] limit their binding affinity to some extent. On the contrary, our VHH library, having a scaffold identical to a human VH and CDRs which, in sequence and length, resemble those found in llama Nbs, should allow selecting human VHs with the binding capacity of Nbs.

We first validated our humanization strategy grafting CDRs of two Nbs (which showed unchanged binding properties after the previous grafting in the llama-derived CFW) into the humanized version of the scaffold: Gcons (anti-GFP Nb, see Chapter 1 for details) and G09cons (anti-murine IgGs Nb, see Chapter 4 for details). Both humanized versions of the Nbs (hGcons and hG09cons respectively) showed a high level of expression and solubility when produced as recombinant proteins in *E. coli*, highlighting an identical solubilizing and stabilizing properties of hCFW if compared with llama version (**Figure 2**). While hG09cons showed unchanged target-binding capacity, an apparent decrease of target affinity was visible only in case of hGcons Nb (**Figure 3**). Since in some Nbs FRs might be involved in target binding, we expected that the modification of the scaffold could have reduced binding capacity, exactly as antibody humanization could lead to loss of target affinity.

After hCFW scaffold validation, following the same protocol for CDRs randomisation and library assembly reported in Chapter 1, a humanized version of the Nb library encoding genes was built by assembling PCR (**Figure 4**). High complexity and quality of the library genes were confirmed through sequencing of a sample of about hundred cloned amplicons which showed that more than 75% of them were correct with CDRs randomisation consistent with expected degeneration.

The amplicon library is now ready to be cloned in a vector for rendering it selectable through phage display method. We chose phage display because it is the most widespread and robust antibodies selection technique, is the easiest one and can be applied in almost every laboratory performing in harsh conditions or difficult target selections[37]. Standard phage display which uses phagemid as cloning vector is very time-consuming since one panning step required 3-4 days: once the selection of Nbs exposing phages is performed and *E. coli* infection is executed, as phagemids are not able to produce phages, a pool of *E. coli* resistant cells are isolated. These cells have to be grown and secondarily infected with a helper phage in order to get final Nbs exposing phages for the subsequent panning step[24]. Fusing Nbs directly to endogenous pIII protein of M13 genome can be an alternative excluding the use of helper phage infection, but fusing peptides with more than 50 amino acids to pIII protein leads generally to not infective phages. Furthermore, since M13 pIII protein is present in five copies on phage particles, the antibody would be pentavalent and a selection against a target could lead to the isolation of low-affinity binders[38].

To speed up phage display selection, here we reported the assembly of a novel vector suitable for rapid panning steps: we modified the genome of an ancient M13 vector introducing in its multiple cloning sites the pIII expressing sequence from pIT2 phagemid and substituting M13 endogenous pIII gene with one derived from trypsin sensitive

Helper phage protein (**Figure 5**). These modifications led to a vector (M13-flash) that is able to autonomously produce complete phages which bear, on their surface, trypsin sensitive version of pIII and, thanks to the leaky activity of pIT2 expressing sequence, no more than one copy of Nb-pIII fused peptide. The expected VHH-pIII/pIII protein ratio of less than 1/5 has yet to be assessed through a western blot experiment on phage protein extract using antibodies against pIII[31]. We finally demonstrated the functionality of M13-flash vector during speedy panning procedures simulating a phage display selection against GFP with a Gcons-derivative contaminated small phage VHH library. After three rounds of panning, which took less than a week, more copies of the correct GFP-binder were recovered (**Figure 6**).

The vector is now ready to receive the humanized semi-random Nb library amplicons but the goal of final library complexity of 10^9 clones could not be reached yet using alternative cloning procedures. For this reason, the vector has been further modified in order to render it suitable for Gateway cloning procedure, which, from early tests, seemed to guarantee higher ligation efficiency[32].

We speculate that once high-efficient ligation is archived and a high complex library is obtained, with a fast selection procedure new Nbs, potentially ready to be used in humans, could be acquired. The speedy phage display technique will improve the number of selection performed at the same time, increasing the possibility to find new potential binders.

5. Bibliography

1. Strohl WR. Current progress in innovative engineered antibodies. *Protein Cell*. 2018;9(1):86-120. doi:10.1007/s13238-017-0457-8.
2. Kashmiri SVS, De Pascalis R, Gonzales NR, Schlom J. SDR grafting - A new approach to antibody humanization. *Methods*. 2005;36(1):25-34. doi:10.1016/j.ymeth.2005.01.003.
3. Ducancel F, Muller BH. Molecular engineering of antibodies for therapeutic and diagnostic purposes. *MAbs*. 2012;4(4):445-457. doi:10.4161/mabs.20776.
4. Hamers-Casterman C, Atarhouch T, Muyldermans S, et al. Naturally occurring antibodies devoid of light chains. *Nature*. 1993;363(6428):446-448. doi:10.1038/363446a0.
5. Ghassabeh GH-, Devoogdt N, Pauw P De, Vincke C, Muyldermans S. Nanobodies and their potential applications. *Nanomedicine*. 2013;8(6):1013-1026.
6. Bannas P, Hambach J, Koch-Nolte F. Nanobodies and nanobody-based human heavy chain antibodies as antitumor therapeutics. *Front Immunol*. 2017;8(NOV):1-13. doi:10.3389/fimmu.2017.01603.
7. Muyldermans S. Nanobodies : Natural Single-Domain Antibodies. 2013. doi:10.1146/annurev-biochem-063011-092449.
8. Kazemi-Lomedasht F, Muyldermans S, Habibi-Anbouhi M, Behdani M. Design of a humanized anti vascular endothelial growth factor nanobody and evaluation of its in vitro function. *Iran J Basic Med Sci*. 2018;21(3):260-266. doi:10.22038/ijbms.2018.24898.6183.
9. Yu Y, Li J, Zhu X, et al. Humanized CD7 nanobody-based immunotoxins exhibit promising anti-T-cell acute lymphoblastic leukemia potential. *Int J Nanomedicine*. 2017;12:1969-1983. doi:10.2147/IJN.S127575.
10. Peyvandi F, Scully M, Kremer Hovinga JA, et al. Caplacizumab for Acquired Thrombotic Thrombocytopenic Purpura. *N Engl J Med*. 2016;374(6):511-522. doi:10.1056/NEJMoa1505533.
11. Duggan S. Caplacizumab: First Global Approval. *Drugs*. 2018;(0123456789). doi:10.1007/s40265-018-0989-0.
12. Vaneycken I, Govaert J, Vincke C, et al. In Vitro Analysis and In Vivo Tumor Targeting of a Humanized, Grafted Nanobody in Mice Using Pinhole SPECT/Micro-CT. *J Nucl Med*. 2010;51(7):1099-1106. doi:10.2967/jnumed.109.069823.
13. Vincke C, Loris R, Saerens D, Martinez-Rodriguez S, Muyldermans S, Conrath K. General strategy to humanize a camelid single-domain antibody and identification of a universal humanized nanobody scaffold. *J Biol Chem*. 2009;284(5):3273-3284. doi:10.1074/jbc.M806889200.
14. Koch-Nolte F, Reyelt J, Schossow B, et al. Single domain antibodies from llama effectively and specifically block T cell ecto-ADP-ribosyltransferase ART2.2 in vivo. *FASEB J*. 2007. doi:10.1096/fj.07-8661com.
15. Vaneycken I, Devoogdt N, Van Gassen N, et al. Preclinical screening of anti-HER2 nanobodies for molecular imaging of breast cancer. *FASEB J*. 2011;25(7):2433-2446. doi:10.1096/fj.10-180331.
16. Behar G, Sibéril S, Groulet A, et al. Isolation and characterization of anti-FcγRIII (CD16) llama single-domain antibodies that activate natural killer cells. *Protein Eng Des Sel*. 2008;21(1):1-10. doi:10.1093/protein/gzm064.
17. Zhai W, Glanville J, Fuhrmann M, et al. Synthetic antibodies designed on natural sequence landscapes. *J Mol Biol*. 2011;412(1):55-71. doi:10.1016/j.jmb.2011.07.018.
18. Prassler J, Thiel S, Pracht C, et al. HuCAL PLATINUM, a synthetic Fab library optimized for sequence diversity and superior performance in mammalian expression systems. *J Mol Biol*. 2011;413(1):261-278. doi:10.1016/j.jmb.2011.08.012.
19. Goldman ER, Andersen GP, Liu JL, et al. Facile generation of heat-stable antiviral and antitoxin single domain antibodies from a semisynthetic llama library. *Anal Chem*. 2006;78(24):8245-8255. doi:10.1021/ac0610053.
20. Moutel S, Bery N, Bernard V, et al. NaLi-H1: A universal synthetic library of humanized nanobodies providing highly functional antibodies and intrabodies. *Elife*. 2016;5(JULY):1-31. doi:10.7554/eLife.16228.
21. Ingram JR, Schmidt FI, Ploegh HL. Exploiting Nanobodies' Singular Traits. *Annu Rev Immunol*.

2018;36(1):695-715. doi:10.1146/annurev-immunol-042617-053327.
22. McMahon C, Baier AS, Pascolutti R, et al. Yeast surface display platform for rapid discovery of conformationally selective nanobodies. *Nat Struct Mol Biol*. 2018;25(3):289-296. doi:10.1038/s41594-018-0028-6.
23. Romao E, Morales-Yanez F, Hu Y, et al. Identification of Useful Nanobodies by Phage Display of Immune Single Domain Libraries Derived from Camelid Heavy Chain Antibodies. *Curr Pharm Des*. 2017;22(43):6500-6518. doi:10.2174/1381612822666160923114417.
24. Lee CMY, Iorno N, Sierro F, Christ D. Selection of human antibody fragments by phage display. *Nat Protoc*. 2007;2(11):3001-3008. doi:10.1038/nprot.2007.448.
25. Sambrook J, W Russell D. Molecular Cloning: A Laboratory Manual. *Cold Spring Harb Lab Press Cold Spring Harb NY*. 2001. doi:10.1016/0092-8674(90)90210-6.
26. Sehr P, Zumbach K, Pawlita M. A generic capture ELISA for recombinant proteins fused to glutathione S-transferase: Validation for HPV serology. *J Immunol Methods*. 2001;253(1-2):153-162. doi:10.1016/S0022-1759(01)00376-3.
27. Quan J, Tian J. Circular polymerase extension cloning for high- throughput cloning of complex and combinatorial DNA libraries. *Nat Protoc*. 2011;6(2):242-251. doi:10.1007/978-1-62703-764-8_8.
28. Clontech (Takara). In-Fusion® HD Cloning Kit User Manual. *In-Fusion Cloning*. 2012;1(011614):1-15. doi:10.1016/0045-6535(92)90022-J.
29. Harmsen MM, Ruuls RC, Nijman IJ, et al. Llama heavy chain V-regions consist of at least four distinct subfamilies revealing novel sequence features. *Mol Immunol*. 2001;37(2000):579-590.
30. Scheuer W, Friess T, Burtscher H, Bossenmaier B, Endl J, Hasmann M. Strongly enhanced antitumor activity of trastuzumab and pertuzumab combination treatment on HER2-positive human xenograft tumor models. *Cancer Res*. 2009;69(24):9330-9336. doi:10.1158/0008-5472.CAN-08-4597.
31. Kramer RA, Cox F, van der Horst M, et al. A novel helper phage that improves phage display selection effciency by preventing the amplification of phages without recombinant protein. *Nucleic Acids Res*. 2003;27(12):2123-2128. doi:10.1093/nar/gng058.
32. Life Technologies Carlsbad CA. Gateway ® Technology with Clonase ™ II A universal technology to clone DNA. *User Man*. 2009;(25). doi:10.3189/172756406781812087.
33. Saerens D, Pellis M, Loris R, et al. Identification of a universal VHH framework to graft non-canonical antigen-binding loops of camel single-domain antibodies. *J Mol Biol*. 2005;352(3):597-607. doi:10.1016/j.jmb.2005.07.038.
34. Mandrup OA, Friis NA, Lykkemark S, Just J, Kristensen P. A Novel Heavy Domain Antibody Library with Functionally Optimized Complementarity Determining Regions. *PLoS One*. 2013;8(10):1-15. doi:10.1371/journal.pone.0076834.
35. Christ D, Famm K, Winter G. Repertoires of aggregation-resistant human antibody domains. *Protein Eng Des Sel*. 2007;20(8):413-416. doi:10.1093/protein/gzm037.
36. Martin F, Volpari C, Steinkuhler C, et al. Affinity selection of a camelized V(H) domain antibody inhibitor of hepatitis C virus NS3 protease. *Protein Eng*. 1997;10(5):607-614. doi:10.1093/protein/10.5.607.
37. Hoogenboom HR. Selecting and screening recombinant antibody libraries. *Nat Biotechnol*. 2005;23(9):1105-1116. doi:10.1038/nbt1126.
38. McConnell SJ, Uveges AJ, Fowlkes DM, Spinella DG. Construction and screening of M13 phage libraries displaying long random peptides. *Mol Divers*. 1996. doi:10.1007/BF01544954.

Chapter 3

Chapter 3: A simple and modular method to produce monoclonal-like antibodies trough SpyTag – SpyCatcher technology

1. Introduction

Since their serendipitous discovery in 1993[1] the variable domains of heavy chain antibodies (nanobodies (Nb) or VHHs) are protagonists of an increasing number of published articles. Due to the convergence of many characteristics like small size (~15 kDa), high solubility, high yield of expression in prokaryotic systems and high specific binding capacity Nbs are good diagnostic and therapeutic tools[2].

Nbs are known for their intrinsic low immunogenicity due to their small size, rapid clearance from the bloodstream[3] and high identity level with human IgG VH III subtype[4]; however the impossibility to create secondary antibodies against them is a limitation in diagnostic field and their lack of effector function restricts their therapeutic applications.

In order to render Nbs detectable through secondary antibodies, to increase their effector function and target affinity trough dimerization, many fusions of these variable domains to immunoglobulins Fc regions are reported in literature[5]. The immunoglobulin *fragment crystallisable* (Fc), composed of CH2 and CH3 domains dimer, is responsible for antibodies effector function throughout Fc-receptor activation on immune cells[6,7]. Fusing this region of immunoglobulins to VHHs leads to variable effects: Nb *in vivo* half-live and avidity can be enhanced increasing the dimension and inducing dimerization of the antibody[8,9]; recruitment of immune response through Fc receptor activation is another possible effect[10] that can be increased through a rational choice of the fusion partner: fusing human IgA Fc region to an anti-enterotoxigenic *Escherichia coli* Nb increased its anti-bacterial activity thanks to canonical IgA Fc interactions in mucosas[11]. Nb fusion to Fc regions can also be used to extend diagnostic applications of the antibody: the fusion of an anti-P2X7 VHH to a rabbit Fc region permitted its application in brain staining[12].

However Fc regions are difficult to express and their fusion to Nbs leads usually to insoluble proteins that have to be expressed in eukaryotic systems like *Pichia pastoris*[13], HEK/NS0/CHO cell lines[9,10,14] or plants[8,11,12].

In our laboratory a consensus framework scaffold (CFW) was produced in order to enhance Nb expression in bacteria (as described in details in Chapter 1); we attempted to fuse our CFW grafted Nbs to immunoglobulin Fc regions and we personally noted the difficulty to obtain soluble and active antibodies.

Thus we developed a simple and low-cost mechanism to obtain monoclonal-like antibodies trough SpyTag and SpyCatcher technology: Nbs and Fc regions were joined through an *in vitro* protein ligation system obtaining molecules which are able to bind their target and possess detectable Fc regions.
SpyTag and SpyCatcher are two part of the same collagen adhesion domain (CnaB2) of *Streptococcus pyogenes* (Spy) fibronectin binding protein (FbaB). CnaB2 domain contains an isopeptide bond between Lys^{31} and Asp^{117} that spontaneously forms during protein assembly. Separating the catalytic domain (SpyCatcher containing Lys^{31}) from the target peptide (SpyTag containing Asp^{117}) a rapid *in vitro* ligation system was developed: cloning SpyTag or SpyCatcher in frame to N/C terminus of two fusion partners leads to their rapid and directional *in vitro* ligation[15].
We fused SpyTag and SpyCatcher to C-terminus of different Nbs and to the N-terminus of different immunoglobulin Fc regions, after *in vitro* ligation combinations always fully functional monoclonal-like antibodies were obtained. These antibodies maintain Nb peculiar binding capacity but, unlike the Nbs alone, are detectable through secondary antibodies rendering them useful for diagnostic applications.

2. Materials and Methods

2.1. Molecular biology reagents and cloning procedures

Standard protocols[16] were used for all basic recombinant DNA procedures. Enzymes were from Takara Bio Europe (Saint-Germain-en Laye, France) and New England Biolabs (Ipswich, MA, USA). Molecular cloning and recombinant protein expression were carried out in BL21 codon plus *E. coli* strain (Stratagene; La Jolla, CA, USA) using pET28 (Merck Millipore, Darmstadt, Germany) plasmid. Following appropriate design, synthesis of murine Fc region and SpyTagRaFc encoding sequences were performed by GenScript (New Jersey, United States); all protein-encoding sequences were optimized with respect to the *E. coli* codon usage (**Table 1**).
Ligation of murine Fc (using NotI and XhoI cloning sites) in pET28 Gcons plasmid (see Chapter 1 for details) and in pET28 Lcons plasmid (using NotI and XhoI cloning sites, see Chapter 1 for details) were performed following standard protocols. Subcloning of LconsMuFc sequence (using NcoI and XhoI cloning sites) in pET28 Strep-Tag (gently provided by Gloria Spagnoli) was performed following standard protocols[16].

Name	Sequence
E.coli codon optimized murine Fc synthetic gene	CCATGGcggccgcaagcttGAACCGCGTGGACCGACAATCAAACCATGCCCT CCGTGCAAATGTCCAGCGCCAAATCTGTTGGGTGGTCCGAGTGTGTTCATCTT TCCGCCGAAAATCAAAGACGTGCTGATGATTAGCCTGTCACCGATTGTTACCT GTGTAGTGGTTGACGTCAGTGAAGATGATCCGGATGTACAGATTTCCTGGTTT GTCAACAATGTTGAGGTGCATACGGCTCAGACGCAAACGCATCGCGAAGATTA CAATTCTACCCTTCGCGTTGTGAGTGCGTTGCCGATCCAGCATCAGGACTGGA TGTCGGGTAAAGAGTTCAAATGCAAAGTGAACAACAAAGACTTACCAGCCCCG ATTGAACGCACCATTAGCAAACCCAAAGGCTCCGTTCGTGCACCGCAAGTGTA TGTACTGCCTCCACCTGAGGAAGAAATGACCAAGAAACAGGTGACACTGACGT GCATGGTTACCGATTTTATGCCCGAGGACATTTATGTAGAATGGACGAATAAT GGCAAAACCGAACTGAACTACAAGAACACAGAACCGGTCTTAGATAGCGATGG CAGCTACTTCATGTACTCGAAACTCCGCGTCGAAAAGAAGAATTGGGTAGAGC GGAACTCCTATTCGTGCTCGGTCGTTCATGAAGGGCTGCACAACCACCACACC ACAAAGTCGTTTTCCCGTACTCCGGGTAAActcgag
E.coli codon optimized SpyTagRaFc synthetic gene	aagcttGTTGCGCCGAGCACCTGCAGCAAGCCGACCTGCCCGCCGCCGGAACT GCTGGGTGGCCCGAGCGTTTTCATTTTCCCGCCGAAGCCGAAGGACACCCTGA TGATCAGCCGTACCCCGGAAGTGACCTGCGTGGTTGTGGATGTGAGCGAGGAC GATCCGGAAGTTCAGTTCACCTGGTACATTAACAACGAACAGGTTCGTACCGC GCGTCCGCCGCTGCGTGAACAGCAATTTAACAGCACCATCCGTGTTGTGAGCA CCCTGCCGATTGCGCACGAGGACTGGCTGCGTGGCAAGGAGTTCAAGTGCAAA GTTCACAACAAAGCGCTGCCGGCGCCGATCGAGAAGACCATTAGCAAAGCGCG TGGTCAGCCGCTGGAACCGAAAGTGTATACGATGGGTCCGCCGCGTGAGGAAC TGAGCAGCCGTAGCGTTAGCCTGACCTGCATGATCAACGGTTTTTACCCGAGC GACATTAGCGTGGAGTGGGAAAAGAACGGCAAAGCGGAGGATAACTATAAAAC CACCCCGGCGGTGCTGGACAGCGATGGTAGCTACTTCCTGTATAGCAAACTGA GCGTTCCGACCAGCGAATGGCAACGTGGCGATGTTTTTACCTGCAGCGTGATG CACGAGGCGCTGCACAACCATTACACCCAGAAAAGCATTAGCCGTAGCCCGGG CAAGctcgag

Table 1 Nucleotide sequences of the synthetic genes used in this chapter. Sequences are shown in standard 5'-3' orientation.

SpyCatcher sequence was PCR-amplified from pET28 HTag-SpyCatcPfTrxL2(20-38) (gently provided by Gloria Spagnoli) plasmid introducing NcoI site at 5' end and NotI site at 3' end. PCR was performed with 1 unit Phusion DNA Polymerase (New England Biolabs, Ipswich, MA, USA) in presence of the SpyF and SpyR (see **Table 2**) oligonucleotides (4 nM each), plus dNTPs (0.8 mM), 1x PCR buffer and 10 ng pET28 HTag-SpyCatcPfTrxL2(20-38) in a final volume of 50 µl: initial denaturation 98°C 1 min; 25 cycles of 10 s at 98°C, 30 s at 55°C, and 60 s at 72°C; additional extension 72°C, 7 min. Ligation of SpyCatcher sequence (using NcoI and NotI cloning sites) and in pET28 murine Fc plasmid was performed following standard protocols[16].

Gcons sequence was PCR-amplified from pET28 Gcons plasmid (see Chapter 1 for details) introducing NcoI site at 5' end and NcoI and SpyTag sequence at 3' end. Three PCR were performed with 1 unit Phusion DNA Polymerase (New England Biolabs, Ipswich, MA, USA) in presence of the consNb(GFP)-SpyTag-FW/consNb(GFP)-SpyTag-RE1 or consNb(GFP)-SpyTag-FW/GFPSpyTag_RE2 or consNb(GFP)-SpyTag-FW/consNb(GFP)-SpyTag-RE3 (see **Table 2**) oligonucleotides (4 nM each), plus dNTPs (0.8 mM), 1x PCR buffer and 10 ng of template in a final volume of 50 µl. First PCR was performed using pET28 Gcons as template obtaining Amplicon1: initial denaturation 98°C 1 min; 25 cycles of 10 s at 98°C, 30 s at 67°C, and 30 s at 72°C; additional extension 72°C, 5 min. Second PCR was performed using Amplicon1 as template obtaining Amplicon2: initial denaturation 98°C 1

min; 25 cycles of 10 s at 98°C, 30 s at 61°C, and 30 s at 72°C; additional extension 72°C, 5 min. Third PCR was performed using Amplicon2 as template obtaining GconsSpyTag sequence: initial denaturation 98°C 1 min; 25 cycles of 10 s at 98°C, 30 s at 60°C, and 30 s at 72°C; additional extension 72°C, 5 min. GconsSpyTag sequence was cloned in pET28 plasmid in NcoI cloning site following standard protocols[16].

Name	Sequence
SpyF	GTTTAACTTTAAGAAGGAGATATACcatgGATAGTGCTACCCATAT
SpyR	cggttcaagcttgcggccgctAATATGAGCGTCACCTTTAGTTG
consNb(GFP)-SpyTag-FW	aattttgtttaactttaagaaggagatataCCATGGGCCAGGTACAGC
consNb(GFP)-SpyTag-RE1	ACGATGTGGGCGGAACCGTGGTGGTGGTGGTGGTGC
GFPSpyTag_RE2	CCTTCGTCGGCTTGTAGGCGTCCACCATCACGATGTGGGCGGA
consNb(GFP)-SpyTag-RE3	gatgatggctgctgcCCATGGTCAACTACCCTTCGTCGGCTTGTAG
consNb(Lys)-SpyTag-FW	aattttgtttaactttaagaaggagatataCCATGGttacccaggtgcag
cNbGFP-SpyCatchFW	TTGTTTAACTTTAAGAAGGAGATATACCATGGGCCAGGTACA
cNbGFP-SpyCatchRE	ATTTAATATGGGTAGCACTATCCATGGaGCGGCCGCTGCT

Table 2 Nucleotide sequences of the primers used in this chapter. Sequences are shown in standard 5'-3' orientation.

Lcons sequence was PCR-amplified from pET28 Lcons plasmid (see Chapter 1 for details) introducing NcoI site at 5' end and NcoI site + SpyTag encoding sequence at 3' end. Three PCR were performed with 1 unit Phusion DNA Polymerase (New England Biolabs, Ipswich, MA, USA) in presence of the consNb(Lys)-SpyTag-FW /consNb(GFP)-SpyTag-RE1 or consNb(Lys)-SpyTag-FW /GFPSpyTag_RE2 or consNb(Lys)-SpyTag-FW /consNb(GFP)-SpyTag-RE3 (see **Table 2**) oligonucleotides (4 nM each), plus dNTPs (0.8 mM), 1x PCR buffer and 10 ng of template in a final volume of 50 µl. First PCR was performed using pET28 Lcons as template obtaining Amplicon1: initial denaturation 98°C 1 min; 25 cycles of 10 s at 98°C, 30 s at 67°C, and 30 s at 72°C; additional extension 72°C, 5 min. Second PCR was performed using Amplicon1 as template obtaining Amplicon2: initial denaturation 98°C 1 min; 25 cycles of 10 s at 98°C, 30 s at 61°C, and 30 s at 72°C; additional extension 72°C, 5 min. Third PCR was performed using Amplicon2 as template obtaining LconsSpyTag sequence: initial denaturation 98°C 1 min; 25 cycles of 10 s at 98°C, 30 s at 60°C, and 30 s at 72°C; additional extension 72°C, 5 min. LconsSpyTag sequence was cloned in pET28 plasmid in NcoI cloning site following standard protocols[16].
Ligation of rabbit Fc (using HindIII and XhoI cloning sites) and in pET28 Gcons plasmid (see Chapter 1 for details) and ligation of rabbit Fc (using HindIII and XhoI cloning sites) in pET28 SpyCatcher plasmid (gently provided by Gloria Spagnoli) were performed following standard protocols[16].
Gcons sequence was PCR-amplified from pET28 Gcons plasmid (see Chapter 1 for details) introducing NcoI sites at 5' and 3' ends. PCR was performed with 1 unit Phusion DNA Polymerase (New England Biolabs, Ipswich, MA, USA) in presence of the cNbGFP-

SpyCatchFW and cNbGFP-SpyCatchRE (see **Table 2**) oligonucleotides (4 nM each), plus dNTPs (0.8 mM), 1x PCR buffer and 10 ng pET28 Gcons in a final volume of 50 µl: initial denaturation 98°C 1 min; 25 cycles of 10 s at 98°C, 30 s at 62°C, and 30 s at 72°C; additional extension 72°C, 5 min. Ligation of Gcons sequence (using NcoI cloning site) in pET28 SpyCatcher plasmid was performed following standard protocols[16].

2.2. Recombinant protein expression and purification

Standard procedures were used for recombinant proteins expression. Briefly, 10 ml of stationary overnight cultures (LB, 50 mg/l of kanamycin and 34 mg/l of chloramphenicol at 37 °C) were inoculated into 1 l cultures of the same media. After reaching an A_{600} value of 0.4-0.6, cultures were induced with 1 mM IPTG and further incubated overnight at 20°C. Following centrifugation (5000 rpm, 15 min), bacterial cell pellets were recovered, suspended in 200 ml of Tris 10 mM pH 8.0 and centrifuged in the same conditions. Bacterial pellet was suspended in 50 ml of Tris-buffered saline (Tris 25 mM pH 8.0, NaCl 0.3 M, freshly supplemented with protease inhibitors), and lysed by sonication (20 min total sonication time performed with 3 sec bursts alternated with 6 sec resting on ice) carried out at constant power (4W/cm2; Sonicator 3000, Misonix). Lysates were then centrifuged (10000 rpm, 30 min) and the resulting supernatants were used as starting material for metal-affinity purification using a built-in 6xHis-tag and a His-select cobalt affinity resin (Sigma-Aldrich, Saint Louis, MO, USA) as per manufacturer's instructions. Bacterial lysates and individual metal-affinity chromatography fractions were analysed by SDS-PAGE on 15%-11% polyacrylamide gels.
SpyCatcherMuFc protein was expressed in presence of pKJE7 plasmid (Takara Bio Europe, Saint-Germain-en Laye, France) in BL21 *E. coli* stain following user's manual instructions; cells lysis and protein purification were performed as described above.
Recombinant green fluorescent protein (GFP) used in this work is enhanced GFP. GST-tagged GFP and thioredoxin, biotinylated lysozyme and thioredoxin were gently provided by collaborators.

2.3. SpyTag – SpyCatcher reactions

All the reactions between SpyTag and SpyCatcher proteins were performed at 20°C for 3 days in TBS buffer (25 mM Tris HCl, 0.3 M NaCl, pH 8.0) in presence of protease inhibitor cocktail (Sigma-Aldrich, Saint Louis, MO, USA) following user's manual instructions. 70 nM of the protein of interest were mixed with 140 nM of the second protein in a final volume of 100 µl. After reactions final fusion proteins were analysed by SDS-PAGE on 11% polyacrylamide gels.

2.4. Gel filtration analysis

Two samples of every monoclonal-like antibodies produced in this chapter (300 µg each) were prepared using the following protocol: one was suspended in 25 mM Tris-HCl (pH 7.5), 150 mM NaCl and 5 mM β-mercaptoethanol, the other was suspended in 25 mM Tris-HCl (pH 7.5), 150 mM NaCl. Both samples were incubated for 1 hr at room temperature and used for analysis. Size exclusion chromatography (SEC) was performed on a Superdex 200 HR10/30 column (24 ml; GE Healthcare) equilibrated in 25 mM Tris-HCl (pH 7.5), 150 mM NaCl, at a flow-rate of 0.7 ml/min, using an ÄKTA Prime Plus pump/monitoring (280 nm) system. A calibration curve was built with the use of thyroglobulin (670 kDa), human ferritin (440 kDa), yeast alcohol dehydrogenase (140 kDa), bovine serum albumin (66 kDa), ovalbumin (44.3 kDa), trypsinogen (24 kDa) and lysozyme (14.5 kDa) as molecular mass standards.

2.5. ELISA tests procedures

GST-ELISA tests performed to verify monoclonal-like antibodies activity were carried out using the following protocol: polystyrene 96-wells microtiter plates were coated overnight at 4°C with casein-glutathione (prepared and used as previously described[17]) dissolved in carbonate buffer (1 vol. 0.5 M Na_2CO_3 : 4 vol. 0.5 M $NaHCO_3$ pH 9.6). Blocking was performed by incubation for 1 hr at room temperature with 0.2% casein in Phosphate-buffered saline (PBS, pH 7.4), followed by a 1 hr incubation at room temperature with the purified GST-tagged proteins in PBS (800 nM each). After incubation with serial 1:3 dilutions of monoclonal-like antibodies (starting from 800 nM) for 1 hr at room temperature, a peroxidase-conjugated anti-mouse IgG (whole molecule) goat antibody (Sigma-Aldrich) diluted 1:5000 in PBS + 0.2% casein was added. Following an additional 1 hr incubation at RT, wells were filled with the 2,2'-azino-di-[3-ethylbenzthiazoline sulfonate (ABTS) substrate (KPL, Gaithersburg, MD, USA) and absorbance was measured at 415 nm with a microplate reader (iMark, Biorad). Wells were washed with PBS containing 0.3% (v/v) Tween20 after each incubation step.
ELISA tests on biotinylated lysozyme and thioredoxin were performed following the same protocol but polystyrene 96-wells microtiter plates were coated overnight at 4°C with 66 nM neutravidin dissolved in PBS. All the ELISA tests were triplicated.

2.6. Western Blot procedures

3 ml of stationary overnight BL21 pET28 GFP or BL21 pET28 culture (LB, 50 mg/l of kanamycin and 34 mg/l of chloramphenicol at 37 °C) were inoculated into 10 ml cultures of the same media. After reaching an A_{600} value of 0.4-0.6, cultures were induced with 1

mM IPTG and further incubated for 3 hr at 37°C. Following centrifugation (5000 rpm, 15 min), bacterial cell pellets were recovered, suspended in 1 ml of Tris 10 mM pH 8.0 and centrifuged in the same conditions. Bacterial pellet was suspended in 1 ml of Tris-buffered saline (Tris 25 mM pH 8.0, NaCl 0.3 M, freshly supplemented with protease inhibitors), and lysed by sonication (10 min total sonication time performed with 30 sec bursts alternated with 1 min resting on ice) carried out at constant power (4W/cm2; Sonicator 3000, Misonix). Lysates were then centrifuged (10000 rpm, 30 min) and the resulting supernatants were analysed by SDS-PAGE on 11% polyacrylamide gels. Supernatant GFP content was evaluated and the same quantity of chicken lysozyme was added in BL21 pET28 supernatant: both supernatants were used as starting material for Western Blot analyses.

Serial 1:2 dilutions of GFP and lysozyme containing *E. coli* supernatants were analysed by SDS-PAGE on 11 and 15% polyacrylamide gels respectively, and were transferred on nitrocellulose membranes (GE Healthcare, Little Chalfont, USA) for 2 hr in transferring buffer (25 mM Tris HCl, 192 mM glycine, 10% methanol, pH 8.3). Transferred membranes were blocked for 2 hr at room temperature with TBS (20 mM Tris HCl, 150 mM NaCl, pH 7.4) + 5% Skin Milk and then 40 nM of monoclonal-like antibodies in TBS + 5% BSA were added. Incubation of the membranes continued o/n at 4°C and the next day anti-rabbit or anti-mouse IRDye antibodies (LI-COR, Lincoln, Nebraska, USA) diluted 1:15000 in TBS + 5% BSA were added. After 1 hr incubation membranes were analysed with Odyssey instrument (LI-COR, Lincoln, Nebraska, USA) at 700 nm. After every incubation three washing steps were performed with TBS+0.3% (v/v) Tween20.

3. Results

3.1. Direct fusion of CFW grafted nanobodies to murine IgG Fc region

3.1.1 Cloning and expression of Gcons and Lcons fused to murine IgG 2a Fc region

To assess the possibility to fuse CFW grafted Nbs to IgG Fc regions we chose murine IgG 2a Fc as first fusion partner because large amounts of secondary anti-mouse antibodies are commercially available. We cloned Gcons and Lcons Nbs encoding genes (anti-GFP and anti-chicken lysozyme natural CDRs grafted in our CFW, see Chapter 1 for details) in frame at the N-terminus to murine Fc encoding region and exploiting pET expression system we obtained GconsMuFc and LconsMuFc proteins respectively.

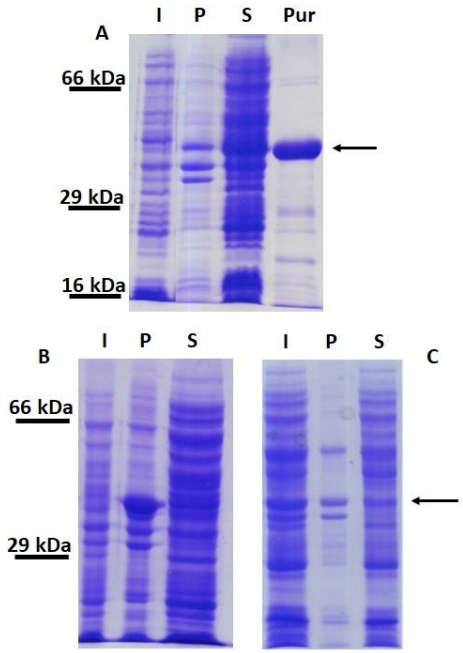

Figure 1 Expression and solubility analysis of GconsMuFc (A) and LconsMuFc His-Tag (B) or Strep-Tag (C). I: induced bacterial lysate; S: bacterial lysate supernatant; P: bacterial pellet; Pur: purified protein. The arrows mark the polypeptide bands corresponding to the fusion proteins. Molecular size of the marker is indicated on the left of the figures (see "Materials and Methods" for details).

After cell lysis, GconsMuFc protein turned out to be soluble and was purified by metal-affinity chromatography using the vector-provided poly-histidine tag (see "Materials and methods" for details) with a final yield of approximately 15 mg of pure protein/L of bacterial culture (**Figure 1A**). LconsMuFc protein was completely insoluble (**Figure 1B**) and the substitution of the poly-histidine tail with Strep-peptide as purification tag did not enhance protein solubility (**Figure 1C**).

3.1.2. Analysis of GconsMuFc structure and functionality

Because of the presence of Fc domain, we expected GconsMuFc assume a monoclonal-like structure (**Figure 3**) due to dimer formation. Thus, the correct dimerization of the protein was verified. Size exclusion chromatography (SEC) was performed and two samples of GconsMuFc were analysed: one sample was incubated for 1 hour in presence of β-mercaptoethanol and the other sample not (see "Materials and Methods" for details).

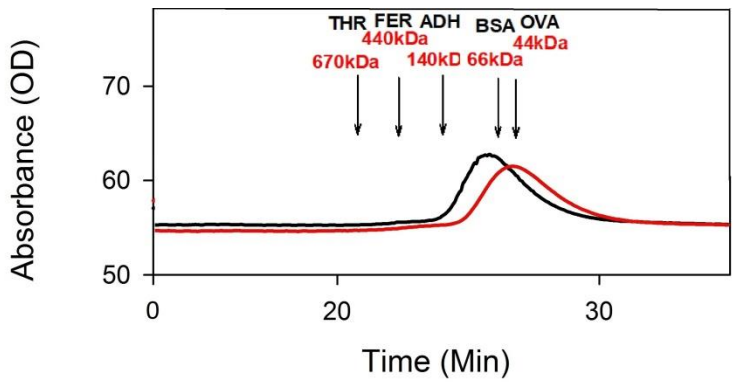

Figure 2 SEC performed on GconsMuFc with Superdex 200 column on ÄKTA system. Sample in red was treated with 5 mM β-mercaptoethanol and sample in black is the not treated counterpart. Elution time of markers is shown on the top (see "Materials and Methods" for details).

As shown in **Figure 2** after treatment with the reducing agent (thus reduction of disulphide bonds responsible of dimerization) a delay in the elution time was observed (in red), if compared with the elution time of the not treated sample (in black).

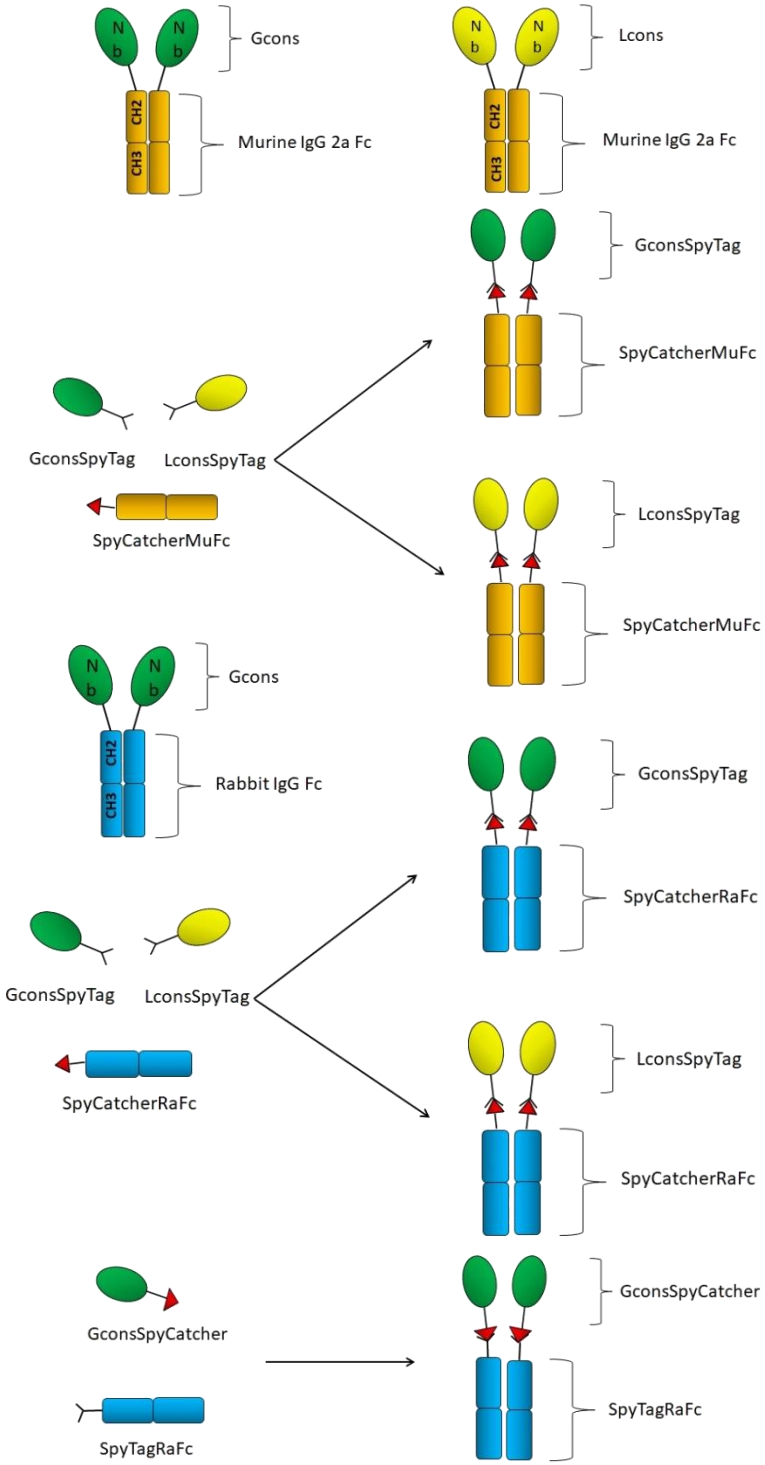

Figure 3 Schematic representation of all the monoclonal-like antibodies and single proteins produced in this chapter.

Comparing elution times with those of protein markers, these results indicated that in solution and in the absence of reducing agents GconsMuFc protein has a molecular weight corresponding to its dimer.

The functionality of GconsMuFc monoclonal-like antibody was assessed in ELISA test and Western Blot. In ELISA, as shown in **Figure 4**, different dilutions of GconsMuFc were tested against its target and an unrelated protein: the antibody was able to recognise specifically GFP and was detectable through secondary anti-mouse antibodies until 0.1-0.03 nM tested concentrations (see "Materials and Methods" for details).

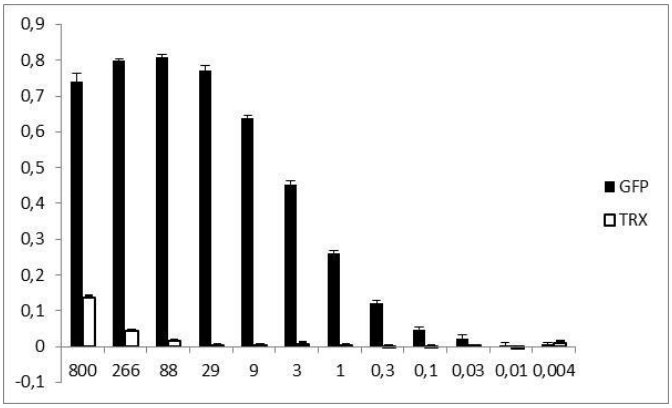

Figure 4 GST-ELISA testing of the GconsMuFc fusion Nb against GFP-GST. An unrelated protein (thioredoxin-GST) served as negative control. Bars represent absorbance measured at 415 nm after addition of the horseradish peroxidase (HRP) substrate, abscissa indicates the serial tested dilution of GconsMuFc (nM) (see "Materials and Methods" for details).

Also in Western Blot (**Figure 5**) GconsMuFc was able to specifically recognise expressed GFP within an *Escherichia coli* lysate until 100 ng of target protein and, in turn, was detected by an secondary anti-mouse antibody (see "Materials and Methods" for details). These results indicate that the direct fusion of our grafted "consensus" Nbs to murine IgG Fc region is feasible but not always the procedure leads to soluble and functional monoclonal-like antibodies, as observed for LconsMuFc.

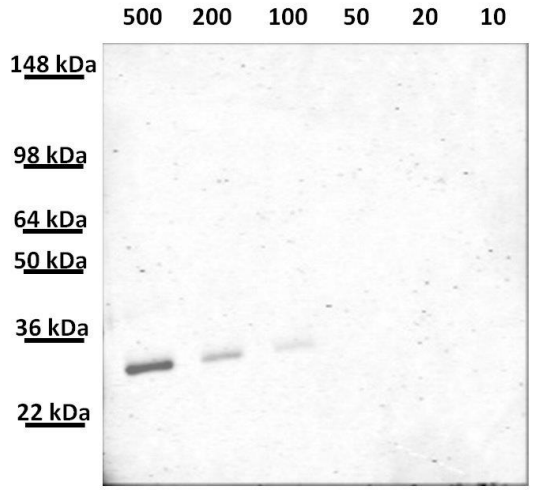

Figure 5 Western Blot performed on serial dilutions of GFP-expressing *E. coli* lysate. GconsMuFc was used as primary antibody and anti-mouse IRDye as secondary antibody. On the top the predicted quantity of GFP in bacterial lysate is indicated (ng) and molecular size of the marker is displayed on the left of the figure (see "Materials and Methods" for details).

3.2. SpyTag - SpyCatcher technology for the production of monoclonal-like antibodies

3.2.1 Cloning and expression of Gcons/Lcons nanobodies fused to SpyTag and SpyCatcher fused to murine IgG 2a Fc region

In order to produce monoclonal-like antibodies avoiding not always successful cloning and expression procedures of the entire molecules, to both Gcons and Lcons Nbs encoding sequence SpyTag nucleotide sequence at C-terminus was added and the corresponding proteins were produced in *E. coli* exploiting the pET28 system. GconsSpyTag and LconsSpyTag were

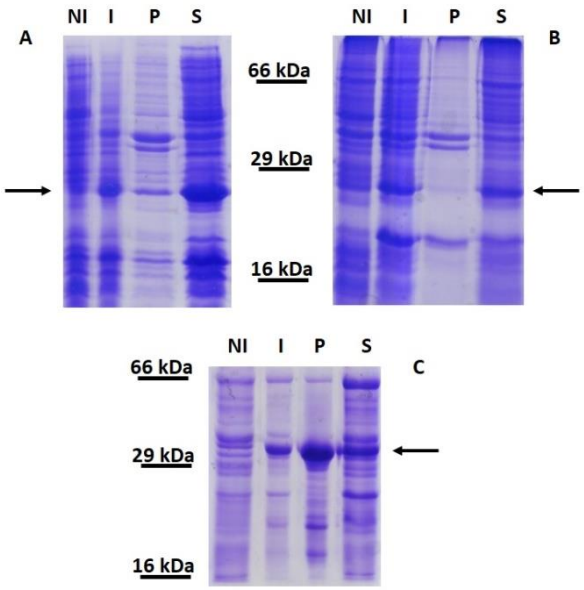

Figure 6 Expression and solubility analysis of GconsSpyTag (A), LconsSpyTag (B) and SpyCatcherMuFc (C). NI: non-induced control; I: induced bacterial lysate; S: bacterial lysate supernatant; P: bacterial pellet. The arrows mark the polypeptide bands corresponding to the fusion proteins. Molecular size of the marker is indicated next to the figures (see "Materials and Methods" for details).

highly expressed and soluble and they were purified by metal-affinity chromatography using the vector-provided poly-histidine tag (see "Materials and methods" for details) with a final yield of approximately 12 mg and 10 mg of pure protein/L of bacterial culture respectively (**Figure 6 A** and **B**).

SpyCatcher gene was fused in frame to N-terminus of murine IgG 2a Fc encoding sequence in pET28 vector and after protein expression, no soluble product was obtained. After the co-transformation of this expressing bacteria with pKJE7 plasmid, bearing DnaK, DnaJ and GrpE chaperones (see "Materials and Methods" for details), almost 100% soluble SpyCatcherMuFc protein was produced and purified by metal-affinity chromatography with a final yield of approximately 4 mg of pure protein/L of bacterial culture (**Figure 6 C**). A schematic representation of GconsSpyTag, LconsSpyTag and SpyCatcherMuFc proteins is visible in **Figure 3**.

3.2.2. Production and analysis of SpyTag – SpyCatcher monoclonal-like murine antibodies

As for GconsMuFc antibody, Fc region of SpyCatcherMuFc protein was expected to allow dimerization and thus size exclusion chromatography (SEC) was performed to check this hypothesis. As showed in **Figure 7** two samples of SpyCatcherMuFc protein were analysed: also in this case, a shift in elution time was visible after treatment of the protein with β-mercaptoethanol (from ~76 kDa of the black peak to ~38 kDa of the red peak). So, we concluded that murine IgG 2a Fc region fused to SpyCatcher domain is still able to dimerize correctly.

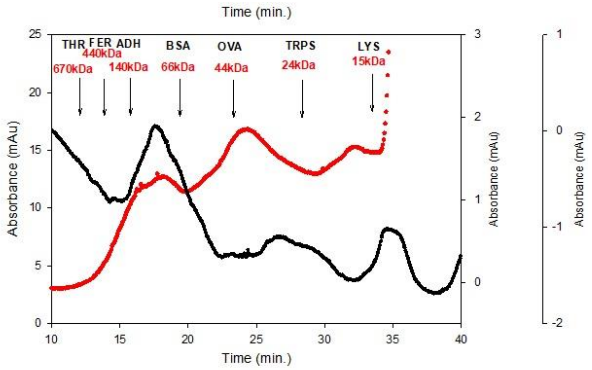

Figure 7 SEC performed on SpyCatcherMuFc with Superdex 200 column on ÄKTA system. Sample in red was treated with β-mercaptoethanol and showed an elution time compatible with monomeric state of the protein, instead of not treated sample (in black) that showed an elution time compatible with a dimeric state. Elution time of markers is shown on the top (see "Materials and Methods" for details).

Once the components have been produced separately, in soluble form, we set up reactions in order to assembled a functional monoclonal-like antibody: GconsSpyTag or LconsSpyTag were mixed with SpyCatcherMuFc in 1:2 molar ratio (excess of SpyCatcherMuFc) to obtain 100% reaction efficiency and to avoid free Nb remainders, which could compete with the reacting monoclonal-like antibody in subsequent analyses. SpyTag and SpyCatcher peptides were expected to react *in vitro* providing a covalent bond between Nbs and murine Fc region. As shown in **Figure 8,** both

reactions reached almost 100% ligation efficiency (Nbs reminders are not visible) and a fusion product was obtained. A schematic representation of the produced SpyTag – SpyCatcher murine monoclonal-like antibodies is reported in **Figure 3**.

After quantification, both GconsSpyTag+SpyCatcherMuFc and LconsSpyTag+SpyCatcherMuFc antibodies were analyzed in an ELISA and Western Blot experiments. During ELISA serial dilutions of GconsSpyTag+SpyCatcherMuFc and LconsSpyTag+SpyCatcherMuFc were tested for the capacity to bind their target compared to an unrelated protein. Both antibodies were able to recognise specifically GFP and lysozyme respectively and both were detectable with anti-mouse secondary antibodies until 0.3-0.1 nM tested concentrations (**Figure 9 A** and **B**).

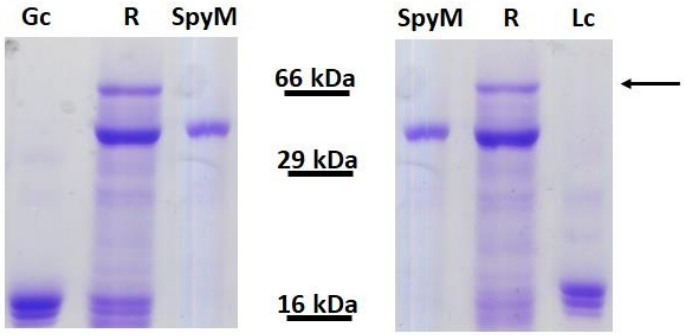

Figure 8 SDS-page analysis of GconsSpyTag (left) and LconsSpyTag (right) reactions with SpyCatcherMuFc protein. Gc: GconsSpyTag; R: reaction; SpyM: SpyCatcherMuFc: Lc: LconsSpyTag. Black arrow indicates the final fusion products. Molecular size of the marker is indicated at the center of the figure (see "Materials and Methods" for details).

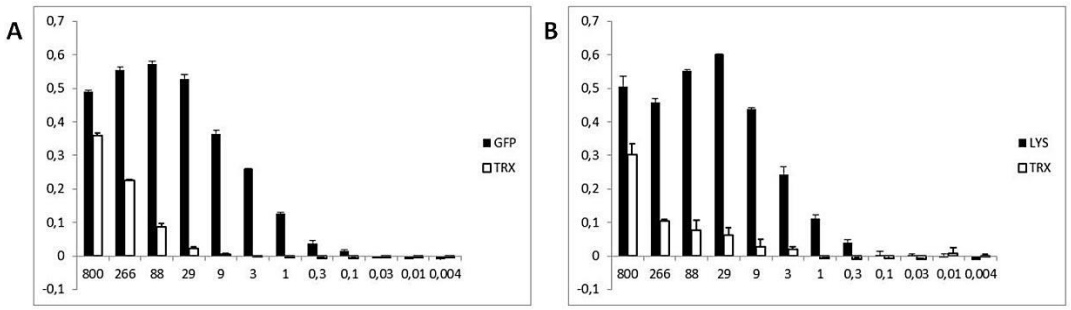

Figure 9 ELISA testing of GconsSpyTag+SpyCatcherMuFc (A) and LconsSpyTag+SpyCatcherMuFc (B) reactions against GFP-GST and biotinylated lysozyme respectively. An unrelated protein (thioredoxin) served as negative control. Bars represent absorbance measured at 415 nm after addition of the horseradish peroxidase (HRP) substrate, abscissa indicates the serial tested dilution of monoclonal-like antibodies (nM) (see "Materials and Methods" for details).

Western Blots were performed analysing serial dilutions of *E. coli* lysates containing GFP or lysozyme. During the procedure, GconsSpyTag+SpyCatcherMuFc and LconsSpyTag+SpyCatcherMuFc respectively were used as primary antibody and a secondary anti-mouse antibody was used for their detection. Both monoclonal-like

antibodies were able to detect their targets (GFP and lysozyme respectively) in cell lysates until 100 ng target amount and to be recognised by secondary anti-mouse antibodies (**Figure 10 A** and **B**).

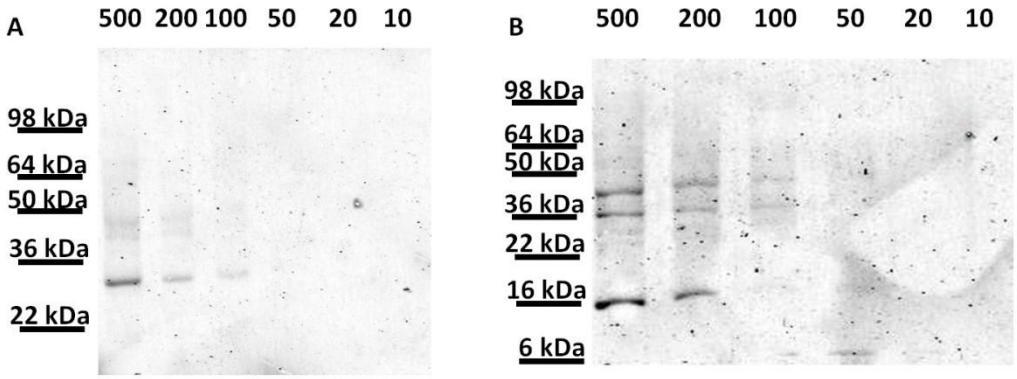

Figure 10 Western Blots performed on serial dilutions of GFP-expressing *E. coli* lysate (A) and lysozyme-containing *E. coli* lysate (B). GconsSpyTag+SpyCatcherMuFc and LconsSpyTag+SpyCatcherMuFc were used respectively as primary antibodies and an anti-mouse IRDye secondary antibody was employed. On the top predicted quantity of GFP and lysozyme in bacterial lysate is indicated (ng) and molecular size of the marker is displayed on the left of the figures (see "Materials and Methods" for details).

These results indicated that monoclonal-like anti-GFP antibody obtained through SpyTag – SpyCatcher technology showed similar activity to GconsMuFc direct fusion in both ELISA tests and Western Blots. Moreover, the SpyTag – SpyCatcher technology proved to be the only one able to provide a functional anti-lysozyme murine monoclonal-like antibody since the corresponding direct fusion protein (LconsMuFc) was completely insoluble.

3.2.3. Cloning and expression of Gcons and SpyCatcher fused to rabbit IgG Fc region

To verify the versatility of SpyTag – SpyCatcher assembly system we decided to assess its functionality attempting the fusion of CFW grafted Nbs to another Fc region: we chose the rabbit IgG constant region because a plethora of anti-rabbit secondary antibody is available.

In order to perform a comparison of SpyTag - SpyCatcher rabbit monoclonal-like antibodies with a Nb – Fc direct fusion, at first we cloned Gcons Nb gene in frame with rabbit IgG Fc region encoding sequence and we expressed the protein in BL21 *E. coli* strain in the pET28 vector. A soluble product was obtained (GconsRaFc, **Figure 11**) and the protein was purified by metal-affinity chromatography using the vector-provided poly-histidine tag (see "Materials and methods" for details) with a final yield of approximately 9 mg of pure protein/L of bacterial culture.

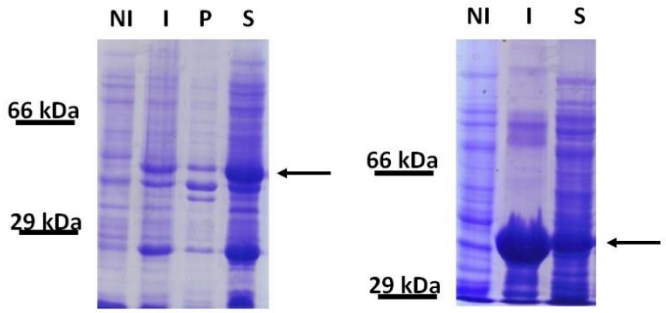

Figure 11 Expression and solubility analysis of GconsRaFc (left) and SpyCatcherRaFc (right). NI: non-induced control; I: induced bacterial lysate; S: bacterial lysate supernatant; P: bacterial pellet. The arrows mark the polypeptide bands corresponding to the fusion proteins. Molecular size of the marker is indicated next to the figures (see "Materials and Methods" for details).

Also the fusion protein SpyCatcher rabbit Fc has been expressed as a soluble protein (SpyCatcherRaFc, **Figure 11**) providing, after metal-affinity chromatography, 15 mg of pure protein/L of bacterial culture. A schematic representation of the produced proteins is visible in **Figure 3**.

3.2.4. Production and analysis of monoclonal-like rabbit antibodies

GconsRaFc and SpyCatcherRaFc were analysed through size exclusion chromatography (SEC) in order to verify their monomeric/dimeric state. As previously mentioned, two samples of both proteins were examined, one treated with β-mercaptoethanol and the other not; results are shown in **Figure 12**.

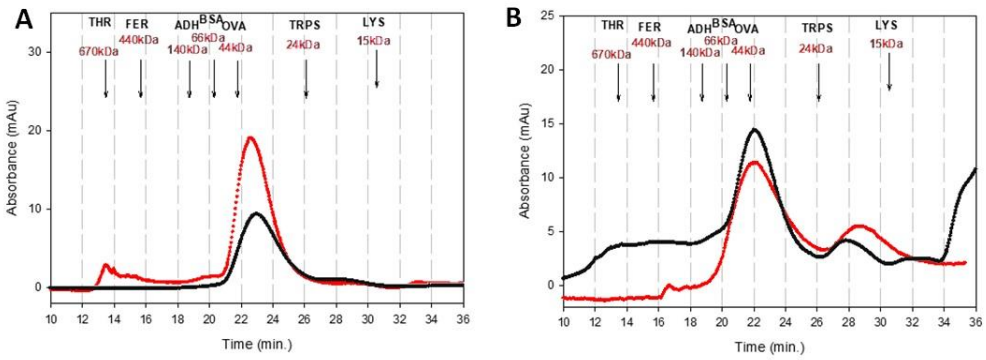

Figure 12 SEC performed on GconsRaFc (A) and SpyCatcherRaFc (B) with Superdex 200 column on ÄKTA system. Samples in red were treated with β-mercaptoethanol, not treated samples are in black. Elution time of markers is shown on the top (see "Materials and Methods" for details).

Any of the rabbit Fc fusion proteins seemed able to dimerize and for both proteins, in presence and absence of a reducing agent, only a peak corresponding to the monomer state was detected. These data confirmed previous observation, where a preferential monomeric state for rabbit IgGs is reported[18].

In order to obtain rabbit monoclonal-like antibodies two reactions were assembled: GconsSpyTag or LconsSpyTag were mixed with SpyCatcherRaFc in 1:2 molar ratio and incubated at 20°C for three days. After reactions incubation products were analysed through SDS-pages (**Figure 13**) confirming the formation of the isopeptide bond between SpyTag and SpyCatcher elements. A schematic representation of the final monoclonal-like rabbit antibodies is reported in **Figure 3**.

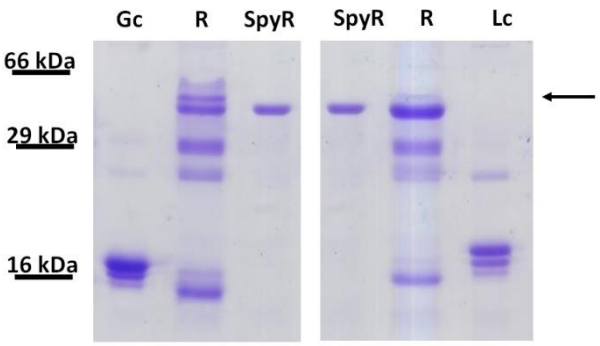

Figure 13 SDS-page analysis of GconsSpyTag (left) and LconsSpyTag (right) reactions with SpyCatcherRaFc. Gc: GconsSpyTag; R: reaction; SpyR: SpyCatcherRaFc: Lc: LconsSpyTag. Black arrow indicates the final fusion products. Molecular size of the marker is indicated on the left of the figure (see "Materials and Methods" for details).

All the obtained monoclonal-like antibodies (GconsRaFc, GconsSpyTag+SpyCatcherRaFc and LconsSpyTag+SpyCatcherRaFc) were examined through ELISA tests and Western Blots. As shown in **Figure 14** serial dilutions of GconsRaFc, GconsSpyTag+SpyCatcherRaFc and LconsSpyTag+SpyCatcherRaFc were tested for their target binding capacity in ELISA and all the antibodies were able to recognise specifically their targets (GFP and lysozyme respectively) and were detectable with commercial secondary anti-rabbit antibodies until their lowest tested concentrations.

Results were confirmed with Western Blot analyses (**Figure 15**) in which antibodies were able to recognise specifically their targets in *E. coli* cell lysates serial dilutions and their presence were detected with secondary anti-rabbit antibodies.

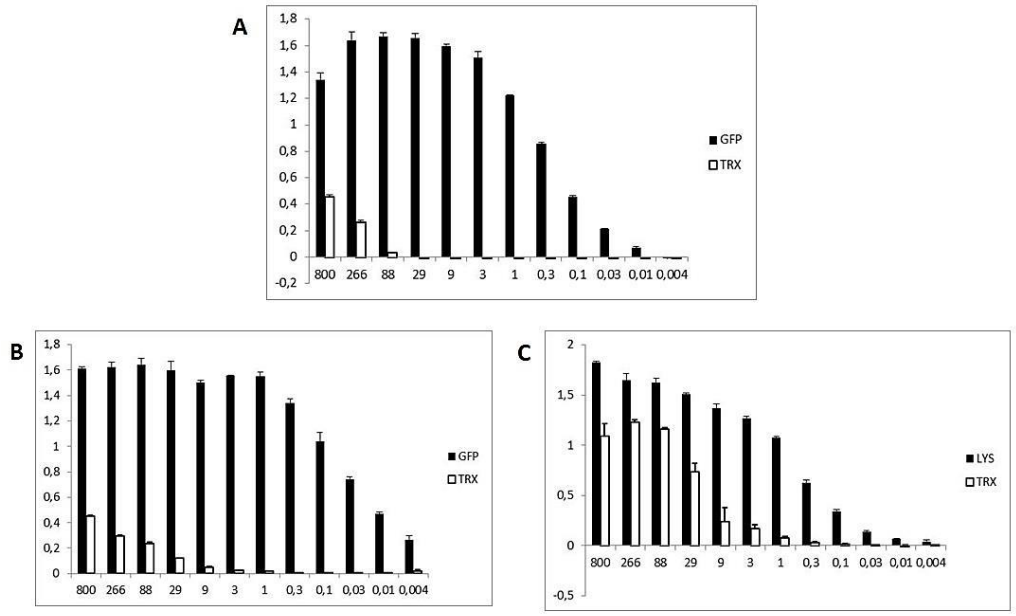

Figure 14 ELISA testing of GconsRaFc (A),GconsSpyTag+SpyCatcherRaFc (B) and LconsSpyTag+SpyCatcherRaFc (C) reactions against GFP-GST and biotinylated lysozyme respectively. An unrelated protein (thioredoxin) served as negative control. Bars represent absorbance measured at 415 nm after addition of the horseradish peroxidase (HRP) substrate, abscissa indicates the serial tested dilutions of monoclonal-like antibodies (nM) (see "Materials and Methods" for details).

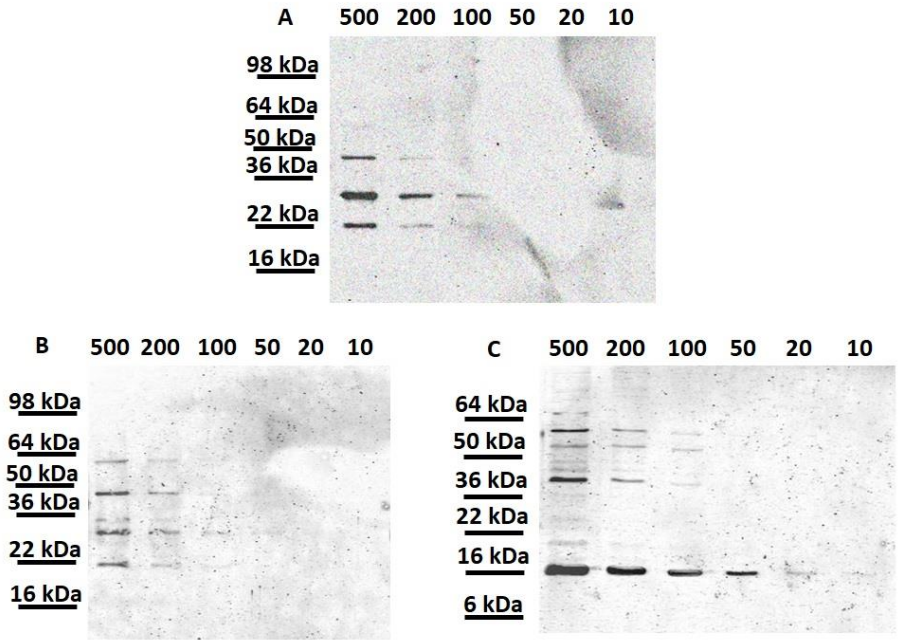

Figure 15 Western Blots performed on serial dilutions of GFP-expressing *E. coli* lysate (A and B) and lysozyme-containing *E. coli* lysate (C). GconsRaFc (A), GconsSpyTag+SpyCatcherRaFc (B) and

LconsSpyTag+SpyCatcherRaFc (C) were used as primary antibody and anti-rabbit IRDye secondary antibody was used for detection. On the top predicted quantities of GFP and lysozyme in bacterial lysate is indicated (ng) and molecular size of the marker is displayed on the left of the figures (see "Materials and Methods" for details).

In all these experiments, SpyTag – Spy Catcher antibody derivatives showed similar activity if compared to GconsRaFc direct fusion. These results indicated the possibility to apply SpyTag – Spy Catcher technology for combining any Nb also to rabbit IgG Fc region and, potentially, to any immunoglobulin Fc region of interest, highlighting the potentiality and versatility of this novel approach.

3.2.5. Cloning and expression of Gcons fused to SpyCatcher and SpyTag fused to rabbit IgG Fc region

One last interesting possibility that remained to be explored in the production of monoclonal-like antibodies was the inversion of SpyTag and SpyCatcher positions in the two joining components.

To check this alternative approach we cloned in frame Gcons gene to N-terminus of SpyCatcher sequence and SpyTag gene to N-terminus of rabbit IgG Fc sequence. Both fusion genes were cloned in pET28 vector, expressed in BL21 *E. coli* strain and, after cells lysis, they were detected in soluble fractions (**Figure 16**). GconsSpyCatcher and SpyTagRaFc proteins were then purified by metal-affinity chromatography using the vector-provided poly-histidine tag (see "Materials and methods" for details) with a final yield of approximately 18 mg and 8 mg of pure protein/L of bacterial culture respectively. A schematic representation of GconsSpyCatcher and SpyTagRaFc proteins is reported in **Figure 3**.

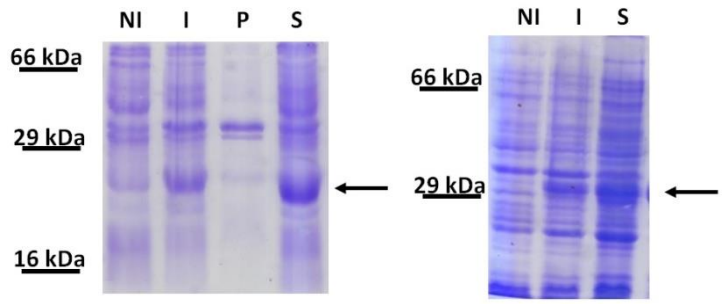

Figure 16 Expression and solubility analysis of GconsSpyCatcher (left) and SpyTagRaFc (right). NI: non-induced control; I: induced bacterial lysate; S: bacterial lysate supernatant; P: bacterial pellet. The arrows mark the polypeptide bands corresponding to the fusion proteins. Molecular size of the marker is indicated next to the figures (see "Materials and Methods" for details).

3.2.6. *Production and analysis of inverted SpyTag - SpyCatcher monoclonal-like rabbit antibody*

Also, SpyTagRaFc protein dimerization state was tested: as described above size exclusion chromatography (SEC) was performed on β-mercaptoethanol treated and not treated protein samples. As shown in **Figure 17** SpyTagRaFc protein was present in solution as a monomer because elution time of both samples corresponded to ~31 kDa molecular size.

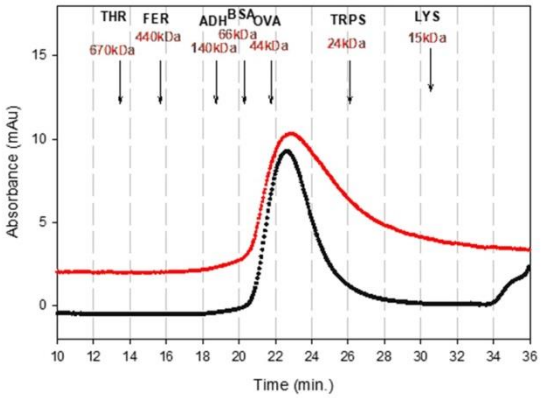

Figure 17 SEC performed on SpyTagRaFc with Superdex 200 column on ÄKTA system. Sample in red was treated with β-mercaptoethanol, not treated sample is in black. Elution time of markers is shown on the top (see "Materials and Methods" for details).

GconsSpyCatcher and SpyTagRaFc single elements were ligated using a 1:2 molar ratio reaction (with an excess of Fc component) and the reaction product was visible on SDS-page as a single band protein (**Figure 18**). A schematic representation of inverted SpyTag - SpyCatcher monoclonal-like rabbit antibody is reported in **Figure 3**.

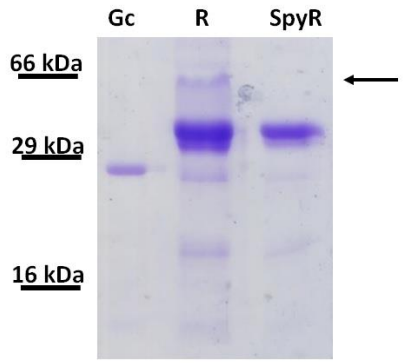

Figure 18 SDS-page analysis of GconsSpyCatcher reaction with SpyTagRaFc. Gc: GconsSpyCatcher; R: reaction; SpyR: SpyTagRaFc. Black arrow indicates the final fusion product. Molecular size of the marker is indicated on the left of the figure (see "Materials and Methods" for details).

GconsSpyCatcher+SpyTagRaFc antibody was examined for its functionality in ELISA tests and Western Blot. As shown in **Figure 19 A** serial dilutions of the tested rabbit monoclonal-like antibody were able to bind specifically GFP (the Nb target) and were detectable with commercial secondary anti-rabbit antibodies until their lowest tested concentrations.

In **Figure 19 B** GconsSpyCatcher+SpyTagRaFc monoclonal-like antibody was used as primary antibody in Western Blot where different dilutions of GFP-expressing *E. coli* lysate were analysed. The activity of the antibody in Western Blot is reported: GFP was specifically recognised and primary antibody could be detected with secondary anti-rabbit antibody.

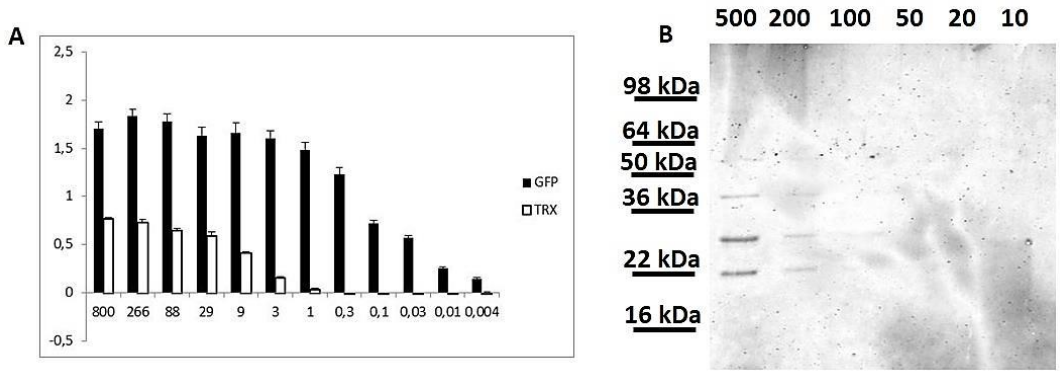

Figure 19 A) GST-ELISA testing of GconsSpyCatcher+SpyTagRaFc reaction against GFP-GST. An unrelated protein (thioredoxin-GST) served as negative control. Bars represent absorbance measured at 415 nm after addition of the horseradish peroxidase (HRP) substrate, abscissa indicates the serial tested dilution of monoclonal-like antibodies (nM). B) Western Blot performed on serial dilutions of GFP-expressing *E. coli* lysate. GconsSpyCatcher+SpyTagRaFc was used as primary antibody and an anti-mouse IRDye as secondary antibody. On the top predicted quantity of GFP in bacterial lysate is indicated (ng) and molecular size of the marker is displayed on the left of the figure (see "Materials and Methods" for details).

4. Discussion

Since 1993 Nbs are new interesting therapeutic and diagnostic tools and nowadays they are widespread in biology and medicine fields[19]. One peculiar VHHs characteristic is their intrinsic low immunogenicity that determined their success as imaging tools[3] but prevented the possibility to produce secondary antibody against them (confirmed by our unpublished data). These Nbs feature inhibited their potential applications; for this reason in literature many direct fusion of Nbs to immunoglobulins Fc regions are reported: fusing Nbs to Fc regions increases their avidity through dimerization, adds an effector function through Fc receptor recruitment and renders Nbs detectable through secondary antibodies[5].

However, fusing VHHs to Fc regions usually leads to difficult-to-express proteins which required complex expression systems or eukaryotic cells usage[20]. Attempts to produce monoclonal-like antibodies in *Escherichia coli* are reported but low expression yields are obtained[21] and to enhance protein expression mutant *E. coli* strains or chaperone-expressing vectors are required[22,23].

We verified the possibility to fuse our "consensus" grafted Nbs to murine IgG 2a Fc region to obtain antibodies that maintain Nb binding capacity but that can be detected through anti-mouse secondary antibodies. The direct fusion of anti-GFP consensus Nb (Gcons) to murine IgG 2a Fc region led to a fully functional monoclonal-like antibody (**Figure 4** and **5**) but on the other hand the fusion of anti-chicken lysozyme consensus Nb (Lcons) to the

same region resulted in a completely insoluble protein (**Figure 1**). These data confirmed how by fusing Nbs directly to Fc regions the success is not guaranteed[22].

Here we reported the introduction of SpyTag – SpyCatcher technology in order to obtain easy to express single components for the assembly of fully functional monoclonal-like antibodies (**Figure 3**). Splitting CnaB2 *S. pyogenes* protein into a single domain (SpyCatcher) and a peptide (SpyTag) a fast and robust *in vitro* ligation system was developed. SpyCatcher and SpyTag elements are able to form an isopeptide bond between them in some hours and in a wide range of different conditions and buffers. The formation of the new bond is very specific, can be performed also in cell cytoplasm and the ligating elements can also be cloned internally to the fusion partners[15]. We chose SpyTag and SpyCatcher ligation system because is more stable then other non-covalent binding such as coiled-coil interactions[24], does not require post-transcriptional or chemical modifications of fusion partners[25] and is not linked to the conjugation to specific sites of the proteins[26].

SpyTag – SpyCatcher technology is not traceless and the ligating elements are finally included in the products but that permits to avoid purification steps after the reaction. For our purpose, we assembled *in vitro* ligations with an excess of the component which remainders will not alter subsequent analyses.

To be sure that the final fusion product could maintain the same target affinity of the original antibody, we decided to fuse SpyTag at the C-terminus of Nbs because is far from their target binding site and SpyTag is also the smallest ligation component. SpyCatcher was fused instead to N-terminus of Fc region for keeping this Fc domain free from structural impediment and capable of forming classical dimer.

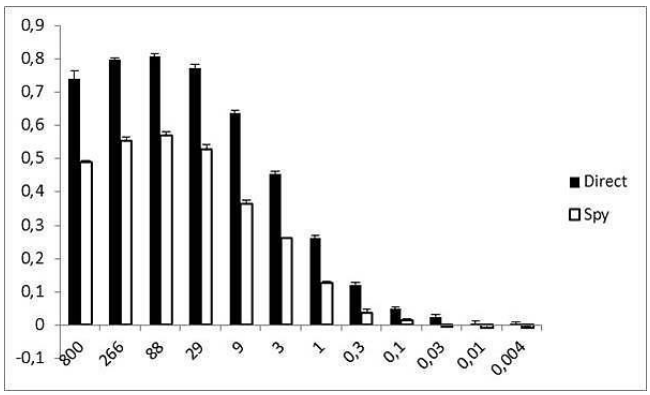

Figure 20 Merge of GFP tested columns of Figure 4 and 9A.

With Nbs fused to SpyTag and SpyCatcher fused to murine Fc region we were able to produce a fully functional anti-GFP monoclonal-like antibody (**Figure 3**) that reacts similarly to the direct fusion GconsMuFc. A small decrease in signal intensity is visible during analyses for GconsSpyTag+SpyCatcherMuFc antibody but both proteins were able to detect till 100 ng of GFP in Western Blot (**Figure 5** and **10**) and could be detected till 0.3-0.1 nM antibody concentration in ELISA tests (**Figure 20**). Also, a functional anti-lysozyme monoclonal-like antibody could be obtained, bypassing

insolubility problems occurred during the direct fusion of Lcons to murine Fc region (**Figure 9** and **10**).

We demonstrated the versatility of the system showing its functionality with rabbit IgG Fc region as well: anti-GFP and anti-lysozyme functional monoclonal-like rabbit antibodies were obtained and they were active in ELISA tests (**Figure 14**) and Western Blots (**Figure 15**).

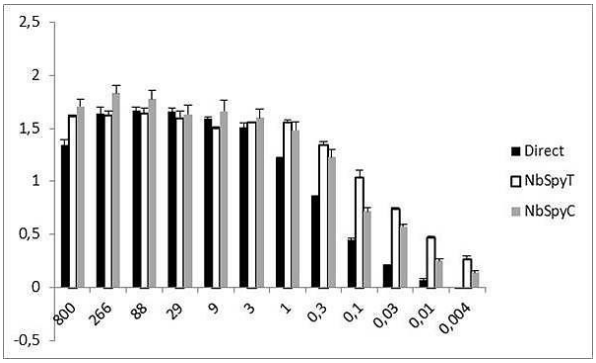

Figure 21 Merge of the GFP columns of Figure 14A, B and 19A.

We demonstrated also the possibility to invert SpyTag and SpyCatcher fusion partners fusing SpyCatcher to C-terminus of the Nb Gcons and SpyTag to N-terminus of the rabbit Fc region: after *in vitro* ligation also in this case a functional antibody was obtained (**Figure 19**). All the three anti-GFP rabbit monoclonal-like antibody (GconsRaFc, GconsSpyTag+SpyCatcherRaFc, GconsSpyCatcher+SpyTagRaFc) showed similar activity in ELISA (**Figure 21**) and Western Blot (**Figure 15** and **Figure 19**).

While murine Fc derivative seemed to assume dimeric structure, all the produced rabbit monoclonal-like antibodies had an apparent monomeric state (**Figure 12** and **18**). We speculate that this could be due to the prevalent monomeric conformation of the native rabbit IgGs (usually more than 75%) and their tendency to lose their dimeric structure also in native conditions. Additionally, rabbit IgGs share high identity sequence with human IgG4 subtype that also presents a monomeric structure[18,27]. Although the fusion to rabbit IgG Fc region did not permit Nb dimerization, the final antibodies could be detected efficiently by secondary anti-rabbit antibodies.

In conclusion, we applied successfully SpyTag – SpyCatcher technology to the production of monoclonal-like antibodies that are functional in ELISA tests and Western Blots. What remains to be asses is the functionality of these antibodies in immunoprecipitation: if they are able to bind protein A and G, they will be functional in most of the diagnostic techniques.

Even if other antibody-like molecules were built with SpyTag - SpyCatcher system[28], this is the first reported fusion of Nbs to Fc regions through *in vitro* ligation technologies. The final fusion antibodies possess the peculiar and specific binding capacity of Nbs[29] and are able to be detected with the most widespread secondary antibodies, maintaining a smaller size than conventional monoclonal antibodies[2]. Furthermore the application of SpyTag – SpyCatcher technology allows an interesting modularity in which any Nb can be

produced with SpyTag tail and can be conjugated with any SpyCatcher-Fc type, avoiding cloning procedure to change Fc partner.
All these features render these simple-to-produce monoclonal-like antibodies perfect novel diagnostic tools.

5. Bibliography

1. Hamers-Casterman C, Atarhouch T, Muyldermans S, et al. Naturally occurring antibodies devoid of light chains. *Nature*. 1993;363(6428):446-448. doi:10.1038/363446a0.
2. Bannas P, Hambach J, Koch-Nolte F. Nanobodies and nanobody-based human heavy chain antibodies as antitumor therapeutics. *Front Immunol*. 2017;8(NOV):1-13. doi:10.3389/fimmu.2017.01603.
3. Chakravarty R, Goel S, Cai W. Nanobody: The "magic bullet" for molecular imaging? *Theranostics*. 2014;4(4):386-398. doi:10.7150/thno.8006.
4. Vu KB, Ghahroudi MA, Wyns L, Muyldermans S. Comparison of llama V(H) sequences from conventional and heavy chain antibodies. *Mol Immunol*. 1997. doi:10.1016/S0161-5890(97)00146-6.
5. Romao E, Morales-Yanez F, Hu Y, et al. Identification of Useful Nanobodies by Phage Display of Immune Single Domain Libraries Derived from Camelid Heavy Chain Antibodies. *Curr Pharm Des*. 2017;22(43):6500-6518. doi:10.2174/1381612822666160923114417.
6. Nimmerjahn F, Ravetch J V. Fc-Receptors as Regulators of Immunity. *Adv Immunol*. 2007. doi:10.1016/S0065-2776(07)96005-8.
7. Abcam. Understanding secondary antibodies. *Int J Oral Maxillofac Surg*. 2012;41(1):121-127. doi:10.1016/j.ijom.2011.06.025.
8. Richard G, Meyers AJ, McLean MD, Arbabi-Ghahroudi M, MacKenzie R, Hall JC. In Vivo Neutralization of α-Cobratoxin with High-Affinity Llama Single-Domain Antibodies (VHHs) and a VHH-Fc Antibody. *PLoS One*. 2013;8(7):1-14. doi:10.1371/journal.pone.0069495.
9. Scheuplein F, Rissiek B, Driver JP, Chen YG, Koch-Nolte F, Serreze D V. A recombinant heavy chain antibody approach blocks ART2 mediated deletion of an iNKT cell population that upon activation inhibits autoimmune diabetes. *J Autoimmun*. 2010;34(2):145-154. doi:10.1016/j.jaut.2009.08.012.
10. Qasemi M, Behdani M, Ali M. Construction and expression of an anti-VEGFR2 Nanobody-Fc fusionbody in NS0 host cell. *Protein Expr Purif*. 2016;123:19-25. doi:10.1016/j.pep.2016.03.004.
11. Virdi V, Coddens A, De Buck S, et al. Orally fed seeds producing designer IgAs protect weaned piglets against enterotoxigenic Escherichia coli infection. *Proc Natl Acad Sci*. 2013;110(29):11809-11814. doi:10.1073/pnas.1301975110.
12. Kaczmarek-hajek K, Zhang J, Kopp R, et al. Re-evaluation of neuronal P2X7 expression using novel mouse models and a P2X7-specific nanobody. *Elife*. 2018:1-29. doi:10.7554/eLife.36217.
13. Ji X, Lu W, Zhou H, et al. Covalently dimerized Camelidae antihuman TNFa single-domain antibodies expressed in yeast Pichia pastoris show superior neutralizing activity. *Appl Microbiol Biotechnol*. 2013;97(19):8547-8558. doi:10.1007/s00253-012-4639-2.
14. Hmila I, Abdallah R BA Ben, Saerens D, et al. VHH, bivalent domains and chimeric Heavy chain-only antibodies with high neutralizing efficacy for scorpion toxin AahI'. *Mol Immunol*. 2008;45(14):3847-3856. doi:10.1016/j.molimm.2008.04.011.
15. Zakeri B, Fierer JO, Celik E, et al. Peptide tag forming a rapid covalent bond to a protein, through engineering a bacterial adhesin. *Proc Natl Acad Sci U S A*. 2012;109(12):E690-7. doi:10.1073/pnas.1115485109.
16. Sambrook J, W Russell D. Molecular Cloning: A Laboratory Manual. *Cold Spring Harb Lab Press Cold Spring Harb NY*. 2001. doi:10.1016/0092-8674(90)90210-6.
17. Sehr P, Zumbach K, Pawlita M. A generic capture ELISA for recombinant proteins fused to glutathione S-transferase: Validation for HPV serology. *J Immunol Methods*. 2001;253(1-2):153-162. doi:10.1016/S0022-1759(01)00376-3.
18. Rayner LE, Kadkhodayi-Kholghi N, Heenan RK, Gor J, Dalby PA, Perkins SJ. The solution structure of rabbit IgG accounts for its interactions with the Fc receptor and complement C1q and its conformational stability. *J Mol Biol*. 2013;425(3):506-523. doi:10.1016/j.jmb.2012.11.019.
19. Steeland S, Vandenbroucke RE, Libert C. Nanobodies as therapeutics: Big opportunities for small antibodies. *Drug Discov Today*. 2016;21(7):1076-1113. doi:10.1016/j.drudis.2016.04.003.
20. Marco A De. Recombinant antibody production evolves into multiple options aimed at yielding reagents suitable for application - specific needs. *Microb Cell Fact*. 2015:1-17. doi:10.1186/s12934-015-0320-7.

21. Simmons LC, Reilly D, Klimowski L, et al. Expression of full-length immunoglobulins in Escherichia coli : rapid and efficient production of aglycosylated antibodies. 2002;263:133-147.
22. Djender S, Schneider A, Beugnet A, et al. Bacterial cytoplasm as an effective cell compartment for producing functional VHH-based affinity reagents and Camelidae IgG-like recombinant antibodies. *Microb Cell Fact*. 2014:1-10. doi:10.1186/s12934-014-0140-1.
23. Nguyen VD, Hatahet F, Salo KEH, Enlund E, Zhang C, Ruddock LW. Pre-expression of a sulfhydryl oxidase significantly increases the yields of eukaryotic disulfide bond containing proteins expressed in the cytoplasm of E . coli. 2011:1-13.
24. Woolfson DN. The design of coiled-coil structures and assemblies. *Adv Protein Chem*. 2002;70(04):79-112. doi:10.1016/S0065-3233(04)70004-2.
25. Howard TS, Cohen RD, Nwajiobi O, et al. Amino-Acid-Catalyzed Direct Aldol Bioconjugation. *Org Lett*. 2018:acs.orglett.8b02265. doi:10.1021/acs.orglett.8b02265.
26. Massa S, Vikani N, Betti C, et al. Sortase A-mediated site-specific labeling of camelid single-domain antibody-fragments: a versatile strategy for multiple molecular imaging modalities. *Contrast Media Mol Imaging*. 2016;11(5):328-339. doi:10.1002/cmmi.1696.
27. Liu H, May K. Disulfide bond structures of IgG molecules. *MAbs*. 2012;4(1):17-23. doi:10.4161/mabs.4.1.18347.
28. Alam MK, Gonzalez C, Hill W, et al. Synthetic Modular Antibody Construction by Using the SpyTag/SpyCatcher Protein-Ligase System. *ChemBioChem*. 2017;18(22):2217-2221. doi:10.1002/cbic.201700411.
29. De Genst E, Silence K, Decanniere K, et al. Molecular basis for the preferential cleft recognition by dromedary heavy-chain antibodies. *Proc Natl Acad Sci*. 2006;103(12):4586-4591. doi:10.1073/pnas.0505379103.

Chapter 4

Chapter 4: NanoNluc, new probes for in vivo imaging

1. Introduction

Antibodies are one of the most important tools in diagnostic field[1] and since the discovery of camelids heavy chain antibodies in 1993[2] a new engineered antibody fragment suitable for diagnostic purposes is available. Heavy chain antibodies bind the target with a single soluble domain called VHH or nanobody (Nb) that if expressed alone in simple organisms like *Escherichia coli* maintains the binding capacity of the entire immunoglobulin. Some features like their small size (~15 kDa, compared to ~150 kDa of an immunoglobulin G), high solubility, low immunogenicity and rapid clearance from the bloodstream render Nbs interesting diagnostic reagents[3].

In vivo imaging is the most direct human application for diagnostic antibodies and a continuous innovation and sensitization of techniques is required[4]. Nbs contributed to the implementation of the field: with their small size they can easily penetrate in tissue where vascularisation is irregular (i.e. cancer tissues) providing good stratified imagines, they are well tolerated after administration because of their high identity with human VH III domain and their rapid clearance from the blood enables fast achievement of optimal signal-to-noise ratio, decreasing analysis duration and patient drug exposure[5]. Recent studies demonstrated also VHHs ability to penetrate blood-brain barrier and their suitability for brain *in vivo* imaging[6]. Thus, it should not surprise that an anti-HER2 Nb, appropriate for breast cancer detection, is currently in Phase I study for PET analysis[7] and a plethora of labelled VHH suitable for *in vivo* imaging are reported in literature[8].

Rather than the common use of radio-labelled antibodies (expensive and toxic for the operator), in preclinical *in vivo* analysis bioluminescence is catching on. Exploiting the ability of nature-derived enzymes, called luciferases, to emit photons in presence of their substrate (luciferin) a novel *in vivo* imaging technique was developed for cancer imaging[9,10], tumor burden evaluation[11] and infections progress analysis[12,13]. With a simple substrate injection, luciferase-labelled targets in high resolution and with low background could be visualized using sensitive charged-coupled devices (CCD) on nude mice[14].

Firefly (Fluc) and *Renilla reniformis* (Rluc) luciferases are the most studied and widespread enzymes but recently a smaller and brighter luciferase derivative has been produced[15]: NanoLuc (Nluc) was obtained from the smaller and bioluminescent subunit (Oluc-19) of the deep sea shrimp *Oplophorus gracilirostris* luciferase and is an optimized, small (19 kDa) and high stable reporter enzyme. It shows a strong glow-type luminescence (~150-fold more than Fluc or Rluc) providing a broader time window for imaging and its specific modified substrate (furimazine) does not oxidize in the bloodstream and has lower

background activity if compared to common luciferin. Furthermore, Nluc does not require post-translational modifications and can be easily obtained with high yield using bacterial expression systems (i.e. *Escherichia coli*).
Despite its blue light emission (460 nm), which usually does not penetrate mammalian tissues, Nluc has been successfully used for imaging in living animals with a limited detection only in deep tissues: *in vivo* Nluc activity reflects directly tumor dimension and its presence in serum can be detected as *ex vivo* biomarker for tumor growth[16].
Taking together all these features the fusion of a small and soluble antibody fragment (i.e. a Nb) with an optimized and small luciferase (i.e. Nluc) should lead to a high specific, penetrating, soluble and stable molecular construct that enables sensitive CCD *in vivo* imaging. Here we reported preliminary results of small probes (NanoNluc) obtained by recombinant fusion of synthetic Nbs to NanoLuc luciferase. Namely, complementary determining regions (CDRs) encoding sequence of three natural Nbs (GFP, chicken lysozyme and murine IgGs binders) were grafted into a synthetic gene coding for a stable and soluble scaffold derived from the alignment of more than 750 llama VHHs (described in details in Chapter 1) and fused in frame with Nluc reporter gene. Functional proteins were expressed and their potential activity confirmed by ELISA analyses. *In vivo* imaging tests were performed with the anti-GFP probe.

2. Materials and Methods

2.4. Molecular biology reagents and cloning procedures

Standard protocols[17] were used for all basic recombinant DNA procedures. Enzymes were from Takara Bio Europe (Saint-Germain-en Laye, France) and New England Biolabs (Ipswich, MA, USA). Molecular cloning and recombinant protein expression were carried out in BL21 codon plus *E. coli* strains (Stratagene; La Jolla, CA, USA), using pET28 (Merck Millipore, Darmstadt, Germany) plasmid. Following appropriate design, synthesis of G09 and G09cons encoding sequences were performed by Eurofins Genomics (Ebersberg, Germany); all protein-encoding sequences were optimized with respect to the *E. coli* codon usage (**Table 1**).
NanoNluc sequence was PCR-amplified from pNL3.2.NF-κB-RE plasmid (Promega, Fitchburg, Wisconsin, United States) introducing HindIII sites at 5' and 3' ends (**Table 1**). PCR was performed with 1 unit Phusion DNA Polymerase (New England Biolabs, Ipswich, MA, USA) in presence of the oligonucleotides (4 nM each), plus dNTPs (0.8 mM), 1x PCR buffer and 10 ng pNL3.2.NF-κB-RE in a final volume of 50 µl: initial denaturation 98°C 1 min; 25 cycles of 10 s at 98°C, 30 s at 58°C, and 60 s at 72°C; additional extension 72°C, 7 min.

Ligations of NanoLuc (using HindIII cloning site) in pET28 Nbs and G09/G09cons (using NcoI and NotI cloning sites) in pET28 plasmids were performed following standard protocols[17].

Name	Sequence
E.coli codon optimized G09 synthetic gene	CCATGGCGCAGGTGCAACTGGTGGAATCGGGAGGTGGCGTGGTTCAACCAGGCGGTTCTCTGCGTCTTT CCTGTGTTGCGTCAGGTCGGAATGTCGAGAATCAGGCAATGGGCTGGTTTCGCCAGACACCGGGCAAAG AACGCGAGTTTGTCGGTACGATCAGCTATTCGGGCGTTACCACCTATTATGCCGACTTCGTAGAAGGGC GTTTCACCATTAGTCGCGATCGCCCGAAAAACGCGCTGTTCCTGCAGATGAACAGCCTCACTCCGGAAG ATACCGCTGTCTACTACTGCAACGTGCATCGCGGTACTGCCTTGACGATGTCCCGTGCTTCACCTGCCG ATTTTGGGTCGTGGGGTCAGGGAACGCTGGTAACCGTGAGCAGCGCAGCGTTAGGCTCTGGCAGTAGCA AGCTTGGAAAACCTATCCCAAACCCTCTCCTAGGACTGGATTCAACGGGCAGCGGTTCTAGTCTAGCGG CCGC
E.coli codon optimized G09cons synthetic gene	ccATGGccaggtacagctgcaggaatcgggtggtggcctggttcaagcaggcggcagtttacgcctgt catgtgcagcgtcaggtCGCAATGTGGAGAATCAGGCAATGGGCTGGTTTCGTCAaACTCCAGGgAAAG AACGcGAGTTTGTGGGCACAATCAGCTATAGCGGGGTTACGACCTACtatgcggattccgtgaaaggac gcttcaccatttctcgggacaatgccaagaaccgtgtatttgcagatgaactccctgaaaccggaag atacggctgtctactattgcgctgcgCATCGTGGTACAGCTCTGACCATGAGTCGTGCCTCGCCTGCGG ACTTTGGCTCAtggggccagggtactcaggtcaccgtaagcagcAAgCTtGGTTCTGGCAGTTCTGGCA AACCGATTCCCAATCCGCTGTTGGGCCTCGATAGCACTGGGTCGGGgagCTCCCATCACCACCACCATC ATGGgagctcTGGTGGACTGAACGACATCTTCGAAGCCCAGAAGATTGAATGGCATGAAGGGTCGtgag cggccgc
Nluc-HindIII-F	TAAATATAAAAAGCTTTCGGGAGGCGGTTCTGGTATGGTCTTCACACTCGAAGAT
Nluc-HindIII-R	AATTATTTTAAAGCTTCGCCAGAATGCGTTCGCAC

Table 1 Sequences of the synthetic genes and primers utilized in this chapter. Sequences are shown in standard 5'-3' orientation.

2.5. Recombinant protein expression and purification

Standard procedures were used for recombinant Nbs and NanoNluc expression. Briefly, 10 ml of stationary overnight cultures (LB, 50 mg/l of kanamycin and 34 mg/l of chloramphenicol at 37 °C) were inoculated into 1 l cultures of the same media. After reaching an A_{600} value of 0.4-0.6, cultures were induced with 1 mM IPTG and further incubated for overnight at 20°C. Following centrifugation (5000 rpm, 15 min), bacterial cell pellets were recovered, suspended in 200 ml of Tris 10 mM pH 8.0 and centrifuged in the same conditions. Bacterial pellets were suspended in 50 ml of Tris-buffered saline (Tris 25 mM pH 8.0, NaCl 0.3 M, freshly supplemented with protease inhibitors), and lysed by sonication (20 min total sonication time performed with 3 sec bursts alternated with 6 sec resting on ice) carried out at constant power (4W/cm2; Sonicator 3000, Misonix). Lysates were then centrifuged (10000 rpm, 30 min) and the resulting supernatants were used as starting material for metal-affinity purification using a built-in 6xHis-tag and a His-select cobalt affinity resin (Sigma-Aldrich, Saint Louis, MO, USA) as per manufacturer's instructions. Bacterial lysates and individual metal-affinity chromatography fractions were analyzed by SDS-PAGE on 15-11% polyacrylamide gels.

Recombinant green fluorescent protein (GFP) used in this work is enhanced GFP. GST-tagged GFP and *E.coli* thioredoxin were gently provided by collaborators.
Cloning and expression of the GconsMuFc protein are described in details in Chapter 3.

2.6. ELISA tests procedures

ELISA tests on GconsNluc were performed using the following protocol: polystyrene 96-wells microtiter plates were coated overnight at 4°C with casein-glutathione (prepared and used as previously described[18]) dissolved in carbonate buffer (1 vol. 0.5 M Na_2CO_3 : 4 vol. 0.5 M $NaHCO_3$ pH 9.6). Blocking was performed by incubation for 1 hr at room temperature with 0.2% casein in Phosphate-buffered saline (PBS, pH 7.4), followed by a 1 hr incubation at room temperature with the purified GST-tagged proteins in PBS (800 nM each). After incubation with serial 1:4 or 1:2 dilutions of GconsNluc (starting from 20 µM or 2.5 µM) for 1 hr at room temperature, 50 µl of PBS were added to wells and plate was read with BertholdTech TriStar2 using 480 nm filter and adding 30 µl of NanoGlo diluted 1:2000 in PBS. Wells were washed with PBS containing 0.3% (v/v) Tween20 after each incubation step.
ELISA performed with Gcons His-tagged protein was performed following the same protocol described above but after Nb incubation an anti-histidine-tagged protein mouse mAb (Merck Millipore) diluted 1:1000 in PBS+0.2% casein was added and incubated for 1 hr. Then a peroxidase-conjugated anti-mouse IgG (whole molecule) goat antibody (Sigma-Aldrich) diluted 1:5000 in PBS+0.2% casein was added. Following an additional 1 hr incubation at RT, wells were filled with the TMB One substrate (Promega, Fitchburg, US) and absorbance was measured at 450-620 nm with a microplate reader (iMark, Biorad).
ELISA performed with G09cons protein in order to evaluate its functionality was carried out using the following protocol: polystyrene 96-wells microtiter plates were coated overnight at 4°C with casein-glutathione dissolved in carbonate buffer (1 vol. 0.5 M Na_2CO_3 : 4 vol. 0.5 M $NaHCO_3$ pH 9.6). Blocking was performed by incubation for 1 hr at room temperature with 0.2% casein in Phosphate-buffered saline (PBS, pH 7.4), followed by a 1 hr incubation at room temperature with the purified GST-tagged proteins in PBS (800 nM each). 800 nM of GconsMuFc were then added and incubated for 1 hr at RT. After incubation serial 1:2 dilutions of G09cons were added and incubated for 1 hr at room temperature. After incubation with an anti-histidine-tagged protein mouse mAb (Merck Millipore) diluted 1:1000 in PBS+0.2% casein for 1 hr, a peroxidase-conjugated anti-mouse IgG (whole molecule) goat antibody (Sigma-Aldrich) diluted 1:5000 in PBS+0.2% casein was added. Following an additional 1 hr incubation at RT, wells were filled with the 2,2'-azino-di-[3-ethylbenzthiazoline sulfonate (ABTS) substrate (KPL, Gaithersburg, MD, USA) and absorbance was measured at 415 nm with a microplate

reader (iMark, Biorad). Wells were washed with PBS containing 0.3% (v/v) Tween20 after each incubation step.

2.7. Stability of GconsNluc in plasma and blood samples

To 1 ml of rat blood and plasma samples (provided by Preclincs, Potsdam, Germany) different quantities (0, 0.6, 3, 15 µg) of GFP (Sigma-Aldrich, Saint Louis, MO, USA) were added. Samples were incubated for 30 min in presence of 20 µg of GconsNluc probe at room temperature in head over rotation. 100 µl of anti-GFP mAb-Magnetic Beads (Mbl International Corp, Woburn, MA, USA) were added and after 30 min of head over rotation three washing steps with PBS containing 0.3% (v/v) Tween20 were performed. Complexes were recovered and suspended with 100 µl of PBS in 96-wells microtiter plate. 30 µl of NanoGlo diluted 1:2000 in PBS were added and the plate was immediately imaged with an ANDOR Ikon M 934 BV camera for 5 min.

2.8. *In vivo* GconsNluc probe experimentation

To explore pharmacokinetics of GconsNluc probe three female NMRI mice were treated: at time point 0, animal 2 received an intravenous administration and animal 3 a subcutaneous administration 1 mg/kg BW (administration volume: 5 ml/kg BW) of GconsNluc probe. Animal 1 remained untreated. At time point 2 hr, all animals were imaged with an ANDOR Ikon M 934 BV camera for 5 min in a darkbox under isofluran anesthesia. Directly before imaging, all animals received an intravenous administration of NanoGlo substrate diluted 1:2000 with PBS (200 µl per animal and imaging).
To verify the capacity of GconsNluc probe in recognizing its target *in vivo* three female of SKHR (hairless) mice were treated: at time 0, 50 µl of GFP coated beads (SiMAG-Glutathione + GFP-GST[19]) dissolved in PBS were injected in the right, dorsal flank (in the area of the pelvis) of mice. At time point 0, animal 1, 2 and 3 were injected with 1, 0.5 and 0.1 mg/kg BW (administration volume: 5ml/kg BW) of GconsNluc, respectively. At time point 3 hr all animals were imaged with an ANDOR Ikon M 934 BV camera for 5 min in a darkbox under isofluran anaesthesia. Directly before imaging, all animals received an intravenous administration of NanoGlo substrate diluted 1:2000 with PBS (200 µl per animal and imaging).

3. Results

3.1. Cloning and expression of NanoNluc probes

To verify the possibility to obtain a functional Nb fused to a bioluminescent Nluc, the encoding sequences of two previously described and functional grafted consensus GFP and chicken lysozyme binders (Gcons and Lcons described in details in Chapter 1) were fused at C-terminus in frame with chemically synthesized DNA sequence coding for NanoLuc. Obtained pET28 vectors were transformed in BL21 codon plus *Escherichia coli* strain and used for bacterial expression. Both GconsNluc and LconsNluc polypeptides were well expressed (**Figure 1**) even if LconsNluc was only 10% soluble. After verifying luminescence in bacterial lysate (indication of soluble peptides presence), the resulting recombinant proteins were purified by metal-affinity chromatography exploiting the vector-provided poly-histidine tag (see "Materials and methods" for details) with a final yield of approximately 10 and 2 mg of pure protein/L of bacterial culture for GconsNluc and LconsNluc respectively.

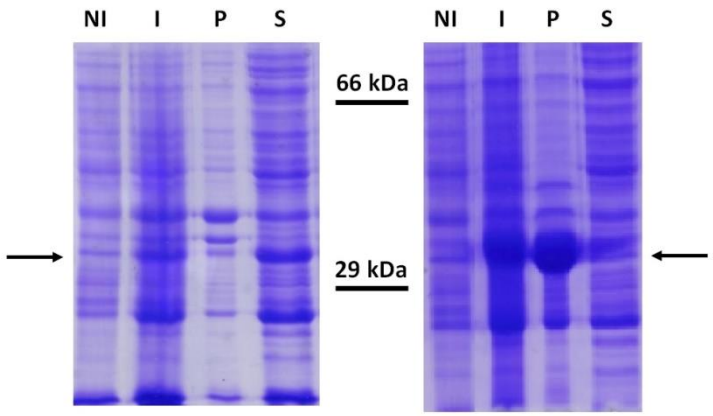

Figure 1 Expression and solubility analysis of GconsNluc (left) and LconsNluc (right). NI: non-induced control; I: induced bacterial lysate; S: bacterial lysate supernatant; P: bacterial pellet. The arrows marks the polypeptide bands corresponding to the fusion proteins. Molecular size of the marker is indicated in the center of the figure (see "Materials and Methods" for details).

A third Nb considered for the construction of a NanoNluc probe was isolated by Isogenica after a CIS-Display[20] screening performed on a Nb library derived from llamas immunized with mouse IgGs (unpublished data). Among 67 promising anti-murine IgGs VHHs, one of them (hereafter designated as G09) showed high capacity to bind different murine IgG subtypes.

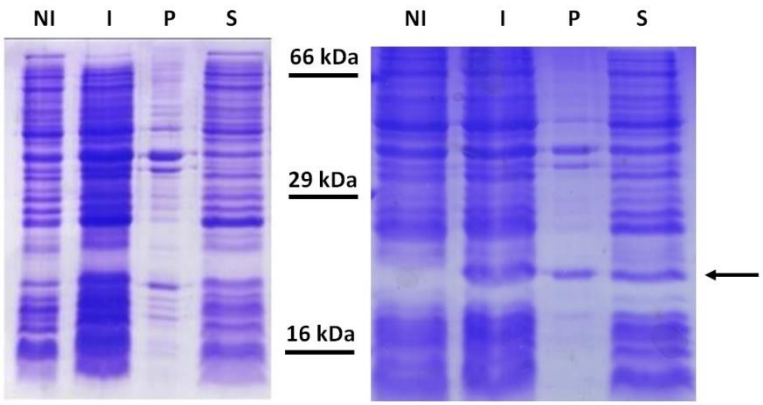

Figure 2 Expression and solubility analysis of G09 (left) and G09cons (right). NI: non-induced control; I: induced bacterial lysate; S: bacterial lysate supernatant; P: bacterial pellet. The arrow marks the polypeptide band corresponding to the expressed Nbs. Molecular size of the marker is indicated in the center of the figure (see "Materials and Methods" for details).

After optimization of G09 DNA sequence for *E. coli* expression and its cloning into pET28 vector, the expression of the protein in BL21 codon plus *E. coli* strain led to low yield of protein recovery (3 mg per liter of culture) (**Figure 2**). So the CDRs of the G09 Nb were grafted in our validated consensus scaffold (described in Chapter 1) and cloned in pET28 vector rising solubility and recovery of new G09cons till 10 mg per liter of culture (**Figure 2**, see "Materials and methods" for details).

Data from Isogenica indicated that G09 clone should bind murine IgGs through their Fc region, so in order to confirm the binding capacity of the grafted G09cons clone an ELISA test was performed in which the Nb was used as secondary antibody to reveal the presence of GconsMuFc protein (a Nb anti-GFP fused to a murine Fc region, described in detail in Chapter 3) (**Figure 3**). Serial dilution of G09cons were tested and all of them were able to recognize GconsMuFc protein (see "Materials and methods" for details).

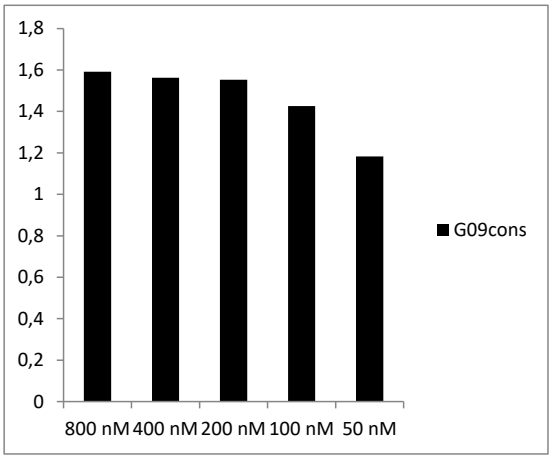

Figure 3 GST-ELISA testing of the G09cons Nb against GconsMuFc protein. Bars represent emission intensity measured at 415 nm after addition of the ABTS substrate, abscissa indicates the serial tested dilution of G09cons (see "Materials and Methods" for details).

With the aim to obtain an anti-IgGs probe G09cons DNA sequence was fused at N-terminus of codon optimized NanoLuc DNA sequence and the obtained pET28 vector was transformed in BL21 codon plus *E. coli* strain. The final probe was soluble and well expressed with an yield of expression of 10 mg of protein per liter of culture and leaded to visible

luminescence if NanoGlo substrate was added to bacterial expressing lysate (see "Materials and methods" for details).

3.2. Evaluation of GconsNluc probe *in vitro* functionality

The GconsNluc fusion protein might be able to bind GFP as a target and emit bioluminescence in presence of the furimazine substrate (NanoGlo). To asses both abilities of the probe an ELISA test was performed (**Figure 4**), which yielded a signal diagnostic of GFP-Nb interaction upon incubation with immobilized GFP-GST but not thioredoxin-GST (negative control, see "Materials and methods" for details).

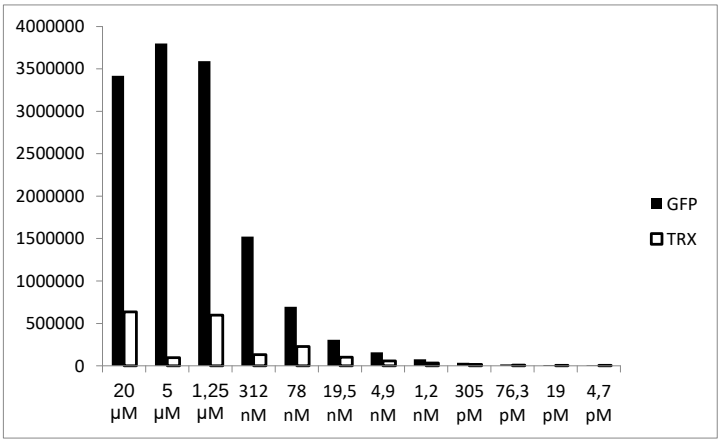

Figure 4 GST-ELISA testing of the GconsNluc fusion Nb against GFP-GST. An unrelated protein (thioredoxin-GST) served as negative control. Bars represent light emission intensity measured at 480 nm after addition of the NanoGlo substrate, abscissa indicates the serial tested dilution of GconsNluc (see "Materials and Methods" for details).

A good light signal, higher than the negative control, was detectable till 19.5 nM GconsNluc concentration indicating specific and high sensitive disclosure even in the presence of low concentrated probe. It is possible to conclude that Nluc luciferase did not alter antibody activity and luminescence is detectable even at low luciferase concentration.

To verify if the observed sensitivity is comparable to a routine ELISA assay in which the presence of the target is reviled with primary and secondary antibodies, a second ELISA test was performed in which His-tagged Gcons (detected with anti-his-tag antibody) was compared to GconsNluc probe (**Figure 5**, see "Materials and methods" for details).

Results indicated clearly a more sensitive detection with GconsNluc which signal remained appreciable till very low probe concentration if compared to conventional colorimetric detection method used for His-tagged Gcons.

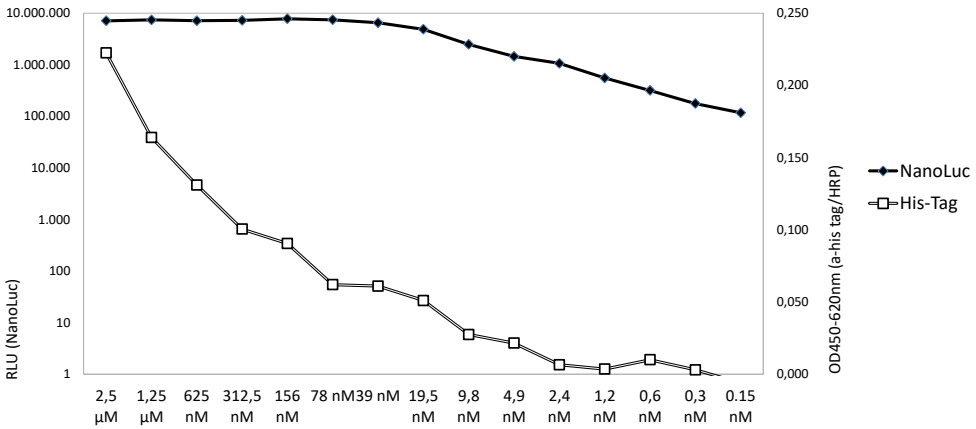

Figure 5 GST-ELISA testing of the GconsNluc fusion Nb against GFP-GST compared to His-tagged Gcons against GFP-GST. Black diamonds represent light emission intensity measured at 480 nm after addition of NanoGlo substrate (left ordinate), white squares represent absorbance at 450-620 nm after addition of TMB One substrate (right ordinate). Abscissa indicates the serial tested dilution of GconsNluc and his-tagged Gcons (see "Materials and Methods" for details).

Necessary features that a probe suitable for *in vivo* imaging should have are stability and target detection in plasma and blood samples. For these reasons different quantities of GFP were added to rat blood and plasma simulating clinically relevant protein concentrations, followed by the addition of GconsNluc to each samples. Using anti-GFP magnetic beads the resulting complexes, consisting of GconsNluc bound to GFP, were recovered from samples and visualize, after NanoGlo addition, with CCD imager (**Figure 6**, see "Materials and methods" for details).

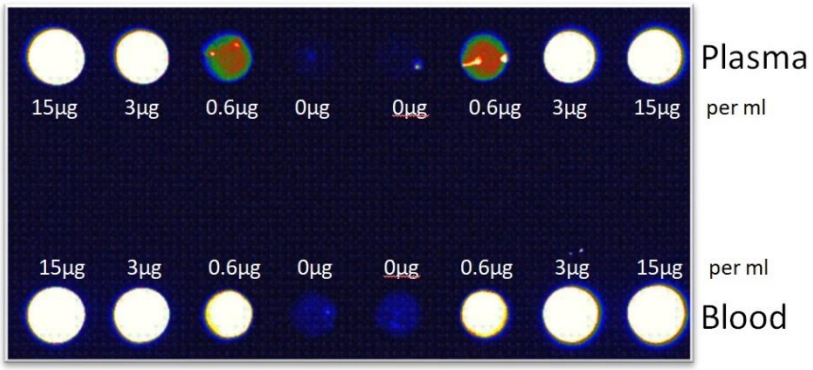

Figure 6 CCD image (upper threshold 3500) of wells containing magnetic anti-GFP beads that collected GconsNluc-GFP complexes from blood and plasma samples. Starting quantities of GFP in plasma and blood are indicated (see "Materials and Methods" for details).

This pool-down experiment showed that GconsNluc is stable and able to bind its target even in plasma and blood samples, confirming also the high sensitivity of the probe which allowed to detect till 0.6 µg/ml of target protein in both plasma and blood samples.

3.3 *In vivo* imaging with GconsNluc probe

Once established the ability of GconsNluc to bind its target in blood and plasma samples a first preliminary *in vivo* pharmacokinetic test was performed. NanoGlo was intravenously administered to female NMRI mice after GconsNluc intravenous or subcutaneous injection (**Figure 7,** see "Materials and methods" for details).

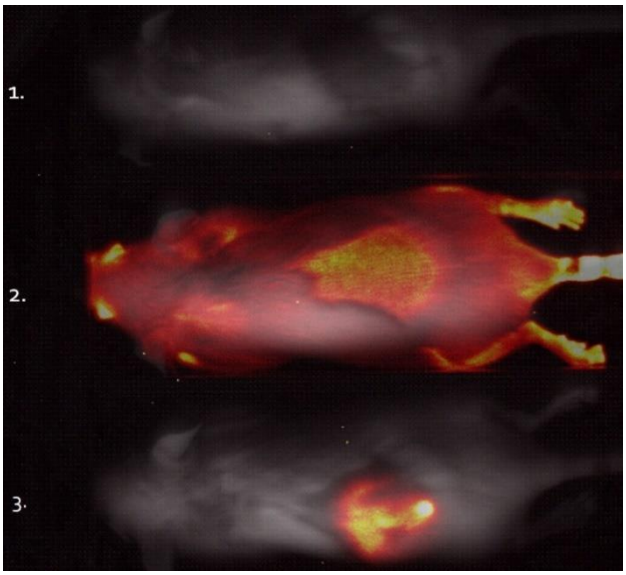

Figure 7 CCD image of intravenous administration of NanoGlo to NMRI mice after no GconsNluc injection (1.), intravenous GconsNluc injection (2.) or subcutaneous GconsNluc injection (3.) (see "Materials and Methods" for details).

The test revealed that GconsNluc is functional and can be detected *in vivo* after intravenous or subcutaneous administration, outputting images consistent with the administration mode.

A second *in vivo* analysis was performed in which GFP (the target of the probe) coated beads were intradermally injected in right hip of three SKHR (hairless) mice; each mouse received subsequently by intravenous administration a different dose of GconsNluc. After three hours of clearance, NanoGlo intravenous injections were performed and CCD images were acquired (see "Materials and methods" for details). How showed in **Figure 8** even at 0.1 mg/kg of probe dose a signal in the right hip of mice is visible indicating a local accumulation of GconsNluc probe probably due to GFP presence. Taken together these

results strongly indicate the possibility to use NanoNluc as a new general system for *in vivo* imaging.

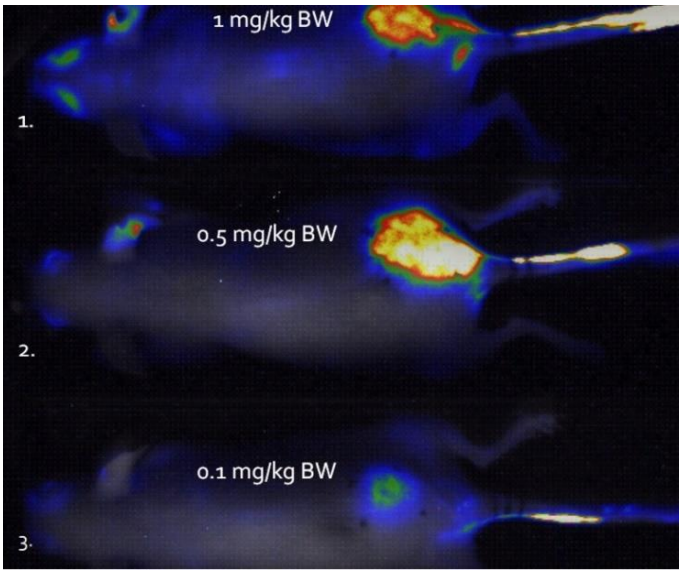

Figure 8 CCD image of SKHR mice after intradermal GFP coated beats injection in the right hip followed by intravenous administration of 1 mg/kg (1.), 0.5 mg/kg (2.) and 0.1 mg/kg (3.) GconsNluc. After three hours since GconsNluc injection NanoGlo was intravenously administrated and images were collected (see "Materials and Methods" for details).

4. Discussion

In vivo imaging filed for diagnostic or preclinical applications needs continuous innovation and sensitization. Recently the discovery of camelids heavy chain antibodies variable domains[5] and the introduction of novel luciferases[14] leads to a significant improvement in imaging technology. Here we created new probes for *in vivo* imaging fusing Nbs to a small and bright luciferase and reported preliminary results of functional tests.

First, the fusion of Nbs to NanoLuc luciferase was validated exploiting three Nbs: Gcons that binds GFP, Lcons that binds chicken lysozyme (both described in Chapter 1) and Isogenica selected G09 that binds murine IgGs grafted in our consensus framework scaffold. Fusing Nluc luciferase to the C-terminus of the antibodies led to high express and soluble proteins using a simple and cheap expression system like *E. coli*. Interesting to note is that the solubility of the fusion proteins probably depended on initial VHH stability; this is evident in **Figure 1** where LconsNluc fusion protein is only 10% soluble as opposed to GconsNluc that is almost 100% soluble, reflecting the stability of sole expressed VHHs as described in Chapter 1.

The functionality of the obtained probes was investigated for GconsNluc which was used as an antibody in ELISA tests. During first analyses the probe binding capacity was evaluated against GFP and an unrelated protein as a negative control; the antibody presence was revealed using Nluc bioluminescence and activity of the fusion protein was confirmed (**Figure 4**). To validate the high sensitivity of GconsNluc we performed a comparative ELISA, in which GconsNluc and Gcons His-tagged proteins were examined. Comparison of the two protocols revealed an evident greater sensibility for luciferase reporter method: luciferase fusion protein showed a high signal even in presence of small amounts of probe (**Figure 5**).

The activity of the GconsNluc protein was further evaluated *in vitro* mixing probe target (GFP) with rat blood and plasma samples simulating clinically relevant concentrations of plasma and blood proteins (**Figure 6**). In all tested dilutions GconsNluc was able to pull down the target showing stability and activity in the tested samples. Furthermore, even low concentration of target protein could be revealed highlighting the possibility to use NanoNluc system as a diagnostic tool for the detection of low concentrated target protein in blood or plasma samples.

Finally, GconsNluc probe was tested *in vivo*: injection of the fusion protein intravenously or subcutaneously in mice revealed a detectable signal compatible with administration method (**Figure 7**). Furthermore, GFP subcutaneous administration led to a GconsNluc accumulation in the GFP injected area (**Figure 8**) with a detectable signal even after administration of 0.1 mg/kg BW probe concentration. To exclude that GconsNluc accumulation in the right hip was due to inflammation response after GFP injection a further control has to be performed in which only PBS or an unrelated protein has to be injected in the right hip of mice before GconsNluc administration. More experiments to assess the optimal lag time for NanoGlo substrate injection time are needed in order to identify the moment where Nb is maximally bond to the target and minimally present in tissues.

All the performed analyses have to be repeated with LconsNluc and G09consNluc probes in order to validate NanoNluc as general system. Additionally, we speculate a possible *in vivo* G09consNluc application in which accumulation of IgGs in case of immune reaction can be detected[21,22]. Experimentally it will be interesting to inject GFP-immunize mice with GFP and verify IgGs accumulation in the injection site through G09consNluc probe.

In conclusion, despite examples of Nbs-luciferase fusion proteins are described in literature[23,24], here we reported the development of the first NanoNluc system suitable for *in vivo* imaging. Even if further validation and evaluation have to be made, preliminary results encourage the deepening of a general system for the production of new cheap and functional imaging probes suitable for preclinical studies.

5. Bibliography

1. Zola H, Mohandas AP, Krumbiegel D. Monoclonal Antibodies: Diagnostic Uses. *eLS*. 2013. doi:10.1097/01.inf.0000223443.80696.5b.
2. Hamers-Casterman C, Atarhouch T, Muyldermans S, et al. Naturally occurring antibodies devoid of light chains. *Nature*. 1993;363(6428):446-448. doi:10.1038/363446a0.
3. Muyldermans S. Nanobodies : Natural Single-Domain Antibodies. 2013. doi:10.1146/annurev-biochem-063011-092449.
4. Freise AC, Wu AM. In vivo Imaging with Antibodies and Engineered Fragments. *Mol Immunol*. 2015;48(0):923-930. doi:10.1016/j.clinbiochem.2015.06.023.Gut-Liver.
5. De Vos J, Devoogdt N, Lahoutte T, Muyldermans S. Camelid single-domain antibody-fragment engineering for (pre)clinical *in vivo* molecular imaging applications: adjusting the bullet to its target. *Expert Opin Biol Ther*. 2013;13(8):1149-1160. doi:10.1517/14712598.2013.800478.
6. Li T, Vandesquille M, Koukouli F, et al. Camelid single-domain antibodies: A versatile tool for in vivo imaging of extracellular and intracellular brain targets. *J Control Release*. 2016;243:1-10. doi:10.1016/j.jconrel.2016.09.019.
7. Keyaerts M, Xavier C, Heemskerk J, et al. Phase I Study of 68Ga-HER2-Nanobody for PET/CT Assessment of HER2 Expression in Breast Carcinoma. *J Nucl Med*. 2016;57(1):27-33. doi:10.2967/jnumed.115.162024.
8. Schoonooghe S, Laoui D, Van Ginderachter JA, et al. Novel applications of nanobodies for in vivo bio-imaging of inflamed tissues in inflammatory diseases and cancer. *Immunobiology*. 2012;217(12):1266-1272. doi:10.1016/j.imbio.2012.07.009.
9. Nogawa M, Yuasa T, Kimura S, et al. Monitoring luciferase-labeled cancer cell growth and metastasis in different in vivo models. *Cancer Lett*. 2005;217(2):243-253. doi:10.1016/j.canlet.2004.07.010.
10. Leary PO, Crown J, Gallagher WM. Generation of a new bioluminescent model for visualisation of mammary tumour development in transgenic mice. *BMC Cancer*. 2012. doi:10.1186/1471-2407-12-209.
11. Gainkam LOT, Keyaerts M, Caveliers V, et al. Correlation between epidermal growth factor receptor-specific nanobody uptake and tumor burden: A tool for noninvasive monitoring of tumor response to therapy. *Mol Imaging Biol*. 2011;13(5):940-948. doi:10.1007/s11307-010-0428-4.
12. Karlsson EA, Meliopoulos VA, Savage C, Livingston B, Mehle A, Schultz-Cherry S. Visualizing real-time influenza virus infection, transmission and protection in ferrets. *Nat Commun*. 2015;6(May 2014):1-10. doi:10.1038/ncomms7378.
13. Coleman SM, Mcgregor A. A bright future for bioluminescent imaging in viral research. *Futur Virol*. 2015;10(2):169-183. doi:10.2217/fvl.14.96.A.
14. Mezzanotte L, van 't Root M, Karatas H, Goun EA, Löwik CWGM. In Vivo Molecular Bioluminescence Imaging: New Tools and Applications. *Trends Biotechnol*. 2017;35(7):640-652. doi:10.1016/j.tibtech.2017.03.012.
15. Hall MP, Unch J, Binkowski BF, et al. Engineered luciferase reporter from a deep sea shrimp utilizing a novel imidazopyrazinone substrate. *ACS Chem Biol*. 2012;7(11):1848-1857. doi:10.1021/cb3002478.
16. Stacer AC, Nyati S, Moudgil P, et al. NanoLuc Reporter for Dual Luciferase Imaging in Living Animals. *Mol Imaging*. 2013;4(164):1-13. doi:10.1126/scisignal.2001449.Engineering.
17. Sambrook J, W Russell D. Molecular Cloning: A Laboratory Manual. *Cold Spring Harb Lab Press Cold Spring Harb NY*. 2001. doi:10.1016/0092-8674(90)90210-6.
18. Sehr P, Zumbach K, Pawlita M. A generic capture ELISA for recombinant proteins fused to glutathione S-transferase: Validation for HPV serology. *J Immunol Methods*. 2001;253(1-2):153-162. doi:10.1016/S0022-1759(01)00376-3.
19. Chemicell. Purification of GST-fusion proteins with magnetic SiMAG-Glutathione particles. :6-8.
20. Mathonet P, Ioannou A, Betley J, Ullman C. CIS display , a DNA-based in vitro selection technology for therapeutic peptides. 2011;29(April):1-3.
21. Juweid M, William Strauss H, Yaoita H, Rubin RH, Fischman AJ. Accumulation of immunoglobulin G at focal sites of inflammation. *Eur J Nucl Med*. 1992. doi:10.1007/BF00173275.

22. Rashidian M, Keliher EJ, Bilate AM, et al. Noninvasive imaging of immune responses. *Proc Natl Acad Sci U S A*. 2015;112(19):6146-6151. doi:10.1073/pnas.1502609112/-/DCSupplemental.www.pnas.org/cgi/doi/10.1073/pnas.1502609112.
23. Bruce VJ, McNaughton BR. Evaluation of Nanobody Conjugates and Protein Fusions as Bioanalytical Reagents. *Anal Chem*. 2017;89(7):3819-3823. doi:10.1021/acs.analchem.7b00470.
24. Li T, Li SL, Fang C, et al. Nanobody-based dual epitopes protein identification (DepID) assay for measuring soluble CD38 in plasma of multiple myeloma patients. *Anal Chim Acta*. 2018;1029:65-71. doi:10.1016/j.aca.2018.04.061.

Conclusions and future perspectives

Conclusions and future perspectives

During my three years of Ph.D. I built and validate a scaffold suitable for nanobody (Nb) expression and selection. Deriving a consensus sequence of Nbs framework regions (FRs) from the alignment of more than 750 llama Nbs, I demonstrated the possibility to graft natural or artificial Nb complementary determining regions (CDRs) in this scaffold obtaining soluble, stable and functional antibodies. In some grafted Nbs, a loss of the target affinity was observed, since FRs are occasionally involved in target binding as well. Thus, when the amino acids involved in target binding are not known, natural Nbs CDRs grafting should be evaluated as the possibility of losing target affinity could vary case-by-case.

Despite the use of the universal consensus framework scaffold (CFW) to enhance and stabilize the expression of natural Nbs is not always the best choice, CFW had proved to be an optimal template for libraries construction. Introducing semi-random CDRs in the scaffold a complex collection of different Nb genes was produced and a functional library suitable for ribosome display (RD) was obtained. The library presented a complexity similar to the natural llama Nb repertoire (not achievable with standard cloning procedures) and new Nbs against Maltose binding protein (MBP) were successfully selected. The constant of dissociation of new anti-MBP Nbs has now to be assessed in order to determine the quality of the RD library and the worth of entire selection procedure. Anyhow if high-affinity binders will not be obtained after this first selection, further steps of affinity maturation can be performed.

Also after sequence humanization, rendering the scaffold identical to human IgG VH IIII FRs, CFW conserved its solubilizing and stabilizing effects; thus a humanized version of the previous library was built. The selection of already humanized Nbs will enhance the probability to obtain antibodies that, without post-selection modifications, can be directly applied for human therapy or diagnosis. The selection technique that I chose for the humanized library was phage display because is easier and more robust than ribosome display and can be performed in almost every laboratory. However, to enhance the speed of selection and thus the probability to find new high-affinity antibodies, I created a novel phage vector suitable for phage display procedure. The novel vector was validated and now the humanized Nb library is ready to be cloned and screened.

Furthermore, I demonstrated the possibility to render my CFW grafted Nbs applicable in diagnostic field conjugating them to Fc regions of immunoglobulins G, but I occasionally obtained insoluble fusion proteins. In order to get quick and soluble Nb-Fc conjugation, I successfully applied the *in vitro* SpyTag – SpyCatcher ligation system to different Nbs and Fc IgG regions, obtaining fully functional antibodies which simulated monoclonal

antibodies features. Thanks to the modularity of this system the Fc fusion partner can be easily exchanged for producing new versions that fit for every specific analysis. If these monoclonal-like antibodies will demonstrate their ability to bind protein A and G, they will be applicable in almost every diagnostic test.

In collaboration with Preclincs company, I validated the stability and functionality of my CFW scaffold also in *in vivo* experiments. I created novel probes suitable for *in vivo* imaging conjugating CFW grafted Nbs to NanoLuc luciferase. The anti-GFP probe was functional and detectable in mice, while the other probes activity remains to be tested for validating the CFW grafted Nbs-NanoLuc conjugation as a general approach.

In conclusion, I set up a functional platform for new Nbs selection and production which will allow soon to isolate and construct novel tools for diagnostic and therapeutic applications.